*from the seniors to the students*

# CONTENTS

## ORIGINAL ARTICLES

# CASE REPORT

acta medica

ORIGINAL ARTICLE

# Unravelling the maternal stress-induced orchestrations: *Fndc5* gene expression dynamics across duodenum, stomach, and whole blood in offspring

Keziban Korkmaz Bayram[1,2]
ORCID: 0000-0002-1228-1298

Aida Nurul Barokah[2,3]
ORCID: 0000-0003-3102-7858

Merve Hilal Dönmez[4]
ORCID: 0000-0001-6286-7038

Şevval Nebahat Işıktan[5]
ORCID: 0009-0009-4280-6372

Arslan Bayram[6]
ORCID: 0000-0002-3682-2140

[1] Department of Medical Genetics, Faculty of Medicine, Ankara Yıldırım Beyazıt University, Ankara, Türkiye

[2] Research and Application Centre, Central Research Laboratory, Ankara Yildirim Beyazit University, Ankara, Türkiye

[3] Department of Translational Medicine, Faculty of Medicine, Ankara Yıldırım Beyazıt University, Ankara, Türkiye

[4] Institute of Biotechnology, Faculty of Process Sciences, Technical University of Berlin, Berlin, Germany

[5] Department of Biotechnology and Molecular Biology, Faculty of Science, Aksaray University, Aksaray, Türkiye

[6] GENTAN, Genetic Diseases Evaluation Centre, İzmir, Türkiye

Corresponding Author: Keziban Korkmaz Bayram
E-mail: k.korkmaz.bayram@aybu.edu.tr

～∞◯ A B S T R A C T ◯∞～

Objective: Maternal stress is a known risk factor for a variety of adverse outcomes in offspring, including metabolic and behavioural abnormalities. The hormone irisin, encoded by the *Fndc5* gene, is believed to mediate stress's effects on metabolism. Two weeks of restraint stress causes stomach inflammation and increases oxidative stress in rodents. Irisin, coded by the *Fndc5* gene, probably suppresses this oxidative stress. In this study, we examined the effect of early-life maternal stress on *Fndc5* gene expression in the duodenum, stomach and whole-blood offspring.

Materials and Methods: This study consists of three groups: a control, an unpredictable maternal separation (MS), and an unpredictable maternal separation combined with unpredictable maternal stress (MSUS). On postnatal (PND) days 1-14, randomly three hours a day, MS and MSUS were exposed to unpredictable maternal separation. MSUS was subjected to extra unpredictable maternal stress. Mice were sacrificed on PND35. Total RNA was isolated from duodenum, stomach, and whole blood samples by Phenol-Chloroform technique, and HiScript II 1st Strand cDNA Synthesis Kit was used for cDNA synthesis. Fndc5 and Gapdh genes expression level was measured by qPCR using FastStart Universal SYBR Green Master. The data obtained were analyzed using One-Way ANOVA tests in GraphPad Prism.

Results: *Fndc5* gene expression did not differ between groups in the duodenum ($p>0.05$), significantly increased in the MSUS group compared to the control (female $p=0.0089$, male $p=0.0053$) and MS (female $p=0.0206$, male $p=0.026$) groups in the stomach. In whole blood samples, it decreased in MS and MSUS group males ($p=0.0011$). In addition, a significant negative correlation ($p=0.0003$) has been established between the stomach and whole blood.

Conclusion: The findings assert the role of irisin in transmitting stress-related effects on metabolism, emphasizing the therapeutic potential of targeting the *Fndc5* gene in preventing and treating stress-related disorders.

Keywords: maternal stress, early life stress, irisin, *Fndc5* gene expression, macrophage.

## INTRODUCTION

Physical and psychological stress have been linked to various adverse effects on the gastrointestinal tract, including gut motility and permeability changes and an increased risk of gastrointestinal disorders (1). Maternal stress, which is both physical and psychological stress during the lactation period, has been shown to alter the composition of milk (2,3) and impact infant development (2). Maternal stress is widely used as a typical rodent model of early life stress (4-6). Moreover, restraint stress is often used as a model to observe stress effects on the gastrointestinal tract (7,8).

The stomach plays a crucial role in the digestive process by mechanically breaking down food and delivering nutrients to the small intestine through rhythmic contractions (9). The mouse stomach comprises three main parts: the forestomach for food storage, the corpus for food digestion, and the antrum that secretes mucus and certain hormones (10). It contains smooth muscle tissue, which is responsible for the contraction and relaxation of the organ during digestion (11). A recent discovery has shown that the smooth muscle layers of the gastrointestinal tract contain a population of immune cells called muscularis macrophages (12). Macrophages in the gastrointestinal tract constitute the largest population in the body (13,14), and control gastrointestinal motility in health and disease (15). A study has observed macrophages in the muscularis propria. Muscularis macrophages are essential for maintaining the gastrointestinal system's (GI) stability and preventing illness. These immune cells are distinct from mucosal macrophages in that they possess an anti-inflammatory phenotype (12). Psychological stress (16) and acute stress (8,17) have been found to affect various physiological functions of the gastrointestinal tract, including gastrointestinal tract motility (18). In addition, it is known that due to the presence of stress, the expression of gastric monocyte/macrophage markers is increased (7).

Fibronectin type III domain containing 5 (*FNDC5*), a protein found in muscle cells, acts as a precursor for irisin, a 111-amino acid peptide (19). Irisin, the active hormone derived from FNDC5, increases fat burning, improves endurance, speeds up recovery after exercise, and potentially protects against muscle damage during exercise. Despite numerous studies conducted on FNDC5/irisin in skeletal muscle and fat tissue during exercise, almost no studies have investigated FNDC5/irisin expression in the gastrointestinal tract in the presence of early-life chronic stress. Irisin is a crucial mediator of inflammatory response, oxidative stress, and cell apoptosis (20). FNDC5/irisin may protect against oxidative stress by improving mitochondrial function and reducing reactive oxygen species in cells (21). The gastrointestinal system is vulnerable to oxidative stress, which occurs when an imbalance between harmful molecules called reactive oxygen species (ROS) and the body's ability to detoxify them. Factors like diet, exposure to pathogens, inflammation, and chronic stress can contribute to oxidative stress (22). This condition is associated with various gastrointestinal disorders, such as ulcers, inflammatory bowel disease, and some types of cancer (23). Despite the differences in basal irisin levels, exercise-induced irisin secretion is complicated (24). Some studies have questioned whether irisin is an exercise-induced factor (25), and different assay kits account for a large portion of this controversy. This study aims to investigate the relationship between early-life chronic stress and *Fndc5* mRNA expression, the precursor for irisin, specifically in gastrointestinal tissues such as the stomach and duodenum. This research is particularly relevant given the controversy surrounding irisin measurement and its potential modulation by exercise.

## Materials and Methods

### Animals

The study was performed with 72 *Balb/c* mice aged five weeks (supplied by Nesa Experimental Animals Laboratory). The mice were five weeks old at the start of the study and were housed in a room with controlled temperature (22°C), humidity (55%) and a 12/12 light/dark cycle. The mice had free access to food and water throughout the study. The mice were treated under European regulations for laboratory animal care, and the study was approved by the Nesa Experimental Animals Laboratory (Ethics Committee Approval No: 016).

## Maternal stress mice model

The study included three groups of 12 male and 12 female mice: a control group, a group subjected to unpredictable maternal separation (MS), and a group subjected to unpredictable maternal separation combined with unpredictable maternal stress (MSUS). For MSUS, dams and litters were subjected to randomly three hours of proximal separation daily from postnatal days 1 to 14 (26-28). During separation, dams were unpredictably exposed to either 20-minute restraint or 6-minute forced swim stress during the final 20 minutes of a three-hour unpredictable separation. Dams were kept in a 50-mL plastic Falcon tube to induce restraint stress for 20 minutes. Holes were created at the tapering end of the Falcon tube to ensure sufficient air supply. Dams were forced to swim for five minutes in a jar of cold water (18°C) as part of the forced swimming test. Control animals were left undisturbed except for a cage change once a week. Once weaned, pups were reared in social groups (3–4 mice/cage) composed of animals subjected to similar treatment but from different dams to avoid litter effects. Litters were sacrificed at PND35.

## RNA isolation and real-time quantitative RT-PCR analysis

All the genetic studies were performed at Ankara Yıldırım Beyazıt University Central Research Laboratory Research and Application Center (MERLAB). From the hearts of sacrificed mice, 0.5 mL of blood was collected using an Etilendiamin tetraasetik asit (EDTA)-washed syringe. Fifty milligrams of the stomach's corpus region and the start zone of the duodenum were removed. Tissues are homogenised by using an ultrasonic homogeniser (Bandelin SONOPULS ultrasonic homogeniser HD 2070, Berlin, Germany). Total RNA was extracted from blood and tissue samples using QIAzol Lysis Reagent (Qiagen, Germany). RNA samples were stored at −80 °C until used. The quantity (absorbance at 260 nm) and quality (ratio of absorbance at 260 nm and 280 nm) of RNA were estimated with NanoDrop 2000 (Thermo Fisher Scientific, Massachusetts, United States of America). All the RNA samples met the following two criteria: 1) The absorbance ratio at 260 nm to 280 nm was within the range of 1.8 to 2.0, and 2) the total RNA concentration was greater than 100 ng/µl. First-strand cDNA synthesis was performed with HiScript II 1st Strand cDNA Synthesis Kit (Vazyme,

China) from total RNA. The obtained cDNA samples were diluted 1:5 by adding nuclease-free water. Quantitative real-time PCR was performed in Rotor-Gene Q (Qiagen, Germany) using specific primers (Table 1) and FastStart™ Universal SYBR® Green Master (Rox) (Roche, Germany) with the following cycling conditions in Table 2.

The study utilised SYBR Green, optimised through agarose gel electrophoresis technique and Melting Curve Analysis (Table 2). It enabled the determination of the melting temperature (Tm) of the expected size amplicon of the target and housekeeping gene. Data were collected in the linear amplification range, and each PCR experiment was repeated at least twice. As a result, delta-delta-Ct (2−ΔΔCt) was carried out using the sample's Ct value within the expected Tm range, and the data were normalised using the mean values obtained in the control group.

## Statistical analyses

Statistical analysis was performed on the mRNA expression data in control, MS, and MSUS using one-way ANOVA or the Kruskal-Wallis test. Tukey's or Dunn's multiple comparisons post hoc were performed using GraphPad Prism 9.1.0 (GraphPad Software, California, United States). The data distribution was evaluated using a histogram, q-q plot, and the Shapiro-Wilk test. Based on David C. Hoaglin and Boris Iglewicz's approach, outliers were identified and removed. Weight data was analyzed using repeated measure ANOVA followed by Tukey's post hoc. When appropriate, Pearson's or Spearman's correlation was used to assess the

**Table 1.** Sequence of primers

| Primer | Sequence (5'-3' | Amplicon Size (bp) |
|---|---|---|
| *Fndc5* | Forward:ATGAAGGAGATGGGGAGGAA Reverse: CGGCAGAAGAGAGCTATAAC | 101 |
| *Gapdh* | Forward:GAGAAACCTGCCAAGTATGATGAC Reverse:TAGCCGTATTCATTGTCATACCAG | 105 |

**Table 2.** Amplification and Melting Curve program profile in Rotor-Gene Q

| Step | Temperature [°C] | Time [min] | Cycle |
|---|---|---|---|
| Holding | 95 | 10:00 | |
| Cycling | 95 | 00:20 | 40 |
| | | 00:45 | |
| Melting curve | 60 – 95 | | |

relationship between the data. All tests were set at a significance level of p < 0.05.

## RESULTS

### Maternal Stress-Induced *Fndc5* mRNA Expression Changes in the Gastrointestinal System and Whole Blood of a Mice Model

This study investigated the mRNA expression level of the *Fndc5* gene in mice exposed to maternal stress in the stomach duodenum and blood samples. Compared to the control group, there was no difference in *Fndc5* gene expression in the duodenum (p>0.05) (Fig.1A). Interestingly, *Fndc5* gene expression was significantly increased in the stomach of the MSUS group in both females (p=0.0089) and males (p=0.0053) compared to the control. In addition, it was also found that *Fndc5* gene expression level was excessively increased in both females (p=0.0206) and males (p=0.026) of the MSUS group compared to MS (Fig.1B). In contrast, in whole blood samples, *Fndc5* gene expression was increased in the female MS group and unchanged in the MSUS group compared to the control group but decreased in MS and MSUS males. In males, this decrease in *Fndc5* mRNA levels in whole blood samples was not statistically significant in the MS group compared to the control (p>0.05), whereas it was statistically significant in the MSUS group (p=0.0011) (Fig.1C).

The analysis indicates no correlation between the expression level of the *Fndc5* gene in the duodenum and whole blood (p= 0.508) (Fig.2A). On the other hand, a significant negative correlation (p= 0.0003) has been established between the stomach and whole blood (Fig.2B).

## DISCUSSION

Even though several studies have investigated the exercise-associated gene expression level of *Fndc5*, the effects of early-life maternal stress on the expression level of *Fndc5* have yet to be previously examined. Therefore, this study explored the impact on *Fndc5* gene expression level in the stomach, duodenum and whole blood of litters of early maternal separation, maternal forced swim test and maternal restraint stress. Restraint stress has increased the amount of taurine in milk via taurine transports from maternal blood to milk in the mammary gland in lactating mice (3). Therefore, changes in taurine concentration in milk are likely to affect the offspring to some extent. The expected effect on the offspring is believed to be synergistic, with one potential effect being a decrease in milk production. Stress may also decrease hypothalamic prolactin gene expression and plasma prolactin levels, which can reduce milk quantity (22,23). It was observed that during the lactation period, mothers who were separated from their litters, especially those exposed to restraint stress and cold water, avoided breastfeeding their infants compared to the control group. It is believed that they were weaned due to stress and that breastfeeding was avoided due to the pain it caused.

Macrophages play a vital role in the immune system by acting as defenders and cleaners. Based on their
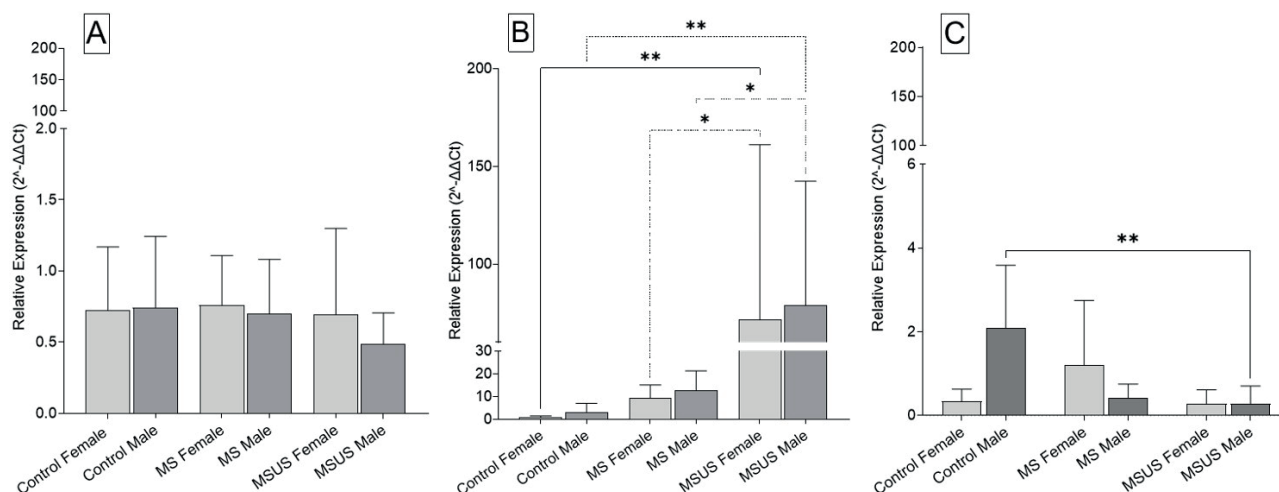


**Figure 1.** Comparison of *Fndc5* mRNA expression levels in the duodenum **(A)**, stomach **(B)**, and whole blood **(C)** of mice from different groups
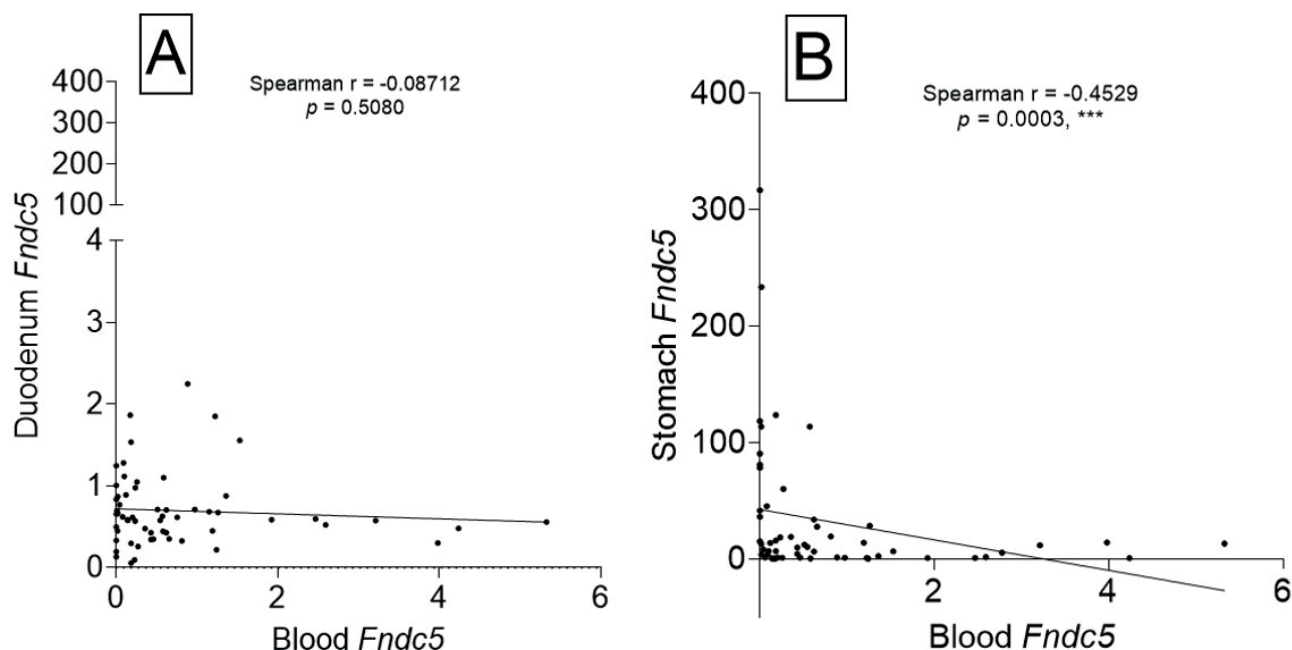
**Figure 2.** Correlation of *Fndc5* gene expression between Blood and Duodenum **(A)**, Blood and Stomach **(B)**.

activation state, they have two primary forms: M1 and M2 macrophages. M1 macrophages act as attackers by releasing inflammatory molecules to exterminate threats like infections or damaged cells and recruit other immune cells. These macrophages play a crucial role in fighting infections but can also cause tissue damage if inflammation persists. On the other hand, M2 macrophages act as healers by promoting tissue repair, reducing inflammation, and facilitating wound healing. Additionally, different types of M2 macrophages perform specialised functions for repairing and dampening inflammation (29).

Mitochondria are the powerhouses of the cell, responsible for energy production. However, damaged mitochondria can leak harmful reactive oxygen species (ROS) that contribute to oxidative stress (30). Mitophagy is a cellular process where damaged mitochondria are targeted for degradation, helping maintain healthy mitochondria and reducing oxidative stress (30,31). Through mitophagy, aged and damaged mitochondria are selectively eliminated through specific retention and engulfment of mitochondria for subsequent lysosomal degradation. Mitophagy is a critical cellular quality control mechanism that maintains homeostasis in normal physiology and under stress (31). Maintaining a balance between M1 and M2 macrophages and ensuring efficient mitophagy is crucial for a healthy immune response and preventing chronic inflammation

and oxidative stress (32). Two weeks of restraint stress causes stomach inflammation and increases oxidative stress in rodents (7). According to studies, taurine supplementation offers defence against diseases linked to mitochondrial defects, including ageing, mitochondrial diseases, metabolic syndrome, cancer, cardiovascular diseases, and neurological disorders (33). Due to oxidative stress, M1 macrophages increase glycolysis and inhibit oxidative phosphorylation, preventing them from polarising to M2 macrophages. M1 and M2 macrophage polarization is critical in maintaining a healthy immune response. However, an imbalance or dysregulation in their activity can result in several diseases. When M1 macrophages are excessively or continuously activated, they release inflammatory molecules that can harm the tissues and promote chronic inflammation (29,33).

Macrophages in the gastrointestinal tract constitute the largest population of macrophages in the body (13,14), and control gastrointestinal motility in health and disease (15). A study has observed macrophages in the muscularis propria, and they suggested that these muscularis macrophages are not only immunomodulatory but also play a housekeeping role and are involved in maintaining normal motility in the healthy gut (15). Psychological stress (16) and acute stress (8,17) have been found to affect various physiological functions of the gastrointestinal tract, including gastrointestinal tract motility (18).

In the presence of stress, the expression of gastric monocyte/macrophage markers is increased (7). Mitochondrial metabolism plays an essential role in regulating macrophage function (34). Studies have demonstrated that metabolism can influence the macrophage phenotype. In active M1 macrophages, mitochondrial oxidative phosphorylation (OXPHOS) is blocked, preventing them from changing into M2 phenotypes. Most cell types rely on mitochondrial OXPHOS as their primary cellular energy production, but this process is blocked in active M1 macrophages (34). Furthermore, a study in mice has shown that M2 macrophages are critical in preventing the development of diabetes-induced delayed gastric emptying (35). In addition, according to Meng L. et al. (32), taurine stabilises energy metabolism and repairs inflammatory damage, helping to prevent chronic diseases and complications. Excessive M1 polarisation of macrophages can lead to the development of inflammatory diseases, but inhibiting M1 polarisation is a protective mechanism against diseases. Taurine transporters in the membrane of macrophages facilitate the transfer of taurine from the extracellular environment to the cytoplasm, which can weaken methionine metabolism and reduce S-adenosylmethionine (SAM) in macrophages. Low SAM is directly sensed by leucine carboxy methyltransferase LCMT-1 and methylesterase PME-1, inhibiting leucine-309 residue of catalytic C-subunit (PP2Ac) methylation, which is required for M1 polarisation. Activation of PTEN-induced kinase 1 (PINK1) promotes the elimination of mitochondria by macrophages via mitophagy for metabolic adaptation, but taurine can block PINK1-mediated mitophagy flux by inhibiting SAM-dependent PP2Ac methylation, resulting in a high mitochondrial density of the M2 phenotype and a low density of the M1 phenotype. This ultimately inhibits the conversion of energy metabolism to glycolysis, which is required for M1 polarisation (36). In addition, Choi et al. (33) found that an increase in taurine content in milk can reduce mitochondrial oxidative stress and increase oxidative phosphorylation in the litter during times of stress. Irisin mediates macrophage proliferation and induces M2 polarisation. Irisin modulates macrophage activity by reducing the overproduction of reactive oxygen species (ROS) (35). *Fndc5* and irisin suppress oxidative stress (18) mediated by mitochondrial dysfunction in macrophages. According to our observations, the

MSUS group subjected to maternal and restraint stress showed a markedly higher expression level of *Fndc5* than the control and MS groups (Fig.1). We suggest that overexpression of *Fndc5* mRNA in the stomach of MSUS groups whose mothers were exposed to extra stress may have occurred to reduce oxidative stress.

Irisin, the active hormone derived from FNDC5, promotes converting white adipose tissue (fat storage) into beige or brown adipose tissue. Brown/beige fat cells are more metabolically active and burn energy for heat production. By increasing the amount of brown/beige fat, irisin helps the body burn more calories during and after exercise. In addition, irisin may also encourage muscle cells to use fat as a fuel source during exercise. Irisin stimulates the creation of new mitochondria within muscle cells (24,37). Mitochondria are the powerhouses of cells where energy is produced (31,38). Irisin enhances the function of existing mitochondria, making energy production more efficient. It allows muscles to work harder and for longer during exercise (30,39). By boosting mitochondrial health, irisin might protect muscle cells from oxidative stress and damage that can occur during intense exercise (24). On the other hand, research on the effect of chronic stress on irisin levels has produced mixed results. While some studies indicate a decrease in irisin with chronic stress (24,40), others have shown no significant alteration (25,41). While directly measuring irisin protein levels would be ideal in the long term, focusing on *Fndc5* mRNA expression in the current study has the following advantages: (1) Transcriptional reflection of the *Fndc5* gene is an earlier indicator of changes in irisin production compared to measuring the protein level of mature irisin. (2) Quantifying *Fndc5* mRNA using qPCR is a well-established and sensitive technique. It allows for a more controlled and potentially more sensitive measurement than techniques for mature irisin protein, which can be more susceptible to degradation and variability. (3) Measuring *Fndc5* mRNA in specific tissues (stomach and duodenum) allows pinpointing potential changes in local production within the GI rather than reflecting systemic irisin levels from other tissues. It provides a more precise picture of how early life stress might affect *Fndc5* expression within GI. In summary, accurately measuring irisin levels can be difficult, and this challenge might be one reason for conflicting research results. It is well-known that stress can negatively impact

the digestive system. However, as it is difficult to accurately measure the irisin level (24), this study investigates the expression of *Fndc5* mRNA in the stomach, duodenal tissue, and blood samples of mice exposed to early-life maternal stress.

Energy metabolism and muscle mass are regulated by testosterone in males (42). The positive impact of testosterone on men's body composition and metabolism is widely recognised, but the exact mechanisms behind these effects still need to be fully comprehended. These mechanisms may be linked to myokines, hormones secreted by the skeletal muscles. One myokine, irisin, has shown potential for beneficial metabolic effects (43). Infants exposed to higher levels of stress in early life due to maternal anxiety and a reduction in breastfeeding interaction may experience an earlier onset of puberty (44,45). This study's limitation is that no tests were explicitly performed for early puberty, and testosterone, taurine and irisin levels were not measured. Based on the knowledge in the literature that early-life chronic stress leads to early puberty, in this study, male mice exposed to early-life maternal stress may have increased testosterone levels due to early puberty. Increased testosterone levels due to precocious puberty (46) in the MS and MSUS groups do not affect *Fndc5* gene expression in duodenal and stomach tissue. However, it causes a significant decrease in whole blood samples in males. (Fig.1). Our study indirectly confirms that maternal stress is the cause of early puberty in males. Probably, the high levels of testosterone in males with maternal stress (MS) and maternal separation with unpredictable stress (MSUS) could lead to a decrease in *Fndc5* gene expression. In our study, we could not identify the precise source of *Fndc5* mRNA expression in the blood. However, we hypothesise that adipose

tissue, brain, liver, and heart tissues likely played a role in this expression. Further research is needed to understand how *Fndc5* mRNA expression in various tissues contributes to *Fndc5* mRNA expression levels in the blood and its impact on normal bodily functions and disease processes.

As a final result, in maternal stress, *Fndc5* gene expression may increase in the stomach to protect against oxidative stress-induced disorders and keep macrophages in the M1 phase. Presumably, increased *Fndc5* gene expression may increase irisin protein, which both reduces M1 polarisation by blocking oxidative stress and enhances M2 polarisation by mediating macrophage proliferation (Fig.3). Stress can cause significant damage in our body, especially in our stomach, but this damage may be compensated at the molecular level thanks to molecules such as irisin and taurine.

The diagram visually represents the pathways affected by maternal stress and the role of Fndc5/Irisin expression in modulating macrophage metabolism. Maternal stress activates oxidative stress (solid arrows), which enhances glycolysis linked to M1 macrophage polarisation and reduces oxidative phosphorylation associated with M2 macrophage polarisation. The introduction of increased Fndc5/Irisin expression (dashed arrows) blocks the effects of oxidative stress, subsequently reducing glycolysis and enhancing oxidative phosphorylation, potentially reversing the effects on macrophage polarisation. This visual aid underscores the complex interplay between stress responses and immune regulation.

## Author contribution

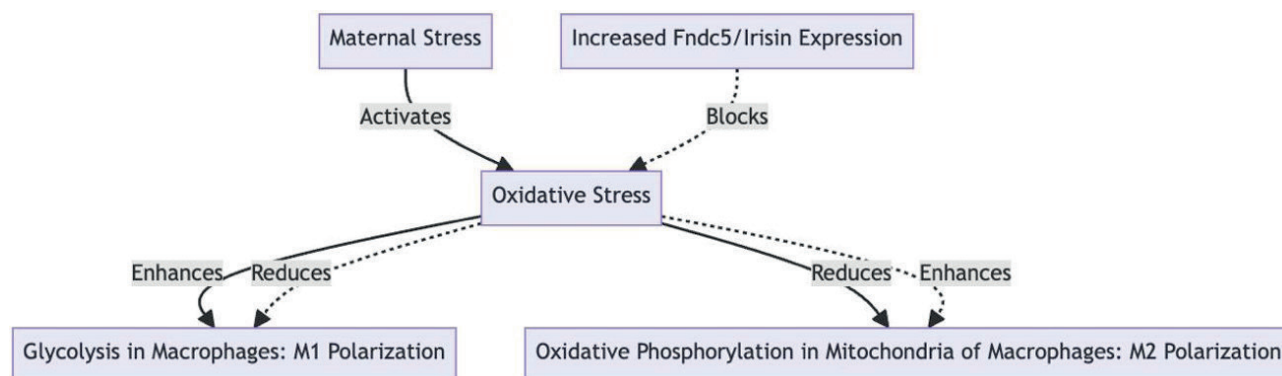Study conception and design: KKB and AB; data collection: KKB, ANB, MHD, and SNI; analysis and



**Figure 3.** Predicted pathway depicting the potential mechanisms underlying M1/M2 macrophage balance disruption in the gastric mucosa following maternal stress

interpretation of results: KKB, ANB and AB; draft manuscript preparation: KKB, ANB and AB. All authors reviewed the results and approved the final version of the manuscript.

## Ethical approval

The study was approved by the Clinical Research Ethics Committee of Nesa Experimental Animals Laboratory (Protocol no. 016, 02 August 2023).

## Funding

## Conflict of interest

The authors declare that there is no conflict of interest.

~~∞◯ REFERENCES ◯∞~~

[1] Caso J, Leza J, Menchen L. The Effects of Physical and Psychological Stress on the Gastrointestinal Tract: Lessons from Animal Models. Curr Mol Med. 2008;8(4):299–312.

[2] Jeličić L, Veselinović A, Ćirović M, Jakovljević V, Raičević S, Subotić M. Maternal Distress during Pregnancy and the Postpartum Period: Underlying Mechanisms and Child's Developmental Outcomes—A Narrative Review. Int J Mol Sci. 2022;23(22):13932.

[3] Nishigawa T, Nagamachi S, Ikeda H. Restraint stress in lactating mice alters the levels of sulfur-containing amino acids in milk. 2018;503–9.

[4] Nishi M. Effects of Early-Life Stress on the Brain and Behaviors: Implications of Early Maternal Separation in Rodents. Int J Mol Sci. 2020;21(19).

[5] Cui Y, Cao K, Lin H, Cui S, Shen C, Wen W, et al. Early-Life Stress Induces Depression-Like Behavior and Synaptic-Plasticity Changes in a Maternal Separation Rat Model: Gender Difference and Metabolomics Study. Front Pharmacol. 2020;11(February):1–13.

[6] Gapp K, Soldado-Magraner S, Alvarez-Sánchez M, Bohacek J, Vernaz G, Shu H, et al. Early life stress in fathers improves behavioural flexibility in their offspring. Nat Commun. 2014;5.

[7] Yisireyili M, Alimujiang A, Aili A, Li Y, Yisireyili S, Abudureyimu K. Chronic Restraint Stress Induces Gastric Mucosal In fl ammation with Enhanced Oxidative Stress in a Murine Model. 2020;383–93.

[8] Zheng J, Dobner A, Babygirija R, Ludwig K, Takahashi T. Effects of repeated restraint stress on gastric motility in rats. Am J Physiol Regul Integr Comp Physiol. 2009;296(5):1358–65.

[9] Prussin C, Scott GD, Fryer AD, Schroeder S, Masterson JC, Fillon S, et al. Eosinophil Cell-Cell Communication. Vol. 5, Eosinophils in Health and Disease. 2013. 329–390 p.

[10] Li X, Zhang C, Gong T, Ni X, Li J 'e, Zhan D, et al. A time-resolved multi-omic atlas of the developing mouse stomach. [cited 2023 Mar 6]; Available from: www.nature.com/naturecommunications

[11] Hafen BB, Burns B. Physiology, Smooth Muscle. StatPearls. 2019.

[12] Cipriani G, Pullapantula S. Macrophages in the Smooth Muscle Layers of the Gastrointestinal Tract. Intech. 2016;225–40.

[13] Hume DA, Loutit JF, Gordon S. The mononuclear phagocyte system of the mouse defined by immunohistochemical localization of antigen f4/80 : macrophages of bone and associated connective tissue don , 1981) and is restricted to this cell lineage in major lymphoid and non-lymphoid. J Cell Sci. 1984;194:189–94.

[14] Lee SH, Starkey PM, Gordon S. Quantitative analysis of total macrophage content in adult mouse tissues. Immunochemical studies with monoclonal antibody F4/80. J Exp Med. 1985;161(3):475-89.

[15] Cipriani G, Gibbons SJ, Kashyap PC, Farrugia G. Intrinsic Gastrointestinal Macrophages: Their Phenotype and Role in Gastrointestinal Motility. Cell Mol Gastroenterol Hepatol. 2016;2(2):120-130.e1.

[16] Mönnikes H, Tebbe JJ, Hildebrandt M, Arck P, Osmanoglou E, Rose M, Klapp B, Wiedenmann B HMI. Role of Stress in Functional. 2001;201–11.

[17] West C, Wu RY, Wong A, Stanisz AM, Yan R, Min KK, et al. Lactobacillus rhamnosus strain JB-1 reverses restraint stress-induced gut dysmotility. Neurogastroenterology and Motility. 2017;29(1):1–11.

[18] Konturek PC, Brzozowski T, Konturek SJ. Stress and the gut: pathophysiology, clinical consequences, diagnostic approach and treatment options. J Physiol Pharmacol. 2011;62(6):591-9.

[19] Norris DO, Carr JA. Chemical Regulation of Feeding, Digestion and Metabolism. Vertebrate Endocrinology. 2013 Jan 1;443–81.

[20] Zhang Y, Zhao L, Gao H, Zhai J, Song Y. Potential role of irisin in digestive system diseases. Vol. 166, Biomedicine and Pharmacotherapy. 2023.

[21] Yano N, Zhao YT, Zhao TC. The Physiological Role of Irisin in the Regulation of Muscle Glucose Homeostasis. Endocrines. 2021;2(3).

[22] Pizzino G, Irrera N, Cucinotta M, Pallio G, Mannino F, Arcoraci V, et al. Oxidative Stress: Harms and Benefits for Human Health. Vol. 2017, Oxidative Medicine and Cellular Longevity. 2017.

[23] Ge L, Liu S, Li S, Yang J, Hu G, Xu C, et al. Psychological stress in inflammatory bowel disease: Psychoneuroimmunological insights into bidirectional gut–brain communications. Vol. 13, Frontiers in Immunology. 2022.

[24] Huh JY, Mougios V, Kabasakalis A, Fatouros I, Siopi A, Douroudos II, et al. Exercise-induced irisin secretion is independent of age or fitness level and increased irisin may directly modulate muscle metabolism through AMPK activation. Journal of Clinical Endocrinology and Metabolism. 2014;99(11).

[25] Pekkala S, Wiklund PK, Hulmi JJ, Ahtiainen JP, Horttanainen M, Pöllänen E, et al. Are skeletal muscle FNDC5 gene expression and irisin release regulated by exercise and related to health? Journal of Physiology. 2013;591(21).

[26] Gapp K, Bohacek J, Grossmann J, Brunner AM, Manuella F, Nanni P, et al. Potential of environmental enrichment to prevent transgenerational effects of paternal trauma. Neuropsychopharmacology. 2016;41(11):2749–58.

[27] Franklin TB, Linder N, Russig H, Thöny B, Mansuy IM. Influence of early stress on social abilities and serotonergic functions across generations in mice. PLoS One. 2011;6(7):1–7.

[28] Weiss IC, Franklin TB, Vizi S, Mansuy IM. Inheritable effect of unpredictable maternal separation on behavioral responses in mice. Front Behav Neurosci. 2011;5(February):1–12.

[29] Ni R, Jiang L, Zhang C, Liu M, Luo Y, Hu Z, et al. Biologic Mechanisms of Macrophage Phenotypes Responding to Infection and the Novel Therapies to Moderate Inflammation. Vol. 24, International Journal of Molecular Sciences. 2023.

[30] Patergnani S, Bouhamida E, Leo S, Pinton P, Rimessi A. Mitochondrial oxidative stress and "mito-inflammation": Actors in the diseases. Vol. 9, Biomedicines. 2021.

[31] Ma K, Chen G, Li W, Kepp O, Zhu Y, Chen Q. Mitophagy, Mitochondrial Homeostasis, and Cell Fate. Front Cell Dev Biol. 2020 Jun 24;8:467.

[32] Meng L, Lu C, Wu B, Lan C, Mo L, Chen C, et al. Taurine Antagonizes Macrophages M1 Polarization by Mitophagy-Glycolysis Switch Blockage via Dragging SAM-PP2Ac Transmethylation. Front Immunol. 2021;12.

[33] Choi KM, Kashyap PC, Dutta N, Stoltz GJ, Ordog T, Shea Donohue T, et al. CD206-Positive M2 Macrophages That Express Heme Oxygenase-1 Protect Against Diabetic Gastroparesis in Mice. Gastroenterology. 2010;138(7).

[34] Qing J, Zhang Z, Novák P, Zhao G, Yin K. Mitochondrial metabolism in regulating macrophage polarization: An emerging regulator of metabolic inflammatory diseases. Acta Biochim Biophys Sin (Shanghai). 2020;52(9):917–26.

[35] Kyoung Moo Choi, Purna C. Kashyap, Nirjhar Dutta, Gary J. Stoltz, Tamas Ordog, Terez Shea Donohue, Anthony J. Bauer, David R. Linden, Joseph H. Szurszewski, Simon J. Gibbons and GF. CD206-positive M2 macrophages that express heme oxygenase-1 protect against diabetic gastroparesis in mice. NIH public acess. 2012;23(1):1–7.

[36] Meng L, Lu C, Wu B, Lan C, Mo L. Taurine Antagonizes Macrophages M1 Polarization by Mitophagy-Glycolysis Switch Blockage via Dragging SAM-PP2Ac Transmethylation. 2021;12(April):1–17.

[37] Zambon AC, McDearmon EL, Salomonis N, Vranizan KM, Johansen KL, Adey D, et al. Time- and exercise-dependent gene regulation in human skeletal muscle. Genome Biol [Internet]. 2003 [cited 2021 Jan 31];4(10):R61. Available from: /pmc/articles/PMC328450/?report=abstract

[38] Picard M, McEwen BS, Epel ES, Sandi C. An energetic view of stress: Focus on mitochondria. Front Neuroendocrinol [Internet]. 2018 Apr 1 [cited 2022 Sep 29];49:72. Available from: /pmc/articles/PMC5964020/

[39] Lebleu VS, O'Connell JT, Gonzalez Herrera KN, Wikman H, Pantel K, Haigis MC, et al. PGC-1α mediates mitochondrial biogenesis and oxidative phosphorylation in cancer cells to promote metastasis. Nat Cell Biol [Internet]. 2014 Oct 1 [cited 2022 Sep 29];16(10):992–1003. Available from: https://pubmed.ncbi.nlm.nih.gov/25241037/

[40] Hellhammer DH, Wüst S, Kudielka BM. Salivary cortisol as a biomarker in stress research. Psychoneuroendocrinology. 2009;34(2).

[41] Wilski M, Brola W, Koper M, Gabryelski J, Łuniewska M, Fudala M, et al. Relationship between physical activity and coping with stress in people with multiple sclerosis: A moderated mediation model with self-efficacy and disability level as variables. International Journal of Clinical and Health Psychology. 2024;24(1).

[42] Haren MT, Siddiqui AM, Armbrecht HJ, Kevorkian RT, Kim MJ, Haas MJ, et al. Testosterone modulates gene expression pathways regulating nutrient accumulation, glucose metabolism and protein turnover in mouse skeletal muscle. Int J Androl. 2011;34(1).

[43] Kamenov Z, Assyov Y, Angelova P, Gateva A, Tsakova A. Irisin and Testosterone in Men with Metabolic Syndrome. Horm Metab Res [Internet]. 2017 Oct 1 [cited 2024 Jan 12];49(10):755–9. Available from: https://pubmed.ncbi.nlm.nih.gov/28759938/

[44] English S, Wright I, Ashburn V, Ford G, Caramaschi D. Prenatal anxiety, breastfeeding and child growth and puberty: linking evolutionary models with human cohort studies. Ann Hum Biol. 2020;47(2).

[45] Tyborowska A, Volman I, Niermann HCM, Pouwels JL, Smeekens S, Cillessen AHN, et al. Early-life and pubertal stress differentially modulate grey matter development in human adolescents. Sci Rep. 2018;8(1).

[46] Duke SA, Balzer BWR, Steinbeck KS. Testosterone and its effects on human male adolescent mood and behavior: A systematic review. Vol. 55, Journal of Adolescent Health. 2014.

acta medica

# Investigating the potential impact of ELF3-associated SNPs on chondrocyte inflammation

Beren Karaosmanoğlu[1]
ORCID: 0000-0001-5564-4813

Büşra Aydın[2]
ORCID: 0000-0003-3922-8953

Gözde İmren[1,2]
ORCID: 0000-0002-2556-0421

Erdal Sağ[3]
ORCID: 0000-0002-6542-2656

Ekim Z. Taşkıran[1,2]
ORCID: 0000-0001-6040-6625

[1] Department of Medical Genetics, Faculty of Medicine, Hacettepe University, Ankara, Türkiye

[2] Department of Medical and Surgical Research, Institute of Health Sciences, Hacettepe University, Ankara, Türkiye

[3] Department of Pediatric Rheumatology, Faculty of Medicine, Hacettepe University, Ankara, Türkiye

Corresponding Author: Beren Karaosmanoğlu
E-mail: berenkaraosmanoglu@gmail.com

~∞◎ A B S T R A C T ◎∞~

Objective: Chondrocyte inflammation is a critical factor in degenerative joint diseases, such as osteoarthritis (OA), significantly impairing quality of life through chronic pain and limited mobility. Genetic predisposition is recognized as a critical factor in the progression of chondrocyte inflammation and OA, with particular focus on the role of genetic variants in the expression and regulation of inflammatory mediators. This study aimed to obtain information about the potential roles of a few genes containing ELF3-associated SNPs in the pathogenesis of chondrocyte inflammation.

Materials and Methods: GVAT Database was used to select top candidate SNPs associated with ELF3, a cardinal transcription factor in chondrocyte inflammation. Inflammation was induced by IL-1β treatment in differentiated chondrocytes to analyze gene expression patterns. Transcriptome analysis was done by RNA sequencing.

Results: The most important SNPs that could potentially affect the binding affinity of ELF3 transcription factor were analyzed. As a result of the analysis, 52% of ELF3-associated SNPs were found in protein-coding regions, 40% in gene-free intergenic regions, and 8% in non-coding RNA sequences. Some of these SNPs are located in regulatory regions (enhancers). A significant increase in expression levels in the ELF3 gene was detected after IL-1β administration, indicating that IL-1β promotes the activity of this transcription factor. mRNA expressions of TLN2, BABAM2, PEPD, and NUDT5 were also increased after IL-1β stimulation.

Conclusion: The presence of ELF3-associated SNPs in the enhancer sequences of TLN2 and BABAM2 genes, in addition to the increased expression of these two genes upon IL-1β stimulation, suggested that TLN2 and BABAM2 genes may be associated with the severity of chondrocyte inflammation and OA.

Keywords: osteoarthritis, ELF3, TLN2, chondrocyte inflammation, IL-1β.

## INTRODUCTION

Osteoarthritis (OA) is one of the most common types of arthritis, affecting millions of people worldwide and significantly reducing quality of life [1]. Typically characterized by joint pain, swelling and reduced mobility, the condition develops as a result of a combination of genetic predisposition, environmental factors and lifestyle [2, 3]. The pathogenesis of OA is characterized by cartilage destruction and degenerative changes in joint structures, the understanding of which is critical in the development of treatment modalities for this disease. Genetic predisposition plays a significant role in the inflammatory processes involved in the progression of OA. While environmental factors and lifestyle have an impact on the development of the disease, genetic predisposition can be decisive in factors such as disease severity, rate of progression and response to treatment.

The ELF3 (E74 Like ETS Transcription Factor 3) gene is a member of the ETS (E26 transformation-specific) transcription factor family and is commonly expressed in epithelial cells [4]. This gene helps regulate critical biological processes such as cell growth, differentiation and renewal [5, 6]. ELF3 binds to various target genes that modulate intracellular signaling pathways and regulate gene expression [7, 8]. It plays an important role in the modulation of inflammation and immune response, and can influence the course of disease by regulating the expression of various cytokines and inflammatory mediators [9]. Both in vitro and in vivo settings, ELF3 was shown to be important specifically in chronic arthritis in different studies [9, 10]. Therefore, a more detailed understanding of the molecular mechanisms of ELF3 may open new avenues for the development of therapeutic strategies for various rheumatologic diseases. Furthermore, studying the effects of genetic variants of ELF3 on the disease process may be critical in the development of more personalized therapies for these diseases.

ELF3, a pivotal regulator of inflammatory and immune responses, emerges as a candidate of interest due to its role in epithelial cell function and potential influence on chondrocyte behavior. The potential role of ELF3-associated Single Nucleotide Polymorphisms (SNPs) in chondrocyte inflammation has not been thoroughly investigated. Exploring these variants could offer new perspectives and aid in developing targeted therapeutic strategies. This highlights the need for continued research on how these SNPs might modulate disease processes through transcriptional regulation. This gap in knowledge presents a critical barrier to the development of targeted therapeutic strategies and underscores the need for research focused on genetic variants that could modulate disease processes through transcriptional regulation. Our study leverages in-silico methods coupled with cellular models to dissect the relationship between ELF3-associated SNPs and chondrocyte inflammation. The existing literature has provided important insights into the complex pathogenesis of OA and the role of genetic factors in the disease process. However, the potential effects of SNPs linked to specific transcription factors such as ELF3 on disease mechanisms are still poorly understood. GVATdb (Genetic Variants Allelic Transcription Factor Binding Database) was used to select top candidate SNPs associated with ELF3. SNPs that alter the binding sites of ELF3 may affect the expression of related genes and consequently influence the severity of chondrocyte inflammation. This study aimed to obtain information about the potential roles of a few genes containing ELF3-associated SNPs in the pathogenesis of chondrocyte inflammation.

## MATERIALS AND METHODS

### Bioinformatic Analysis

ELF3 associated SNPs were identified using the GVATdb, which contains the results of SNP-SELEX (Single Nucleotide Polymorphism Evaluation by Exponential Enrichment with Systematic Evolution of Ligands by Exponential Enrichment), ultra-high-throughput multiprotein-DNA binding experiments to assess the binding affinity of 270 human transcription factors to selected variants which provides comprehensive information on genomic locations, allelic frequencies and their potential impact on gene expression [11]. The top 25 SNPs were selected according to the lowest p-values indicating significant associations. Detailed data on the specific locations and allelic frequencies of these SNPs were meticulously

compiled in a tabular format to understand their distribution within the structure of the gene and their potential importance.

In order to determine the allele frequencies for selected ELF3-associated SNPs, the most reliable frequency data was obtained from the Genome Aggregation Database (gnomAD), which has a large collection of exome and genome sequencing data. This data repository facilitated the acquisition of Minor Allele Frequencies (MAFs) for most of the SNPs and ensured the robustness of the frequency estimates. However, some SNPs did not have MAF data in gnomAD, which required searching alternative databases. For these cases, the search was expanded as to include other reputable genomic databases, maintaining the integrity of our dataset (1000Genomes data). Genomic position information of SNPs was added to the table according to GRCh38. University of California, Santa Cruz (UCSC) Genome Browser was used in order to identify the SNP locations, in terms of regulatory regions, within the human genome [12]. None of the SNPs detected contained ClinVar entries. Therefore, no information was available in terms of pathogenicity. The JASPAR database was used to examine transcription factor binding sites.

### Cell Culture

Human Bone Marrow Mesenchymal Stem Cells (MSCs) were obtained from ATCC (No: PCS-500-012, Lot: 63208778), cultured in DMEM-LG supplemented with 10%FBS, 1% L-glutamine and 1% Penicillin-Streptomycin in standard culture conditions (37°C with 5% CO2). Passage 3 cells were used for further experiments. Chondrogenesis differentiation was induced with Stem Pro Chondrogenesis Differentiation Kit (Cat. No: A1007101, Thermo Fisher Scientific) for 21 days, according to the manufacturer's instructions. In order to trigger inflammation, on the 10th day of differentiation, cells were treated with 1 ng/ml IL-1β.

### RNA-Sequencing and Data Analysis

Total RNA was isolated with TRIzol (Roche), according to the manufacturer's instructions, and quality control was measured spectrophotometrically (NanoDrop One, Thermo Fisher Scientific). RNA-Seq library was prepared from equal amounts of each RNA by Lexogen SENSE mRNA-Seq Library Prep Kit (Lexogen GmbH) and run was performed on Ion Proton Semiconductor Sequencing Platform

(Thermo Fisher Scientific). The raw data were analyzed with the Transcript Per Million (TPM) method by RaNA-Seq software [13]. TPM values were calculated after read numbers mapped to each gene. Differential expression analysis was performed with DESeqR package. Genes with an adjusted p value lower than 0.05 were assigned as differentially expressed. The expression values were visualized with GraphPad Prism (v8.0) (www.graphpad.com/scientific-software/prism/).

## RESULTS

### Analysis of ELF3-Associated SNPs and Their Implications for Gene Regulation

The most significant SNPs that potentially affect the binding affinity of the ELF3 transcription factor were selected for further analysis in this study (Table 1). The distribution of single nucleotide polymorphisms (SNPs) associated with the ELF3 gene examined in this study is summarized in Figure 1. While 52% (n=13) of ELF3-associated SNPs were found in protein-coding regions, 40% (n=10) were localized in intergenic regions (regions containing no genes) and 8% (n=2) in non-coding
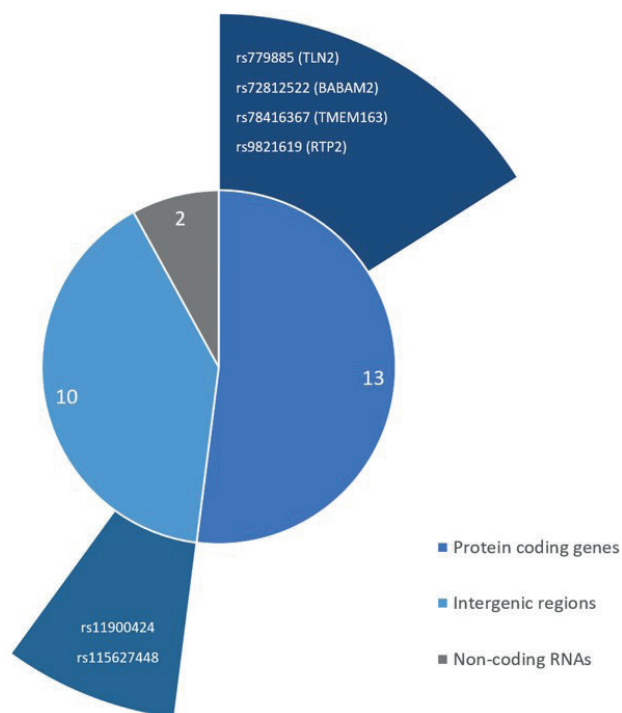


**Figure 1.** Graph for SNP numbers that associated with ELF3. Protein coding genes, Intergenic regions and non-coding RNA targets are given. Critical SNPs within the regulatory regions in each group are shown in the outer ring. rs: reference SNP number

**Table 1.** All SNPs associated with ELF3, analyzed with GVAT database, that could be significant importance for rheumatologic diseases and their details. rs ID: reference SNP number, ref: reference base, alt: alternative base.

| rs ID | Genomic region (GRCh38) | ref | alt | p-value | Global MAF (GnomAD) | Gene | Regulatory region |
|---|---|---|---|---|---|---|---|
| rs4745991 | chr10:69523734 | C | T | 0 | C=0.449334 | TSPAN15 (intronic) | None |
| rs562897 | chr10:78770483 | G | A | 0 | A=0.400848 | Intergenic | None |
| rs10404460 | chr19:33469490 | T | C | 0 | C=0.145462 | PEPD (intronic) | None |
| rs73279624 | chr20:44449217 | G | A | 0 | A=0.021152 | LINC01430 (intronic) | None |
| rs13318430 | chr3:11908851 | T | C | 0 | C=0.242005 | Intergenic | None |
| rs62262911 | chr3:123805176 | G | A | 0 | A=0.038679 | MYLK (intronic) | None |
| rs7068603 | chr10:79012784 | C | T | 0.00002 | T=0.193161* | ZMIZ1-AS1 (intronic) | None |
| rs11900424 | chr2:5849827 | G | C | 0.00002 | C=0.216115* | Intergenic | EH38E1969349 distal enhancer-like signature |
| rs7017487 | chr8:94910524 | C | T | 0.00002 | C=0.395885 | NDUFAF6 (intronic) | None |
| rs115627448 | chr9:21674924 | T | C | 0.00002 | C=0.027165 | Intergenic | EH38E2687073 distal enhancer-like signature |
| rs779885 | chr15:62470173 | C | T | 0.00003 | C=0.394861 | TLN2 (intronic) | EH38E1768118 distal enhancer-like signature |
| rs28549270 | chr15:62528241 | G | C | 0.00003 | C=0.015287 | TLN2 (intronic) | None |
| rs72812522 | chr2:27966013 | T | C | 0.00003 | C=0.028585 | BABAM2 (intronic) | EH38E1983168 distal enhancer-like signature |
| rs9471049 | chr6:39293745 | T | C | 0.00003 | C=0.012014 | Intergenic | None |
| rs10977092 | chr9:8432445 | T | G | 0.00005 | G=0.279858 | PTPRD (intronic) | None |
| rs10842946 | chr12:27592997 | T | A | 0.00008 | A=0.269119 | PPFIBP1 (intronic) | None |
| rs78416367 | chr2:134468413 | T | C | 0.00008 | C=0.031631 | TMEM163 (intronic) | EH38E2034674 distal enhancer-like signature |
| rs3758379 | chr10:12194774 | G | A | 0.0001 | A=0.092262 | NUDT5 (intronic) | None |
| rs9821619 | chr3:187703248 | G | A | 0.00012 | A=0.389633 | RTP2 (intronic) | EH38E2266715 proximal enhancer-like signature |
| rs10121752 | chr9:81472715 | C | T | 0.00012 | T=0.036575 | Intergenic | None |
| rs16921782 | chr9:4670573 | C | T | 0.00013 | T=0.460724 | Intergenic | None |
| rs7641618 | chr3:186537260 | A | G | 0.00017 | G=0.049333 | Intergenic | None |
| rs617523 | chr2:160748153 | C | T | 0.00021 | T=0.024147 | Intergenic | None |
| rs116004702 | chr11:93042150 | T | G | 0.00025 | G=0.015590 | Intergenic | None |
| rs6749329 | chr2:134716795 | T | C | 0.00031 | C=0.207290 | TMEM163 (intronic) | None |

* The MAF scores for these SNPs are presented from the 1000Genomes data.

RNA sequences. Among the 25 SNPs, 6 were located in regulatory sequences (enhancers); 4 of them are located in protein coding genes (rs779885, rs72812522, rs78416367, and rs9821619), other 2 are in intergenic regions (rs11900424 and rs115627448) (Figure 1).

Considering the possibility that SNPs located in the introns of protein-coding genes may lead to alterations in the expression of these genes, this group was first analyzed. There were two SNPs associated with both TLN2 (rs779885 and rs28549270) and TMEM163 (rs78416367 and rs6749329). Moreover, rs779885 was localized in a

regulatory region within the TLN2 gene. This region, referred to as 'EH38E1768118 distal enhancer-like signature' in the UCSC, was predicted to regulate the expression of the TLN2 gene. A similar situation was also observed for rs78416367 in the TMEM163 gene. This genomic region had an 'EH38E2034674 distal enhancer-like signature' according to the UCSC database. Two different SNPs in the introns of RTP2 (rs9821619) and BABAM2 (rs72812522) were also located within the regulatory sequences (Table). Among the 10 SNPs located in intergenic regions, only 2 were in regulatory sequences (rs11900424 and rs115627448). The two SNPs were within the intronic sequences of two different non-

coding RNAs (LINC01430 and ZMIZ1-AS1) and were not associated with regulatory regions.

**Impact of IL-1β Stimulation on Gene Expression**

The transcriptomic dataset in which IL-1β treated chondrocytes was used to determine whether the candidate genes (containing ELF3-associated SNPs) were associated with the chondrocyte inflammation. The results of transcriptomic analysis revealed the effects of IL-1β on gene expression compared to the control group. Significant increases in ELF3 expression was observed after IL-1β administration compared to the control group. This, in line with the literature, suggests that ELF3 plays an increasing role in inflammatory processes and that IL-1β promotes the transcriptional activity of this transcription factor [14]. In addition to ELF3, the demonstration of increased expression of MMP13 is also an important finding for the accuracy of the established inflammatory cell model. Similarly, TLN2, BABAM2, PEPD and NUDT5 genes have also increased mRNA expression after IL-1β stimulation (Figure 2). There was no change

in expression in the MYLK gene, while there was a decrease in expression in the PPFIBP1 gene, and no expression of other protein-coding genes and non-coding RNAs was detected in chondrocytes.

## DISCUSSION

This study highlights the significant role of ELF3 and its associated SNPs in chondrocyte inflammation and OA pathogenesis through in-silico analysis and expression assays. In particular, SNPs in regulatory sequences may be important for ELF3's activity as a transcription factor and its regulatory functions on target genes. Our findings suggest that these SNPs may affect ELF3 activity on these target genes and consequently the course of OA. These effects were also seen in animal studies as well, where ELF3 knockout mice had attenuated cartilage loss proving its pro-catabolic role in cartilage degradation and re-modelling [10, 15]. Studying the effects of ELF3 gene and its associated SNPs on OA is considered as an important step in this field.
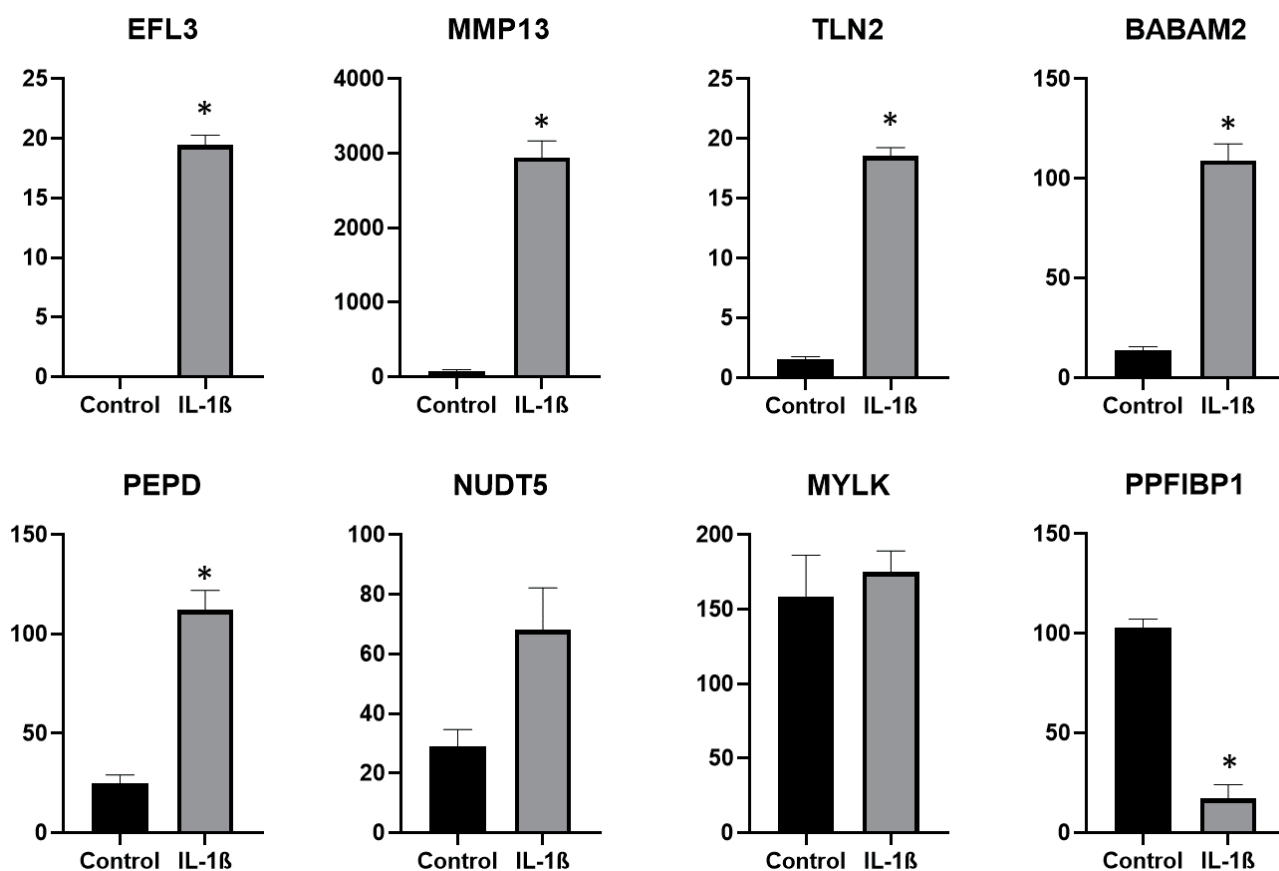


**Figure 2.** mRNA expression levels of the genes in IL-1β Treated Chondrocytes. The y-axis represents the expression levels measured in Transcripts Per Million (TPM). Based on TPM values, significant increases were observed in the expression of ELF3, TLN2, BABAM2 and PEPD genes after IL-1β treatment (*: $p < 0.05$). While no significant change was observed in MYLK and NUDT5 genes, a significant decrease was observed in PPFIBP1 gene

With this aim, this study was designed, and the results revealed an important link between ELF3-associated SNPs and the genomic background of OA. These findings underscore the need to explore specific SNPs and their regulatory roles in gene expression.

Among the SNPs analyzed in this study, rs779885 (TLN2), rs72812522 (BABAM2), rs78416367 (TMEM163), and rs9821619 (RTP2) SNPs, which are located in protein coding regions and regulatory regions, draw attention. In our opinion, the candidate genes containing ELF3-associated SNPs whose expression is increased in the chondrocyte inflammation model are of critical importance. The increased expression of TLN2 and BABAM2 in the chondrocyte inflammation model, which is noteworthy due to SNPs in their enhancer regions, suggests that these genes may be related to the pathogenesis and severity of OA (Figure 3). These SNPs may have important roles in regulating gene expression and cellular functions. Figure 3 illustrates the binding motifs of ELF3 and the locations of

critical SNPs within the TLN2 and BABAM2 genes, highlighting the potential regulatory impact of these SNPs on ELF3 binding.

In addition to TLN2 and BABAM2, the 'EH38E2034674 distal enhancer-like signature' region where rs78416367 is located in the TMEM163 gene indicates a regulatory effect on the transcriptional activity of the gene. The rs11900424 and rs115627448 SNPs in intergenic regions are localized within regulatory sequences and may play a role in regulating gene expression and modulating inflammatory responses. The presence of these specific SNPs strengthens the hypothesis that they may modulate the functionality of ELF3 in processes such as cellular adhesion, signal transduction and inflammation, and thereby serve as critical factors in the pathogenesis of OA.

Given the importance of SNPs in regulatory regions, those located in enhancer sequences can affect ELF3 activity significantly. The 'enhancer-like signature' findings in the UCSC database indicate that the SNPs analyzed are located in enhancer
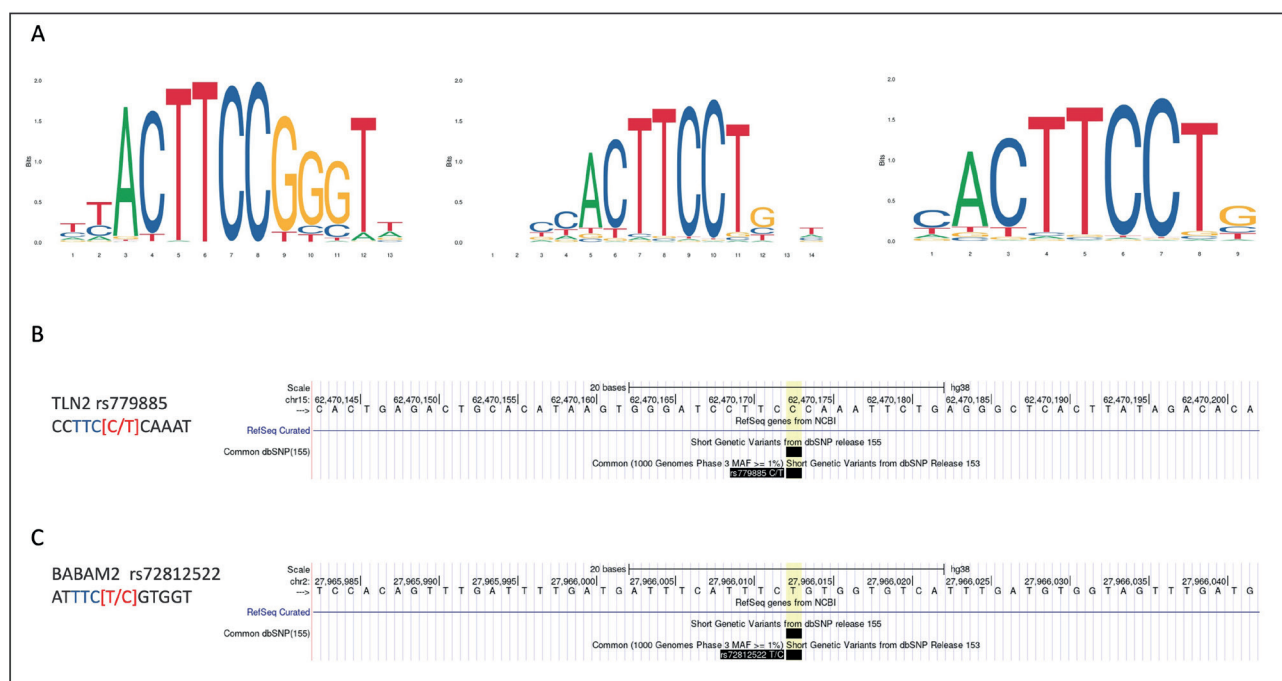


**Figure 3.** ELF3 Binding Motifs and SNPs Locations. A. Position weight matrix of ELF3 binding site motifs. The sequence logos represent the binding motifs of ELF3, illustrating the probability of each nucleotide at specific positions within the binding site. These motifs were obtained from the JASPAR database, highlighting the critical nucleotides that are essential for ELF3 binding. The height of each letter corresponds to the frequency of the nucleotide at that position, with higher letters indicating a higher likelihood of being involved in ELF3 binding. B. The sequence surrounding the SNP rs779885 within the TLN2 gene. The sequence is shown with the critical bases of the ELF3 binding motif highlighted in blue (TTC) and the alternative alleles (C/T) at the SNP location are indicated in red. This SNP falls within the TTCC core motif of ELF3. C. The sequence surrounding the SNP rs72812522 within the BABAM2 gene. Similar to TLN2, the sequence is shown with the essential bases of the ELF3 binding motif highlighted in blue (TTC) and the alternative alleles (T/C) at the SNP location are indicated in red. This SNP falls within the TTCC core motif of ELF3

regions that contribute to genetic regulation. These regions can function as binding sites of transcription factors and play critical roles in the remote regulation of gene expression. In particular, concerning the activity of a transcription factor such as ELF3, which plays central roles in inflammation and immune response, the presence of these enhancer-like sequences may indicate a potential influence in the modulation of the expression of target genes and thus, cellular responses. Therefore, we hypothesized that the SNPs identified in this study and thought to be associated with ELF3 are important regulatory factors in the pathogenesis of rheumatologic diseases.

Potential interactions between ELF3 and TLN2 genes in the pathogenesis of OA may contribute to a better understanding of these diseases and the development of new therapeutic approaches. Functional studies are required to elucidate the effects of intronic SNPs such as rs779885 and rs28549270 on transcriptional or post-transcriptional mechanisms mediated by ELF3. These studies can determine what role these SNPs play in ELF3-responsive gene expression. In this context, the discovery of the role played by SNPs in the TLN2 gene in OA thought to be associated with ELF3 will deepen the understanding of genetic mechanisms and novel targetable molecular pathways. Given the roles of Talin-2 in cellular adhesion and signal transduction, these SNPs may be involved in the modulation of pathways regulated by ELF3. When the role of ELF3's contribution in the inflammatory response and immune response is considered, this may indirectly influence the effects of SNPs in the TLN2 gene on cell-matrix interactions and migration of immune cells. Impairments in the function of TLN2 may contribute to cartilage degradation and OA development by weakening the interactions of chondrocytes with the matrix. In addition, TLN2 gene is also draw attention as an OA related SNP in a GWAS study [16]. TMEM163, a member of the Zinc Efflux Transporter Family, may also be associated with the severity of the inflammatory response, suggesting that SNPs in this gene may play a role in OA. TSPAN15, which has an ELF3-related rs4745991 SNP in its intronic region, is the subunit of the ADAM10 complex and is directly associated with inflammation. Given the capacity of ELF3 to regulate the expression of this gene, it is conceivable that this SNP could affect gene expression levels and could have indirect effects on cellular adhesion and peptide processing mechanisms. Another SNP (rs7017487), located in mitochondrial complex I assembly factor NDUFAF6, also related to ELF3 binding activity. The correlation of this SNP with ELF3 activity may elucidate the complex interplay between genetic predisposition and the emergence of OA. Alterations in mitochondrial function may affect cellular metabolism and influence the chronic inflammation characteristic of these diseases [17].

While some genes such as BABAM2, PTPRD, PPFIBP1, NUDT5, and RTP1 currently have no known relationship with OA, their critical cellular roles warrant further investigation. However, BABAM2 and NUDT5 have roles in DNA damage and repair [18, 19], PTPRD and PPFIBP1 are involved in cancer development [20, 21]. According to our current knowledge, although these genes are not directly associated with OA, should kept in mind due to their critical roles in critical cellular processes. The role of BABAM2 in DNA damage response and repair is crucial in maintaining the genomic stability of chondrocytes. Dysfunctions in DNA repair mechanisms may contribute to OA's pathogenesis by accelerating cartilage tissue's degradation, leading to cellular senescence and apoptosis in chondrocytes. These functions of BABAM2 may become more prominent especially when cartilage tissue is under mechanical stress.

Each of the SNPs may alter the effects of ELF3 on gene expression, which in turn may affect cellular pathways associated with the pathogenesis of OA. Understanding these pathways and genetic interactions could help discover potential targets for the treatment of OA. Furthermore, these SNPs may allow for a better understanding of the genetic networks regulated by ELF3 and more detailed exploration of the molecular mechanisms of OA.

It is also important to note the limitations of the study. Although the GVAT database provides a large SNP data, the functional consequences of these SNPs on ELF3 activity and subsequent gene regulation should be experimentally validated. In addition, the impact of environmental factors on gene expression was beyond the scope of this study and warrants further investigation in the future. By addressing these gaps, future research can further our understanding of ELF3-mediated pathways and their therapeutic potential.

In conclusion, our findings expand the understanding the ELF3's role in OA and set the stage for future research to explore the therapeutic potential of targeting ELF3-mediated pathways. Such research could ultimately lead to novel treatments that more effectively address the genetic underpinnings of these complex conditions. The findings of the study suggest that the interaction between ELF3 and specific SNPs may be helpful in predicting disease course and response to treatment to facilitate more personalized treatment plans based on individual genetic background.

## Author contribution

Study conception and design: BK, ES, and EZT; data collection: BK, BA, GI, and EZT; analysis and interpretation of results: BK, GI, ES, and EZT; draft manuscript preparation: BK and EZT. All authors reviewed the results and approved the final version of the manuscript.

## Ethical approval

This study did not require ethical approval as it exclusively utilized publicly available data and commercially purchased cell lines.

## Funding

The authors declare that the study received no funding.

## Conflict of interest

The authors declare that there is no conflict of interest.

## ～ REFERENCES ～

[1] Glyn-Jones S, Palmer AJ, Agricola R, et al. Osteoarthritis. Lancet 2015; 25;386(9991): 376-87. https://doi.org/10.1016/S0140-6736(14)60802-3

[2] Brandt KD, Dieppe P, Radin E. Etiopathogenesis of osteoarthritis. Med Clin North Am 2009; 93(1): 1-24. https://doi.org/10.1016/j.mcna.2008.08.009

[3] Sinusas K. Osteoarthritis: diagnosis and treatment. Am Fam Physician 2012; 85(1): 49-56.

[4] Subbalakshmi AR, Sahoo S, Manjunatha P, et al. The ELF3 transcription factor is associated with an epithelial phenotype and represses epithelial-mesenchymal transition. J Biol Eng 2023; 17(1): 17. https://doi.org/10.1186/s13036-023-00333-z

[5] Sengez B, Aygün I, Shehwana H, et al. The Transcription Factor Elf3 Is Essential for a Successful Mesenchymal to Epithelial Transition. Cells 2019; 8(8): 858. https://doi.org/10.3390/cells8080858

[6] Wang H, Yu Z, Huo S, et al. Overexpression of ELF3 facilitates cell growth and metastasis through PI3K/Akt and ERK signaling pathways in non-small cell lung cancer. Int J Biochem Cell Biol 2018; 94: 98-106. https://doi.org/10.1016/j.biocel.2017.12.002

[7] Kopp JL, Wilder PJ, Desler M, et al. Different domains of the transcription factor ELF3 are required in a promoter-specific manner and multiple domains control its binding to DNA. J Biol Chem 2007; 282(5): 3027-3041. https://doi.org/10.1074/jbc.M609907200

[8] Otero M, Peng H, Hachem KE, et al. ELF3 modulates type II collagen gene (COL2A1) transcription in chondrocytes by inhibiting SOX9-CBP/p300-driven histone acetyltransferase activity. Connect Tissue Res 2017; 58(1): 15-26. https://doi.org/10.1080/03008207.2016.1200566

[9] Kouri VP, Olkkonen J, Nurmi K, et al. IL-17A and TNF synergistically drive expression of proinflammatory mediators in synovial fibroblasts via IκBζ-dependent induction of ELF3. Rheumatology (Oxford) 2023; 62(2): 872-885. https://doi.org/10.1093/rheumatology/keac385

[10] Wondimu EB, Culley KL, Quinn J, el al. Elf3 Contributes to Cartilage Degradation in vivo in a Surgical Model of Post-Traumatic Osteoarthritis. Sci Rep 2018; 24;8(1): 6438. https://doi.org/10.1038/s41598-018-24695-3

[11] Yan J, Qiu Y, Ribeiro Dos Santos AM, et al. Systematic analysis of binding of transcription factors to noncoding variants. Nature 2021; 591(7848): 147-151. https://doi.org/10.1038/s41586-021-03211-0

[12] Kent WJ, Sugnet CW, Furey TS, et al. The human genome browser at UCSC. Genome Res 2002; 12(6): 996-1006. https://doi.org/10.1101/gr.229102

[13] Prieto C, Barrios D. RaNA-Seq: Interactive RNA-Seq analysis from FASTQ files to functional analysis. Bioinformatics 2019; 15:btz854. https://doi.org/10.1093/bioinformatics/btz854

[14] Peng H, Tan L, Osaki M, et al. ESE-1 is a potent repressor of type II collagen gene (COL2A1) transcription in human chondrocytes. J Cell Physiol 2008; 215(2):562-73. https://doi.org/10.1002/jcp.21338

[15] Otero M, Plumb DA, Tsuchimochi K, et al. E74-like factor 3 (ELF3) impacts on matrix metalloproteinase 13 (MMP13) transcriptional control in articular chondrocytes under proinflammatory stress. J Biol Chem 2012; 287(5): 3559-72. https://doi.org/10.1074/jbc.M111.265744

[16] Boer CG, Hatzikotoulas K, Southam L, et al. Deciphering osteoarthritis genetics across 826,690 individuals from 9 populations. Cell 2021; 184(18): 4784-4818.e17. https://doi.org/10.1016/j.cell.2021.07.038

[17] Dela Cruz CS, Kang MJ. Mitochondrial dysfunction and damage associated molecular patterns (DAMPs) in chronic inflammatory diseases. Mitochondrion 2018; 41: 37-44. https://doi.org/10.1016/j.mito.2017.12.001

[18] Chung CYT, Lo PHY, Lee KKH. Babam2 Regulates Cell Cycle Progression and Pluripotency in Mouse Embryonic Stem Cells as Revealed by Induced DNA Damage. Biomedicines 2020; 10;8(10): 397. https://doi.org/10.3390/biomedicines8100397

[19] Qi H, Grace Wright RH, Beato M, et al. The ADP-ribose hydrolase NUDT5 is important for DNA repair. Cell Rep 2022; 20;41(12): 111866. https://doi.org/10.1016/j.celrep.2022.111866

[20] Shang X, Zhang W, Zhang X, et al. PTPRD/PTPRT mutation as a predictive biomarker of immune checkpoint inhibitors across multiple cancer types. Front Immunol 2022; 29;13: 991091. https://doi.org/10.3389/fimmu.2022.991091

[21] Siemion K, Reszec-Gielazyn J, Kisluk J, et al. What do we know about inflammatory myofibroblastic tumors? - A systematic review. Adv Med Sci 2022; 67(1) :129-138. https://doi.org/10.1016/j.advms.2022.02.002

![acta medica]

ORIGINAL ARTICLE

# Exploring the inhibitory potential of hormone replacement therapy drugs on glutathione transferase P1-1

Yaman Muşdal[1,2]
ORCID: 0000-0003-0999-3179

Bengt Mannervik[2,3]
ORCID: 0000-0002-6416-064X

~∞∞ A B S T R A C T ∞∞~

Aim: Glutathione transferase P1-1 (GST P1-1) plays a crucial role in the human phase II detoxication system and is implicated in drug resistance in certain cancer cells. Analogs of drugs used in Hormone Replacement Therapy (HRT) have been reported to exhibit inhibition of various GSTs. This study aims to investigate the inhibitory potential of several HRT drugs on GST P1-1 for the possible use of counteracting drug resistance and for other therapeutic purposes.

Materials and Methods: GST P1-1 was expressed and then purified in a single step using Nickel Sepharose affinity chromatography. Synthetic drugs that are used in HRT were screened for inhibition of GST P1-1 using 1-chloro-2,4-dinitrobenzene as the substrate. The IC50 value of the most potent compound was calculated and binding location and formation of bonds to GST P1-1 were identified through docking analysis.

Results: Screening the inhibitory effect of eight synthetic estrogenic drugs reveals that estradiol valerate is the most potent inhibitor, showing 72 ± 4% inhibition of GST P1-1. This effect is followed by estradiol cypionate 53 ± 5%, mestranol 39 ± 4%, and estradiol propionate 35 ± 2%. The most potent compound estradiol valerate has an IC50 value of 30 ± 2 μM. According to docking analysis, it binds to the H-site of the enzyme where the residues Phe9, Arg14, Val36, Trp39, Ile105, Tyr109, Pro203, Asn207, and Gln210 were within 5 Å proximity of the ligand. Estradiol valerate forms Pi-alkyl interactions with Phe9 and Val36, as well as an alkyl interaction with Ile104.

Conclusion: Estradiol valerate is a modest inhibitor for hGST P1-1, however it fits in the area of H-site of the enzyme and forms bonds with critical key residues. Understanding its binding site on the enzyme is critical for designing other inhibitors targeting GSTs or possibility for the potential use as a substrate with other GSTs.

Keywords: Glutathione transferase P1-1, synthetic estrogens, enzyme inhibition, cancer, docking analysis.

[1] Department of Pediatric Genetics, Faculty of Medicine, Hacettepe University, Ankara, Turkey

[2] Department of Biochemistry and Biophysics, Stockholm University, Stockholm, Sweden

[3] Department of Chemistry, Scripps Research, La Jolla, CA, USA

Corresponding Author: Yaman Musdal
E-mail: ymusdal@hacettepe.edu.tr

## INTRODUCTION

Glutathione transferases (GSTs; EC 2.5.1.18) is a diverse and essential enzyme family widely distributed across living organisms. They play multifaceted roles, primarily associated with the detoxication of both endogenously and exogenously produced compounds. These enzymes catalyze the conjugation of glutathione (GSH) to electrophilic regions present on hydrophobic molecules, increasing their solubility for elimination from the organisms [1]. Apart from the canonical detoxication functions, human GSTs catalyze isomerization reactions involved in steroid hormone biosynthesis and participate in intracellular transport by binding small ligands such as: bilirubin, steroids, drugs, etc. Moreover, they play a key point in modulating apoptosis through their influence on c-Jun-N-terminal kinase [2-4].

In mammals, seven classes of cytosolic GSTs (alpha, pi, mu, zeta, sigma, omega, and theta) are found, and several of the classes contain multiple isoenzymes [5]. Each GST exhibits unique tissue distribution and substrate specificity, contributing to the body's overall detoxication capacity and other functions. For instance, alpha, mu and pi are involved in detoxication processes, sigma in prostaglandin synthesis, zeta in tyrosine metabolism, omega in oxidative stress response, and theta in the metabolism of various xenobiotics [1,4]. With the advance of database information and utilization of artificial intelligence, it is predicted that the human GST family is more extensive than previously known, with additional members and unknown functions [6]. The enzymes exist in dimeric forms, with each subunit containing an active site composed of two distinct binding sites known as G-site and H-site. The G-site, where GSH binds to specific amino acid residues, is conserved among the GSTs, whereas the residues in the H-site are variable [7].

GST P1-1, also known as GST Pi, is the most extensively studied isoenzyme in humans. Due to its high-level expression in some cancer cells, cause of chemoresistance, and regulatory role in apoptosis, it is of interest in cancer research [8,9]. Consequently, specific and potent inhibitors for GST P1-1 are being pursued by screening large libraries of compounds, including diuretics, antidepressants, antifungals, insecticides, antimalarials, etc [10]. Repurposing of

established drugs is an alternative to the design of novel agents, and the pharmacology and safety of estrogens have been studied extensively. The aim of this study was to evaluate the inhibitory potential of various estrogen derivatives on human GST P1-1. The inhibitory effects of these compounds were screened, the IC50 of the most potent inhibitor was calculated, and the binding residues in the enzyme were identified.

## MATERIALS and METHODS

### Expression and purification of human GST P1-1

The human GST P1-1 gene obtained from a K562 erythroleukemia cDNA library expressing the *GSTP1*A* allele was available in the pKXHP1 plasmid [11]. *Escherichia coli* XL-1 Blue cells were transformed with the plasmid via heat shock and grown on agar plates. A single colony was selected and inoculated in 2YT media, incubated overnight (ON) at 37 °C in a shaking incubator. A new 2TY culture was obtained by addition of 1:1000 of the ON culture, further grown, and induced with isopropyl β-D-thiogalactopyranoside (0.2 mM) when absorbance (OD600) of the culture reached around 0.4. The culture was incubated for an additional 16 hr. Cell pellets obtained by centrifugation (5000 g for 8 min at 4 °C) were resuspended in lysis buffer (10 mM Tris HCl, 1 mM EDTA, 0.2 mM DTT, pH 7.0) supplemented with lysozyme, subjected to sonication (4 cycles of 20 sec), and centrifuged (10000 g, 50 min at 4 °C), resulting in a supernatant fraction [11].

The lysate was applied to a Nickel-Sepharose affinity column (Cytiva), equilibrated with binding/washing buffer (20 mM sodium phosphate, 500 mM NaCl, 20 mM imidazole, pH 7.4), and thoroughly washed. The matrix-bound GST P1-1 underwent elution with buffer (washing buffer including 300 mM imidazole), and dialyzed (10 mM Tris-HCl buffer, pH 7.8, containing 0.2 mM DTT and 1 mM EDTA).

### Enzymatic assay

Enzymatic measurements were performed in quartz cuvettes with the contents 0.1 M phosphate buffer (pH 6.5), 1 mM EDTA, and the substrates 1 mM GSH and 1 mM CDNB (1-chloro-2,4-dinitrobenzene) [12]. The synthetic drugs obtained from MicroSource

Discovery Systems were dissolved in DMSO at 10 mM concentration. The percentage (1% v/v) of solvent present in the assay system has no inhibitory effect on enzyme activity. The inhibitor was added just before CDNB, and initial absorbance change was monitored for 1 min at 340 nm using Shimadzu UV-2501 spectrophotometer.

## Docking analysis

Molecular docking studies were perfomed with Autodock Vina, provided in the Chimera Software [13,14]. The crystal structure of human GST P1-1 (PDB: 6GSS) and the ligand (estradiol valerate) were downloaded from the websites (https://www.rcsb.org/ and https://pubchem.ncbi.nlm.nih.gov/) in pdb and sdf formats, respectively. Water molecules, and ligands were removed from the protein structure. Incomplete side chains, hydrogens, and Gasteiger charges were added using using Dock Prep Tools. Similar preparations were carried out for the ligand including minimization and addition of hydrogen and Gasteiger charges. The entire protein was centered, and docking was executed. Results were visualized and analyzed using UCSF Chimera and Discovery Studio Softwares.

## Statistical analysis

All measurements were made in triplicate and each point in the figures was given with standard deviation of the mean value. The IC50 value was calculated using the regression analysis program of GraphPad Prism 4.0. The IC50 represents the concentration that exhibits 50% of remaining enzyme activity.

## RESULTS

In this study, the inhibition effect of synthetic estrogen derivatives used in Hormone Replacement Theraphy (HRT) on human GST P1-1 are studied. A total of eight compounds, distinguished by different side chains were screened in a concentration of 33 μM. Among the results, estradiol valerate exhibited the highest potency, significantly reducing enzyme activity by 72 ± 4% at the tested concentration. The other compounds showed moderate inhibition, estradiol cypionate at 53 ± 5%, mestranol at 39 ± 4%, and estradiol propionate at 35 ± 2%, respectively. However, estriol, estrone, ethinyl estradiol and estradiol benzoate showed no inhibition (Table 1).

**Table 1.** Screening the inhibition of estrogen derivatives with human GST P1-1. Table shows percentage of inhibition of GST P1-1 in the presence of 33 μM synthetic drugs assayed with CDNB substrate

| Compound | Structure | Inhibition (%) |
|---|---|---|
| estradiol valerate |  | 72 ± 4 |
| estradiol cypionate |  | 53 ± 5 |
| mestranol |  | 39 ± 4 |
| estradiol propionate |  | 35 ± 2 |
| estriol |  | no inhibition |
| estrone |  | no inhibition |
| ethinylestradiol |  | no inhibition |
| norethindrone acetate |  | no inhibition |
| estradiol benzoate |  | no inhibition |
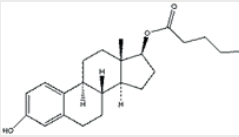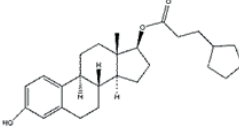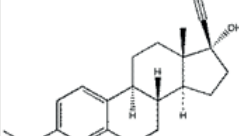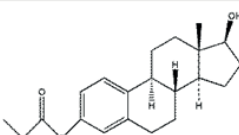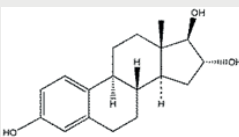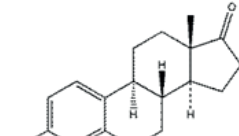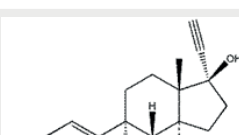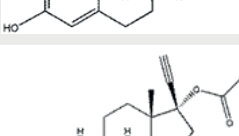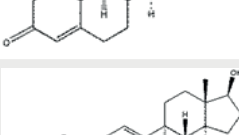
Estradiol valerate was the most promising compound for further analysis. Inhibition analysis with varying concentrations of estradiol valerate, with saturated levels of GSH and CDNB, revealed

an IC50 value of 30 ± 2 μM (Figure 1). However, due to solubility limitations in measurements and turbidity observed at higher concentrations in spectrophotometer cuvettes, further kinetic experiments to elucidate the precise mechanism of binding and inhibition kinetics were impeded. Therefore, binding analysis of estradiol valerate docking to GST P1-1 was conducted using computer software.

The analysis, utilizing Autodock Vina software with the structures of estradiol valerate and GST P1-1, aimed to elucidate the ligand binding location on the enzyme and interactions with amino acid residues. Ten different docking analysis results were obtained, and the one with the lowest energy, scoring -8.4 kcal/mol, was selected. The docking studies showed that the ligand, estradiol valerate fits the H-site region of human GST P1-1. Amino acid residues within the range of 5 Å of the ligand included Phe9, Arg14, Val36, Trp39, Ile105, Tyr109, Pro203, Asn207, and Gln210 (Figure 2). Notably, estradiol valerate formed π-alkyl interactions with Phe9 and Val36, and an alkyl interaction with Ile105 (Figure 3).

## DISCUSSION

In cancer research, GST P1-1 holds significant importance, particularly in understanding and overcoming drug resistance. Increased activity of
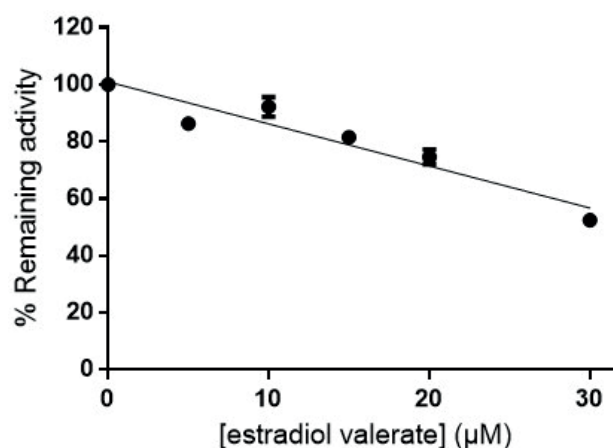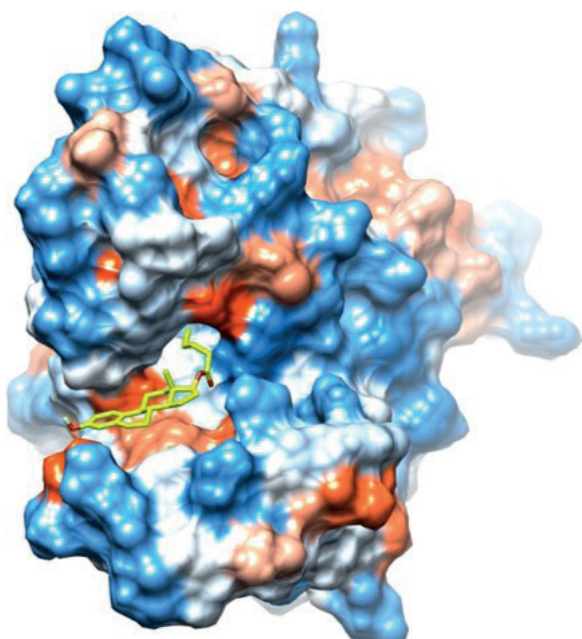


**Figure 1.** Inhibition profile of estradiol valerate for GST P1-1 with the substrate CDNB.
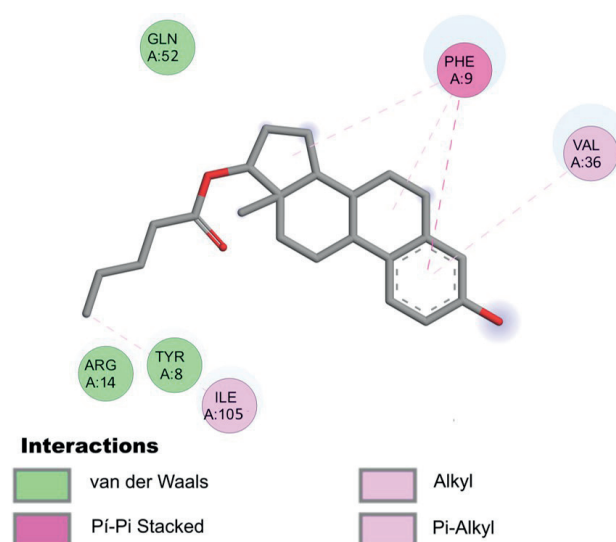


**Figure 3.** 2D view of interactions of estradiol valerate with GST P1-1.
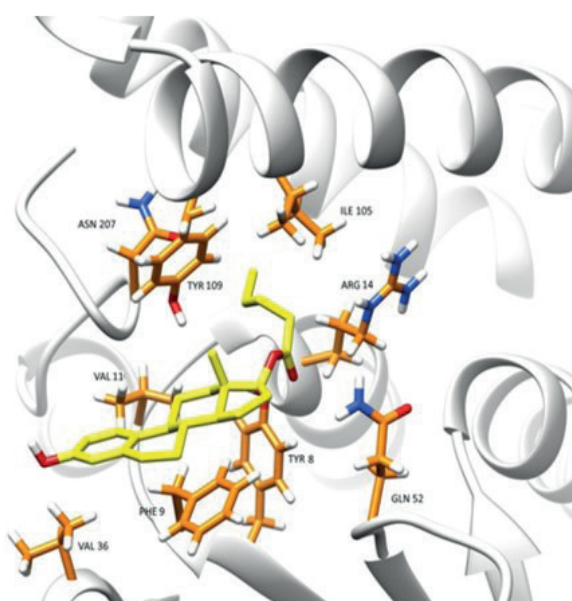


**Figure 2.** 3D structure of docking analysis. **(left)** Surface of GST P1-1 colored according to electrostatic potential with estradiol valerate (yellow). **(right)** Residues of amino acids within 5 Å proximity of estradiol valerate.

GST P1-1 leads to drug inactivation, contributing to resistance against drugs such as chlorambucil, brostallicin, and cyclophosphamide [15,16]. This inactivation might be accompanied by modulating apoptosis through its roles in signaling pathways and transport systems [17]. Based on these premises, several research techniques are being used to suppress GST P1-1 and enhance the efficacy of drugs in chemotheraphy through using specific and potent inhibitors, produgs and antisense cDNA [18,19].

Hormone replacement therapy remains a primary approach for managing menopausal symptoms caused by decreased estrogen levels, involving the administration of synthetic drugs to alleviate symptoms and restore hormonal balance. However, concerns have been raised regarding the potential risk of breast cancer associated with the use of these drugs [20]. Intriguingly, various compounds used in HRT have been described in research papers for their inhibitory effects on various GST from different classes [10,21]. The most potent inhibitors identified in the literature are ethacrynic acid, its analogs, Telintra compounds (TLK117, TLK199), NBDHEX, tin compounds (tributyltin bromide, triphenyltin chloride), and merbromine, all have IC50 values at concentrations <5 μM [10,22-24]. In this study, we identified estradiol valerate as the most potent compound, with an IC50 of $30 \pm 2$ μM, making it a modest inhibitor (Figure 1).

In humans, all GSTs share a similar protein fold with less than approximately 30% of the amino acid composition preserved among the different classes. The diversity of amino acids in the active H-site enables the binding of a wide array of compounds, including drugs, hormones, enviromental pollutants, inhibitors, substrates, etc., attributing to various functions. According to data obtained from crystal structures of GST P1-1, Tyr8, Phe9, Arg14, Val36, Trp39, Tyr109, Asn207, Gly208 are the amino acids involved in the H-site of GST P1-1. These residues line the active site cleft and play a crucial role in binding and catalyzing the conjugation reactions between glutathione and electrophilic substrates [25]. According our docking results, estradiol valerate forms π-alkyl interactions with Phe9 and Val36, and an alkyl interaction with Ile105 (Fig 3). The contact with Ile105 is noteworthy since it is the signature

residue of the *GSTP1*A* allele, the most frequently occurring variant [26]. Residue 105 in the *GSTP1*B* allele is Val. Additionally Phe9, Ile105, Tyr109 and Gln210 are found within 5Å proximity of the ligand with other residues (Figure 2). The docking location of estradiol valerate indicates that the ligand fits in the area of H-site of the protein. Inhibitors binding to the H-site may also act as substrates provided that they contain electrophilic groups. The steroid nucleus of the estrogen derivatives studied here do not contain double bonds that can undergo a GST-catalyzed double-bond isomerization like 5-pregnen-3,20-dione or 5-androsten-3,17-dione, as demonstrated in our previous studies of GSTs from human and other mammalian sources as well as in the mosquito *Anopheles gambiae* [3,27,28]. However, it is well established that GSTs may display esterolytic activities [29] and recent studies demonstrate activity of GST P1-1 with fluorescein esters [30]. Therefore, estradiol valerate and other estrogen derivatives may also be worth testing as substrates of the members of the GSTome.

In conclusion, synthetic estrogen drugs that we studied have minor inhibition effect on human GST P1-1. Even the most potent estradiol valerate is a modest inhibitor. However, the knowledge about its binding location and formation of bonds with the critical residues might assist in the design new inhibitors or substrates targeting GSTs.

## Author contribution

Study conception and design: YM and BM; data collection: YM; analysis and interpretation of results: YM and BM; draft manuscript preparation: YM and BM. All authors reviewed the results and approved the final version of the manuscript.

## Ethical approval

No ethical approval is required for this study.

## Funding

## Conflict of interest

The authors declare that there is no conflict of interest.

## ～ひこ REFERENCES こわ～

[1] Mannervik B, Morgenstern R. Glutathione transferases in "Comprehensive Toxicology". Chapter 10.16, 4th ed. New York: Elsevier; 2024.

[2] Kamisaka K, Habig WH, Ketley JN, Arias M, Jakoby WB. Multiple forms of human glutathione S-transferase and their affinity for bilirubin. Eur J Biochem 1975;60(1):153-61.

[3] Johansson AS, Mannervik B. Human glutathione transferase A3-3, a highly efficient catalyst of double-bond isomerization in the biosynthetic pathway of steroid hormones. J Biol Chem 2001;276(35):33061-5.

[4] Josephy PD, Mannervik B. Molecular toxicology. 2nd ed. Oxford, UK ; New York: Oxford University Press; 2006.

[5] Mannervik B, Board PG, Hayes JD, Listowsky I, Pearson WR. Nomenclature for mammalian soluble glutathione transferases. Methods Enzymol 2005;401:1-8.

[6] Oakley AJ. Hidden Glutathione Transferases in the Human Genome. Biomolecules 2023;13(8).

[7] Armstrong RN. Structure, catalytic mechanism, and evolution of the glutathione transferases. Chemical Research in Toxicology 1997;10(1):2-18.

[8] Tsuchida S, Sato K. Glutathione transferases and cancer. Crit Rev Biochem Mol Biol 1992;27(4-5):337-84.

[9] Simic P, Pljesa I, Nejkovic L, et al. Glutathione Transferase P1: Potential Therapeutic Target in Ovarian Cancer. Medicina (Kaunas) 2022;58(11).

[10] Musdal Y, Hegazy UM, Aksoy Y, Mannervik B. FDA-approved drugs and other compounds tested as inhibitors of human glutathione transferase P1-1. Chem Biol Interact 2013;205(1):53-62.

[11] Kolm RH, Stenberg G, Widersten M, Mannervik B. High-level bacterial expression of human glutathione transferase P1-1 encoded by semisynthetic DNA. Protein Expr Purif 1995;6(3):265-71.

[12] Habig WH, Pabst MJ, Jakoby WB. Glutathione S-transferases. The first enzymatic step in mercapturic acid formation. J Biol Chem 1974;249(22):7130-9.

[13] Pettersen EF, Goddard TD, Huang CC, et al. UCSF Chimera--a visualization system for exploratory research and analysis. Journal of Computational Chemistry 2004;25(13):1605-12.

[14] Seeliger D, de Groot BL. Ligand docking and binding site analysis with PyMOL and Autodock/Vina. J Comput Aided Mol Des 2010;24(5):417-22.

[15] Townsend DM, Tew KD. The role of glutathione-S-transferase in anti-cancer drug resistance. Oncogene. 2003;22(47):7369-75.

[16] Pljesa-Ercegovac M, Savic-Radojevic A, Matic M, et al. Glutathione Transferases: Potential Targets to Overcome Chemoresistance in Solid Tumors. Int J Mol Sci 2018;19(12).

[17] Laborde E. Glutathione transferases as mediators of signaling pathways involved in cell proliferation and cell death. Cell Death Differ 2010;17(9):1373-80.

[18] t Hoen PA, Out R, Commandeur JN, et al. Selection of antisense oligodeoxynucleotides against glutathione S-transferase Mu. RNA 2002;8(12):1572-83.

[19] Allocati N, Masulli M, Di Ilio C, Federici L. Glutathione transferases: substrates, inihibitors and pro-drugs in cancer and neurodegenerative diseases. Oncogenesis 2018;7(1):8.

[20] Sourouni M, Kiesel L. Menopausal Hormone Therapy and the Breast: A Review of Clinical Studies. Breast Care (Basel) 2023;18(3):164-71.

[21] Abel EL, Lyon RP, Bammler TK, et al. Estradiol metabolites as isoform-specific inhibitors of human glutathione S-transferases. Chem Biol Interact 2004;151(1):21-32.

[22] Mannervik B, Danielson UH. Glutathione transferases--structure and catalytic activity. CRC Crit Rev Biochem 1988;23(3):283-337.

[23] Ricci G, De Maria F, Antonini G, et al. 7-Nitro-2,1,3-benzoxadiazole derivatives, a new class of suicide inhibitors for glutathione S-transferases. Mechanism of action of potential anticancer drugs. J Biol Chem 2005;280(28):26397-405.

[24] Dong SC, Sha HH, Xu XY, et al. Glutathione S-transferase pi: a potential role in antitumor therapy. Drug Des Devel Ther 2018;12:3535-47.

[25] Oakley AJ, Lo Bello M, Battistoni A, et al. The structures of human glutathione transferase P1-1 in complex with glutathione and various inhibitors at high resolution. J Mol Biol 1997;274(1):84-100.

[26] Allan JM, Wild CP, Rollinson S, et al. Polymorphism in glutathione transferase P1 is associated with susceptibility to chemotherapy-induced leukemia. Proceedings of the National Academy of Sciences of the United States of America 2001;98(26):11592-7.

[27] Mannervik B, Ismail A, Lindstrom H, Sjodin B, Ing NH. Glutathione Transferases as Efficient Ketosteroid Isomerases. Front Mol Biosci 2021;8.

[28] Musdal Y, Ismail A, Sjodin B, Mannervik B. Potent GST Ketosteroid Isomerase Activity Relevant to Ecdysteroidogenesis in the Malaria Vector Anopheles gambiae. Biomolecules 2023;13(6).

[29] Keen JH, Jakoby WB. Glutathione Transferases - Catalysis of Nucleophilic Reactions of Glutathione. Journal of Biological Chemistry 1978;253(16):5654-7.

[30] Fujikawa Y, Nampo T, Mori M, Kikkawa M, Inoue H. Fluorescein diacetate (FDA) and its analogue as substrates for Pi-class glutathione S-transferase (GSTP1) and their biological application. Talanta 2018;179:845-52.

acta medica

# Outcomes of multidisciplinary management of pulmonary nodules in a tertiary center

Özge Öztürk Aktaş[1]
ORCID: 0000-0002-1939-2636

Ahmet Uğur Demir[1]
ORCID: 0000-0003-4803-6224

Ziya Toros Selçuk[1]
ORCID: 0000-0003-4220-8128

⁓◎ A B S T R A C T ◎⁓

Objective: A multidisciplinary approach is recommended for managing pulmonary nodules. This study aimed to examine the malignancy rates, malignancy determinants, and follow-up results of patients with pulmonary nodules whom the multidisciplinary team evaluates.

Methods: Clinical characteristics of the patients, radiological and histological characteristics of the nodules, and the follow-up outcomes were documented retrospectively. A total of 94 patients with solitary pulmonary nodules (SPNs) (n=58) and multiple pulmonary nodules (MPNs) (n=36) were included in the study.

Results: Our study showed that malignancy risk increased with irregular nodule margins (p < 0.008). Patients who had tissue sampling from suspected nodules exhibited markedly higher rates of previous malignancy than those who did not (58.5% vs. 19.5% p<0.001). For the patients with solitary pulmonary nodule (SPN), the group for whom biopsy was planned had more underlying malignancy (p=0.011) and had a bigger nodule size of 10 mm (range, 8.0-13.25 mm) vs 15.00 mm (range, 10.0-19.75 mm) (p=0.003). Among the patients who have multiple pulmonary nodules (MPN), eighty-four percent of patients in the biopsy group had underlying malignancy diagnoses, whereas this rate was 26% in the CT follow-up group (p=0.002). Adenocarcinoma was the most common SPN histology and squamous cell carcinoma for MPNs. The Multidisciplinary Thoracic Oncology Board identified malignancy in 60% of patients with SPNs and 92.3% of those with MPNs/

Conclusions: Patients evaluated in the multidisciplinary tumor board consist of a very diverse patient group. Discerning between malignant and benign conditions relies heavily on examining nodule features and assessing malignancy history.

Keywords: pulmonary nodule, multidisciplinary board, multiple pulmonary nodules.

[1] Department of Chest Diseases, School of Medicine, Hacettepe University, Ankara, Türkiye

Corresponding Author: Özge Öztürk Aktaş
E-mail: ozgeozturaktas@gmail.com

## INTRODUCTION

Pulmonary nodules are frequently discovered incidentally during CT scans performed for other reasons, and the frequency of nodule detection on a given scan increased from 24 to 31% [1,2]. In patients with a solitary pulmonary nodule (SPN), the overall frequency of malignancy ranges from 2% to 23% [3]. Various guidelines have been published to evaluate pulmonary nodules [4-6]. Tumor boards provide the highest level of patient evaluation for complex cases. Multiple studies have indicated that multidisciplinary care benefits patients with malignancy[7-9]. Although most Multidiciplinary Throacic Oncology Boards (MTB) adhere to guidelines, some judgments deviate owing to patient characteristics [10]. All characteristics should be taken into account when evaluating the risk of malignancy in this complex patient population. At our center, patients reviewed

by the board undergo a comprehensive evaluation using a multidisciplinary approach based on current guidelines. This study aimed to examine the malignancy rates, malignancy determinants, and follow-up results of patients with pulmonary nodules whom the Hacettepe University Medical Faculty Thoracic Oncology Board evaluated.

## METHODS

This study was designed retrospectively, and the Hacettepe University Medical Faculty Ethics Committee, Turkey, approved the study protocol (13.02.2013, LUT 12/163-11). Patients with pulmonary nodules that evauated by The Multidisciplinary Board that held weekly with representatives from Chest Diseases, Cardiovascular and Thoracic Surgery, Radiology, Radiation Oncology, Nuclear Medicine, and Pathology at Hacettepe University between June 2003 and February 2013 included to the study. The patients with solitary pulmonary nodules (SPNs) and multiple pulmonary nodules (MPNs) were recorded. Age, gender, smoking habits, history of other malignancies, and the results of thorax CT scans of the patients, nodule characteristics, pathology results examined. Dominant nodule was sampled for patients with multiple nodules. The follow-up results and post-procedure complications recorded. The study examined the incidence of malignancy in

patients who had diagnostic testing and calculated the efficacy of the MTB in detecting malignancies.

The Statistical Package for the Social Sciences (SPSS) Ver. 18 program was used for the statistical analyses; categorical variables were calculated using frequency, and continuous variables were calculated using median and standard deviation. Nominal variables were analyzed using the Chi-square test, and the interval variables of the two groups were analyzed using the t-test. A p-value of <0.05 was considered significant.

## RESULTS

A total of 94 patients, 58 with SPN and 36 with MPN were included in the study. Of the 58 patients with SPNs, 30 were advised to undergo surgical biopsy, 10 were suggested to undergo transthoracic biopsy, and the remaining 18 underwent thorax CT scans for follow-up per the Board's directive.

Out of the total cohort of 36 patients identified with multiple pulmonary nodules (MPNs), surgical intervention was advised for nine patients, while transthoracic biopsy was deemed appropriate for four patients. The remaining 23 subjects were suggested to undergo follow-up examinations with computed tomography (CT) scans. Sankey diagram of study is shown in Figure 1.
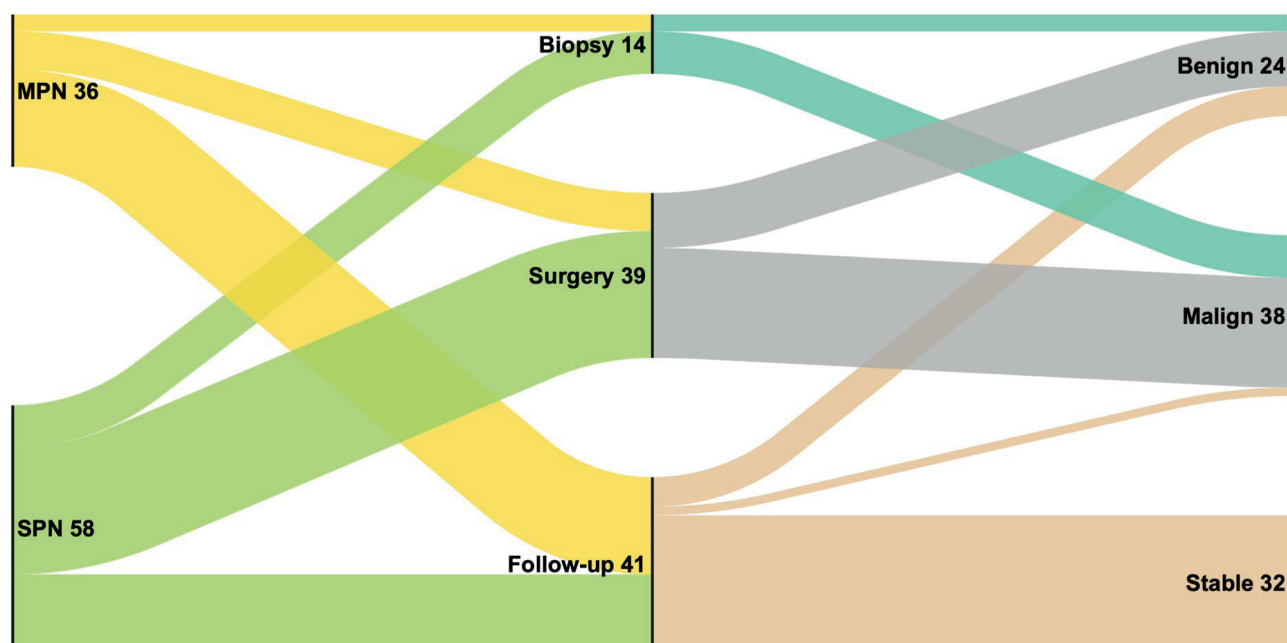


**Figure 1.** Sankey diagram of outcome of all the pulmonary nodules evaluated by Multidisciplinary Thoracic Oncology Board. SPN: Solitary pulmonary nodule, MPN: Multiple pulmonary nodule. (Numbers represent the number of patients in the relevant group).

The mean age of the patients was 62 years. Thirty-two (34%) of the patients were women, and 62 (66%) were men. The demographic characteristics of all patients were categorized based on whether they had tissue sampling. Patients who had tissue sampling exhibited markedly higher rates of previous malignancy than those who did not (58.5% vs. 19.5% p<0.001). Among patients with SPN, for whom biopsy was planned, 50% of patients had underlying malignancy diagnoses, whereas this rate was 11% in the follow-up group (p=0.011). The mean nodule size of patients in the follow-up group was 10 mm (range, 8.0-13.25 mm) [6-19], whereas it was 15.00 mm (range, 10.0-19.75 mm) [6-26] in the biopsy group (p=0.003) (Table 1).

Thirteen (81.3%) of the sharp-borders SPNs were benign, and 8 (33.3%) were malignant. Three irregular-borders SPNs were benign (18.8%), and 16 were malignant (66.7%). SPNs with irregular borders revealed a higher prevalence of malignant histology (p=0.008) (Table 2).

Twenty-one nodules were identified in the upper lobes; however, no significant relation with the location was confirmed in terms of being malignant or benign (p=0.50).

The pathologic results of all three spiculated nodules were determined as malignant. According to the pathology results, 16 nodules had benign histology, and 24 were malignant. Although patients with malign histology had more smoking history, these associations weren't statistically significant. When evaluating the pathology results of patients with SPNs, benign causes were diagnosed in 16 patients, and malignant etiology was diagnosed in 24 patients. Adenocarcinoma (54.6%) was identified most commonly among the malignancies, followed by squamous cell (12.5%) ca and typical carcinoid (12.5%). Chronic inflammation/fibrotic causes (37.5%) were identified most frequently among benign causes, followed by chondroid hamartoma (25%), necrotizing granulomatous inflammation (25%), and lung parenchymal tissue (12.5%).

**Table 1.** Comparison of baseline characteristics of patients with SPN and MPN who underwent tissue sampling and were followed up

| | Patients with Solitary Pulmonary nodule (n= 58) | | | Patients with Multiple Pulmonary nodule (n=) | | |
|---|---|---|---|---|---|---|
| | Follow- up (n: 18) | Tissue sampling (n: 40) | p value | Follow- up (n: 23) | Tissue sampling (n: 13) | p value |
| Age, (mean±SD) years | 66±13.7 | 59.7±12.4 | 0.058 | 64.26±11.17 | 62.69±14.20 | 0.71 |
| Sex, n (%) | | | | | | |
|   Male | 14 (77.8) | 26 (65.0) | 0.50 | 17 (73.9) | 5(38.5) | 0.082 |
|   Female | 4 (22.2) | 14 (35) | | 6 (26.1) | 8(61.5) | |
| Smoking history +, n, (%) | 9 (50.0) | 24 (60.0) | 0.67 | 12 (52.2) | 4 (30.8) | 0.37 |
|   Pack/years, (mean±SD*) | 35.22±25.17 | 28.13±30.49 | 0.45 | 21.36±10.53 | 9.50±2.51 | 0.04 |
| COPD, n, (%) | 3 (16.7) | 12 (30.0) | 0.45 | 4 (17.4) | 5 (38.5) | 0.317 |
| Emphysema, n, (%) | 5 (27.8) | 14 (35.0) | 0.81 | 7 (30.4) | 5 (38.5) | 0.90 |
| Underlying malignancy, n, (%) | 2 (11.0) | 20 (50.0) | **0.011** | 6(26.1) | 11 (84.6) | **0.002** |
| Nodule size, mm, range, median (IQR**) | 10 (8.0-13.25) [6-19] | 15.0 (10.0-19.75) [6-26] | **0.003** | N/A | | |
|   Nodule type, n, (%) | | | | N/A | | |
|     Non-solid, ground glass | 2 (11) | 14 (35) | 0.117 | N/A | | |
|     Solid | 16 (88.9) | 26 (65) | | N/A | | |
|   Egde type, n, (%) | | | | N/A | | |
|     Irregular | 6 (33.3) | 19 (47.5) | 0.47 | N/A | | |
|     Sharp | 12 (66.7) | 21 (52.5) | | N/A | | |
|   Nodule localization, n, (%) | | | | N/A | | |
|     Upper lobes | 12 (66.0) | 18 (45) | 0.21 | N/A | | |

*SD standart deviation ,N/A not applicable

** Interquartile range

**Table 2.** Demographic and radiological characteristics of patient wtih SPN according to pathology

| | Benign (n: 16) | Malign (n: 24) | p value |
|---|---|---|---|
| Age, (mean±SD*) years | 58.1±7.6 | 60.7±14.9 | 0.52 |
| Sex, n (%) | | | |
|    Male | 10 (62.5) | 16 (66.7) | 1.00 |
|    Female | 6 (37.5) | 8 (33.3) | |
| Smoking history, n, (%) | 6 (37.5) | 10 (41.7) | 1.00 |
| Pack/ years,(mean±SD*) | 24.1±17.7 | 30.5±22.5 | 0.56 |
| COPD, n, (%) | 5 (31.3) | 7 (29.2) | 1.00 |
| Emphysema, n, (%) | 6 (37.5) | 8 (33.3) | 1.00 |
| Underlying malignancy, n, (%) | 5 (31.3) | 15 (62.5) | 0.10 |
| Nodule size mm, range, median (IQR**) | 15 (10.5-18.0) [9-22] | 16.5 (10.0-24.25) [6-26] | 0.45 |
| Nodule type, n, (%) | | | |
|    Non-solid, ground glass | 6 (37.5) | 8 (33.3) | 1.00 |
|    Solid | 10 (62.5) | 16 (66.7) | |
| Egde type, n, (%) | | | |
|    Irregular | 3 (18.8) | 16 (66.7) | **0.008** |
|    Sharp | 13 (81.3) | 8 (33.3) | |
| Nodule localization, n, (%) | | | |
|    Upper lobes | 7 (43.8) | 15 (62.5) | 0.50 |
|    Right middle lobe | 3 (18.8) | 3 (12.5) | |
|    Lower lobes | 6 (37.5) | 6 (25.0) | |

*Standart deviation

** Interquartile range

The mean follow-up duration of nodules was 6-12 months (range, 3-36 months). It was confirmed that two nodules disappeared after 3 months, and two regressed. Among the patients with MPNs, 84% of patients in the biopsy group had underlying malignancy diagnoses, whereas this rate was 26% in the CT follow-up group (p=0.002). Also, it was similar for the patients with MPN; the most common malign pathology among multiple nodules was adenocarcinoma (33.3%), and one patient that was diagnosed as benign was chronic inflammation. Nodules disappeared in 3 of the 23 follow-up patients, and one of the nodules grew in one patient. The growing nodule was identified as malignant using transthoracic biopsy. Nineteen patients' nodules were stable. Considering that the patients who underwent tissue biopsy were predicted to be malignant, the malignancy detection success of the MTB was 60% for SPN and 92.3% for MPN. One of the 18 follow-up patients with an SPN was determined to have a malignant disease. Post-procedure pneumothorax in 2 patients, air leak in 3 patients, pneumonia in 1 patient, and renal dysfunction in 1 patient was observed.

## DISCUSSION

Over the past ten years, there has been a consistent rise in the detection of incidental pulmonary nodules on chest CT scans, which has been linked to an increase in the number of stage I lung cancer diagnoses[11]. Guidelines recommend discussing patients with malignancy suspicion by multidisciplinary tumor boards. According to previous studies, a multidisciplinary approach is the most effective way to provide patients with suspected malignancy [7,12] Multidisciplinary tumor boards are supposed to enhance overall treatment and results for patients at high risk; MTB recommendations deviate from the management clinicians' original plan [13].

According to a study; age, female sex, cancer background in the family, emphysema, large nodule size, nodule being in the upper lobe, being half-solid, being few, and spiculation were predictors for cancer risk [14,4]. In a large series of studies, results show that nodules in the upper lobe increase the risk of malignancy [15,16,7]. This may be related to more carcinogens being inhaled in the upper lobes, depending on smoking. In our study,

the majority of malignant solitary nodules (62.5%) were located in the upper lobes. In a recent study among individuals with SPNs, smoking increased the probability of developing lung cancer in men. However, there was no substantial correlation found between smoking and the diagnosis or mortality of lung cancer in women with an SPN [17]. This may be related to more carcinogens being inhaled in the upper lobes, depending on smoking. In our study, most malignant solitary nodules (62.5%) were in the upper lobes. In a recent study among individuals with SPNs, smoking increased the probability of developing lung cancer in men. However, there was no substantial correlation found between smoking and the diagnosis or mortality of lung cancer in women with an SPN [18]. A recent meta-analysis, only centrilobular emphysema was significantly associated with lung cancer [19]. These results support the existence of different malignancy variables for different patient groups. Similarly, in our study, there was no significant relation between smoking, COPD, and radiologic emphysema diagnosis in patients with malignant and benign results, but all nodules with spiculated borders were found to be malignant, and irregular-edged SPNs showed significantly more malignant features when compared with those with smooth edges. A study investigating the clinical practice consensus guidelines for Asia has found that the populations used to validate the models for assessing pretest may not be accurate when applied to Asian populations due to several factors including high rates of granulomatous and other infectious diseases, air pollution, and the occurrence of lung cancer among nonsmokers [20]. This result supports the finding that unique characteristics can be seen in different patients subgroups including multidisciplinary board patients.

The present study determined malignancy histopathologically in 38 (40.4%) patients. The pathology results of 13 (32%) of 40 patients with SPNs and 5 (38%) of 13 patients with multiple nodules who underwent biopsy were diagnosed as adenocarcinoma. Similar to our study, in a study by Gould et al., most SPNs were diagnosed with adenocarcinoma (50%). The increased solid content in ground-glass nodules shows more invasive pathologic conditions [14]. A study shows sub-solid lesions have a 34% malignancy risk, whereas solid lesions have 7% [21]. In our study, the pathology

of malignant SPN patients who had a malignancy history showed 40% cancer metastasis, 35% primary lung cancer, and 25% benign pathology. According to a study examining the surgical results of 131 patients with solitary pulmonary nodules with a previous cancer history, metastases were detected in 65 patients, primary lung cancer in 57 patients, and benign lesions in 9 patients [22].

Our study observed benign pathology in 40% of patients with SPNs who underwent sampling. The MTB had a 60% success rate in identifying cancer in patients who underwent tissue sampling and were expected to have malignant diseases. This rate was 92.3% for patients with MPN. Although the general frequency of malignancy in patients with solitary pulmonary nodule (SPN) varies between 2% and 23% in the literature [3], the high rate of malignancy observed in MTB in our study supports that tissue biopsy should be prioritized for the diagnosis of malignancy in MTB patients, even if the patients do not have other malignancy criteria.

The primary limitation of this study is the limited sample size. The lack of significance of malignancy-risk variables in our study can be attributed to the fact that our study did not screen and instead focused on a specific population. The patient cohort deliberated by the MTB exhibits a higher prevalence of comorbidities and necessitates the implementation of interdisciplinary techniques for both diagnosis and therapy. Furthermore, our research was limited to the available data because we used existing data from hospital records. Therefore, the study could not include additional important information, such as the effects of PET CT.

## CONCLUSIONS

Multidisciplinary board patients present unique subgroup characteristics. When deciding on the light of the guidelines, it should be kept in mind that the patient group may not show classical features due to its complexity, and a patient-specific plan should be made.

### Author contribution

Study conception and design: OOA, AUD, and ZTS; data collection: OOA ; analysis and interpretation of results: OOA and AUD; draft manuscript preparation:

## ~ᴔ◯ REFERENCES ◯ᴓᴏ~

[1] Gould MK, Tang T, Liu IL, et al. Recent Trends in the Identification of Incidental Pulmonary Nodules. Am J Respir Crit Care Med. 2015;192(10):1208-14.

[2] Mazzone PJ, Lam L. Evaluating the Patient With a Pulmonary Nodule: A Review. Jama. 2022;327(3):264-73.

[3] Cruickshank A, Stieler G, Ameer F. Evaluation of the solitary pulmonary nodule. Intern Med J. 2019;49(3):306-15.

[4] Gould MK, Donington J, Lynch WR, et al. Evaluation of individuals with pulmonary nodules: when is it lung cancer? Diagnosis and management of lung cancer, 3rd ed: American College of Chest Physicians evidence-based clinical practice guidelines. Chest. 2013;143(5 Suppl):e93S-e120S.

[5] Chen B, Li Q, Hao Q, et al. Malignancy risk stratification for solitary pulmonary nodule: A clinical practice guideline. J Evid Based Med. 2022;15(2):142-51.

[6] Farjah F, Monsell SE, Smith-Bindman R, et al. Fleischner Society Guideline Recommendations for Incidentally Detected Pulmonary Nodules and the Probability of Lung Cancer. J Am Coll Radiol. 2022;19(11):1226-35.

[7] Davies AR, Deans DA, Penman I, et al. The multidisciplinary team meeting improves staging accuracy and treatment selection for gastro-esophageal cancer. Dis Esophagus. 2006;19(6):496-503.

[8] Freeman RK, Van Woerkom JM, Vyverberg A, Ascioti AJ. The effect of a multidisciplinary thoracic malignancy conference on the treatment of patients with esophageal cancer. Ann Thorac Surg. 2011;92(4):1239-42; discussion 43.

[9] Freytag M, Herrlinger U, Hauser S, et al. Higher number of multidisciplinary tumor board meetings per case leads to improved clinical outcome. BMC Cancer. 2020;20(1):355.

[10] Krause A, Stocker G, Gockel I, et al. Guideline adherence and implementation of tumor board therapy recommendations for patients with gastrointestinal cancer. J Cancer Res Clin Oncol. 2023;149(3):1231-40.

[11] Hendrix W, Rutten M, Hendrix N, et al. Trends in the incidence of pulmonary nodules in chest computed tomography: 10-year results from two Dutch hospitals. Eur Radiol. 2023;33(11):8279-88.

[12] Specchia ML, Frisicale EM, Carini E, et al. The impact of tumor board on cancer care: evidence from an umbrella review. BMC Health Serv Res. 2020;20(1):73.

[13] Schmidt HM, Roberts JM, Bodnar AM, et al. Thoracic multidisciplinary tumor board routinely impacts therapeutic plans in patients with lung and esophageal cancer: a prospective cohort study. Ann Thorac Surg. 2015;99(5):1719-24.

[14] McWilliams A, Tammemagi MC, Mayo JR, et al. Probability of cancer in pulmonary nodules detected on first screening CT. N Engl J Med. 2013;369(10):910-9.

[15] Horeweg N, van der Aalst CM, Thunnissen E, et al. Characteristics of lung cancers detected by computer tomography screening in the randomized NELSON trial. Am J Respir Crit Care Med. 2013;187(8):848-54.

[16] Winer-Muram HT. The solitary pulmonary nodule. Radiology. 2006;239(1):34-49.

[17] Chilet-Rosell E, Parker LA, Hernández-Aguado I, et al. The determinants of lung cancer after detecting a solitary pulmonary nodule are different in men and women, for both chest radiograph and CT. PLoS One. 2019;14(9):e0221134.

[18] González Maldonado S, Delorme S, Hüsing A, et al. Evaluation of Prediction Models for Identifying Malignancy in Pulmonary Nodules Detected via Low-Dose Computed Tomography. JAMA Netw Open. 2020;3(2):e1921221.

[19] Yang X, Wisselink HJ, Vliegenthart R, et al. Association between Chest CT-defined Emphysema and Lung Cancer: A Systematic Review and Meta-Analysis. Radiology. 2022;304(2):322-30.

[20] Bai C, Choi CM, Chu CM, et al. Evaluation of Pulmonary Nodules: Clinical Practice Consensus Guidelines for Asia. Chest. 2016;150(4):877-93.

[21] Henschke CI, Yankelevitz DF, Mirtcheva R, McGuinness G, McCauley D, Miettinen OS. CT screening for lung cancer: frequency and significance of part-solid and nonsolid nodules. AJR Am J Roentgenol. 2002;178(5):1053-7.

[22] Rena O, Davoli F, Boldorini R, et al. The solitary pulmonary nodule in patients with previous cancer history: results of surgical treatment. Eur J Surg Oncol. 2013;39(11):1248-53.

acta medica

# Identification of bio-markers for insulin resistance and sensitivity through multi-omics analysis

İdil Yet[1]
ORCID: 0000-0002-1227-0716

~∞⊙ A B S T R A C T ⊙∞~

Aims: This study aims to identify multi-omics bio-markers for insulin resistance and sensitivity using machine learning approaches on a dataset integrated from several omics.

Methods: The study included 362 patients with Insulin Resistance and Insulin Sensitivity from the Integrative Personal Omics Profiling (iPOP) database. Combining the multi-omics data from the Integrative Human Microbiome Project, this study used machine learning to reveal the relationship between insulin resistance and insulin sensitivity.

Results: Of 362 patients 186 were insulin resistance and 176 were insulin sensitivity. 11,585 features were used, including clinical features, RNA transcripts, gut microbiota, cytokines, proteins, and metabolomics. We found 21 features capable of distinguishing insulin resistance from insulin sensitivity using a well-known artificial neural network (ANN) method. The model had an area under the receiver operating characteristic (AUC) of 0.97 in the validation dataset and 0.89 in the test dataset. The ANN model's performance was compared with Random Forest model. Of the 21 new findings, two metabolites (methyl-uric acid and methylxanthine) are xenobiotics, and three RNA transcripts (*SERPINF1, SLC2A2*, and *CHL1*).

Conclusion: A small number of multi-omics features identified from 11,585 potential candidates for a machine learning model can accurately predict insulin resistance and sensitivity.

Keywords: microbiome, metabolomics, multi-omics, type II diabetes mellitus, artificial neural network.

[1] Department of Bioinformatics, Graduate School of Health Sciences, Hacettepe University, Ankara, Türkiye.

Corresponding Author: İdil Yet
E-mail: idil.yet@hacettepe.edu.tr

## INTRODUCTION

Type II diabetes mellitus (T2D) affects more than 10% of the world population, and another 30% are diagnosed with prediabetes and are at risk of developing diabetes in the coming years [1, 2]. T2D is a complex disease; little is known about changes during the initial prediabetes stage, modifications in biological processes, or its alteration to T2D. Both conditions are connected with insulin resistance, which is used to investigate the earliest stages of diabetes. Innovations in next-generation sequencing (NGS) and mass spectrometry (MS) have made it possible to report novel bio-markers and pathways across several diseases, including

T2D. Biological data created with NGS and MS experiments help more accurately predict health outcomes [3-5]. Massive cohort studies use data generated from NGS to identify genetic variants associated with complex diseases, such as genome-wide association studies (GWAS). GWAS-associated T2D has identified more than 300 genetic variants. However, using GWAS alone is not sufficient for a thorough understanding of complex diseases and their mechanisms as GWAS only focuses on genetic factors [6]. The past two decades have witnessed progress in the diversity of molecular data, including genomics, epigenomics, transcriptomics,

and proteomics. These multi-omics profiling approaches can be used to screen the change of molecules in diseases and examine the variation within the traits. To address these challenges and to study dynamic changes in hosts under several diseases, the Integrated Human Microbiome Project (iHMP) was established by The National Institutes of Health (NIH) [2]. Previous iHMP projects have mainly focused on the longitudinal analysis of prediabetes patients [7]. In the past decade, microbiota and metabolomics have become very popular for uncovering the associations related to health or disease conditions [8,9]. Several cohort studies try to create an atlas for biomarkers using association studies involving metabolite-wide association studies (MeWAS) and microbiome-wide association studies (MWAS) [4,10]. Prediabetes and T2D signature has also been studied at a single omic level using microbiome [11], metabolomics [12], proteomics [13], epigenomics [14]. Overmyer et al. investigated associations between the oral microbiome and metabolomics in subjects with prediabetes [15]. These studies mainly focused on prediabetes patients, but the relationships among multi-omics elements in insulin resistance were not thoroughly studied. Machine learning is a promising tool for analysing multi-omics data and identifying bio-markers for disease risk ].

Additionally, the system biology field has been moving from only generating data to effectively analysing this high-dimensional data using many machine learning techniques [17-20]. These studies mostly try to predict metastasis or help clinicians effectively in cancer diagnosis, prognosis, and treatment selection [18,19]. However, high-dimensional models with different multi-omics elements make it challenging to develop accurate models and lead to overfitting problems. This study aims to identify potential biomarkers for insulin resistance (IR) and insulin sensitivity (IS) using machine learning. Combining data from multiple omics including laboratory features, gut microbiota, RNA transcripts, metabolomics, cytokines and proteins, we investigated 11,585 potential features for predicting IR and IS. We identified 21 potential biomarkers that can make accurate predictions of IS and IR using feature selection approaches.

## METHODS

The iPOP Project omics data was used (http://hmp2-data.stanford.edu/). iHMP Type II Diabetes Mellitus Data were obtained from iPOP [21]. Each omics data is downloaded separately from the data portal and merged using the visiting ID of samples. Ethics approval is not needed, and the Declaration of Helsinki's ethical rules and principles were followed in all procedures. We designed a cross-sectional study ignoring the longitudinal data of prediabetes patients. The samples were selected according to the steady-state plasma glucose level (SSPG) by iPOP. Individuals with an SSPG greater than 150 mg/dL were logged as IR, and below the same threshold were logged as IS [2]. The data consisted of 186 individuals classified as IR and 176 as IS. In total, 11,585 features were used (302 proteins from plasma, 66 cytokines, 51 clinical laboratory features, 96 gut microbiota, 10,346 RNA transcripts, and 724 metabolomics) (Figure 1).

Features that have missing values were excluded and data was scaled with z-score normalisation. The data was analysed using two machine learning methods: artificial neural networks (ANN) and Random Forests. To develop a model for classifying IR and IS, subjects were divided randomly in an 8:2 model training dataset to test-validation dataset ratio. The test-validation dataset was used only to verify the model performance and was randomly divided into a 5:5 ratio to obtain the test and validation datasets. A Multi-Layer Perceptron classifier from the scikit-learn library in Python programming language was used for ANN [22]. Model parameter optimisation was performed using Grid search, and the best parameters were selected for each model. All the predefined parameters are fitted with the Adaptive Movement Estimation (Adam) algorithm to adjust the learning rate dynamically, sigmoid for calculating predictions, and the remaining layers are activated with the Rectified Linear Unit (ReLU) function. The Sequential Feature Selector function was used with forward selection (Sequential Forward Selection (SFS)) for feature selection. A Random Forest Classifier from the scikit-learn library in Python programming language was used for Random forest [22]. The gini function to measure the quality
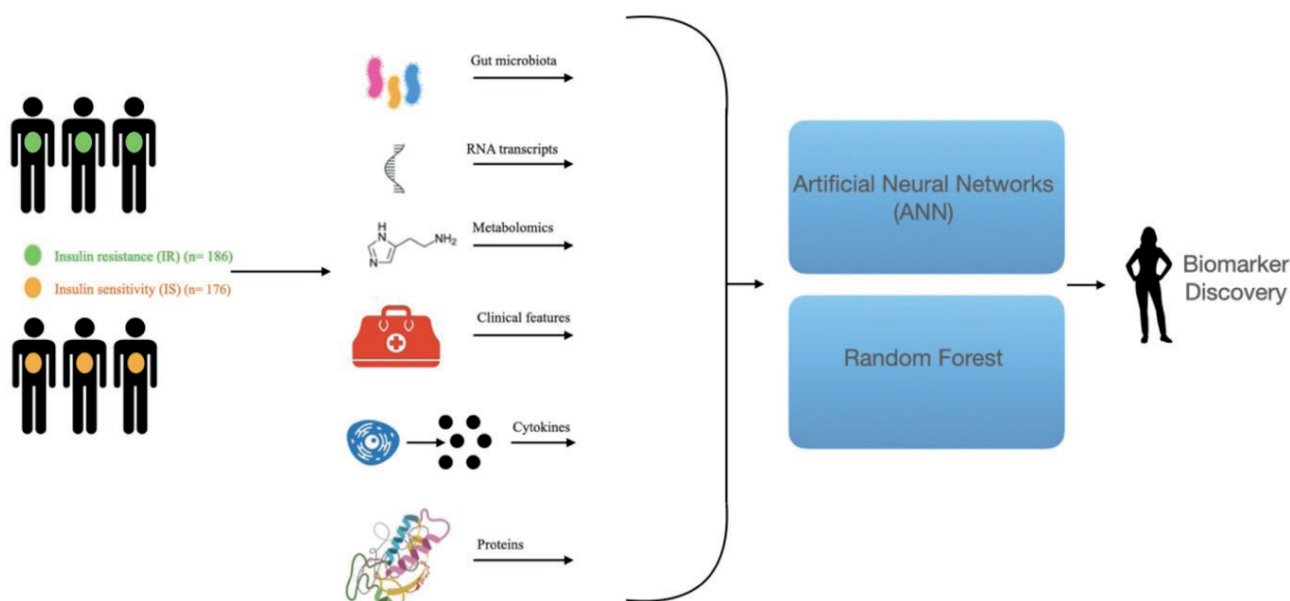
**Figure 1.** Summary of the multi-omics study design

of a split was selected. It ensures that each tree makes effective splits that contribute to accurate predictions when combined with others in the forest. The comparisons of ANN and Random Forest models were based on the area under the receiver operating characteristic (AUC) curve, accuracy, precision, recall and f1-score. AUC was plotted with ggroc function from ggplot library using R programming language [23]. The performance of the ANN algorithm model was compared with the Random Forest algorithm [24].

## RESULTS

The study consisted of 186 patients with IR and 176 patients with IS. To develop a model capable of distinguishing IR from IS, subjects were divided randomly in an 8:2 model training to test-validation dataset ratio. We set the hidden_layer_size inside the Multi-Layer Perceptron Classifier to (6,6,6,6) in ANN model. This means we add four hidden layers with six hidden units in each, including the Adam algorithm, the ReLU function, and 500 iterations. The model resolved with 21 features with the forward selection function from 11,585 features from the data (Table 1).

The first ANN models of IR and IS data were built using training sets. Then, the model was evaluated with validation and test datasets. The same data-splitting procedure is applied to the Random Forest model. We set the n_estimators (number of trees in

the forest) as "1000" in Random Forest Classifier. The function to measure the quality of a split is selected as "gini". The prediction performances of ANN model were also evaluated and compared with Random Forest model (Table 2).

**Table 1.** Selected 21 features with forward selection in the ANN algorithm model

| Bio-marker | Omic | Total | p-value |
|---|---|---|---|
| IGHM | Proteomics | 3 | <0.001 |
| APOE | | | <0.001 |
| LPA | | | 0.01 |
| LEPTIN | Cytokines | 6 | 0.007 |
| SCF | | | <0.001 |
| GMCSF | | | <0.001 |
| MCP1 | | | <0.001 |
| FASL | | | 0.014 |
| IL7 | | | <0.001 |
| HDL | Clinical Laboratory | 6 | 0.006 |
| Monoab | | | 0.05 |
| MCV | | | <0.001 |
| CR | | | <0.001 |
| TGL | | | <0.001 |
| EOTAXIN | | | <0.001 |
| genus_Coprococcus | Gut Microbiota | 1 | 0.015 |
| methyluric acid | Metabolomics | 2 | <0.001 |
| methylxanthine | | | <0.001 |
| SERPINF1 | Transcriptomics | 3 | <0.001 |
| SLC2A2 | | | <0.001 |
| CHL1 | | | 0.05 |

**Table 2.** Model performance metrics

| Models | Performance | Accuracy | Precision | Recall | f1-score |
|---|---|---|---|---|---|
| ANN | AUC=0.89 | 0.89 | 0.89 | 0.85 | 0.87 |
| Random Forest | AUC=0.94 | 0.94 | 0.94 | 0.89 | 0.91 |

Receiver operating characteristic (ROC) curve of the ANN and Random Forest models are plotted in Figure 2.

The AUC was 0.97 in the validation set and 0.89 in the test dataset. The accuracy, precision, recall and f1-score for the validation dataset are 0.91, 0.95, 0.87, and 0.91, respectively. The test dataset's accuracy, precision, recall and f1-score are 0.89, 0.89, 0.85, and 0.87, respectively. The Random Forest algorithm method was used to validate the ANN model. The AUC was 0.93 in the validation set and 0.94 in the test dataset. Of the 11,585 features, 21 features were chosen in the final model. There were three proteins (IGHM, APOE, LPA), six cytokines (LEPTIN, SCF, GMCSF, MCP1, FASL, IL7) and six clinical laboratory features (HDL, Monoab, MCV, CR, TGL, EOTAXIN), one gut microbiota (*genus_Coprococcus*), three RNA transcripts from RNAseq (*SERPINF1*, *SLC2A2*, and *CHL1*), and two from metabolites (methyl uric acid and methylxanthine. The 21 features for the final model are listed and can be found in Table 1.
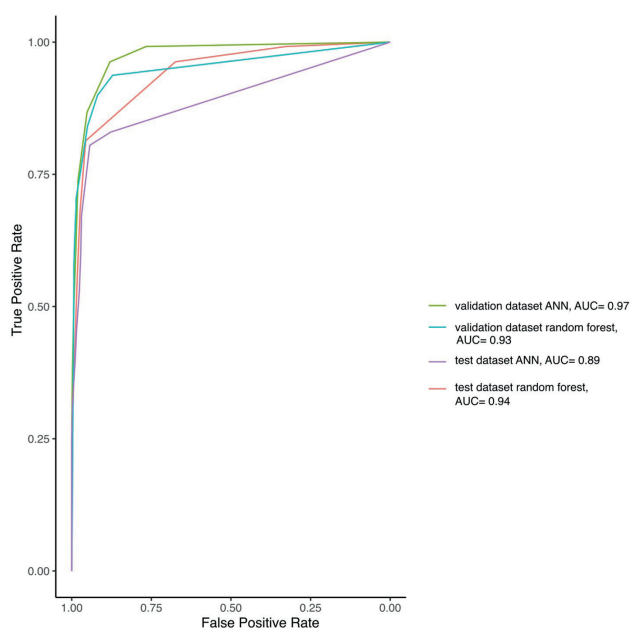


**Figure 2.** ROC curve of the two models (ANN and random forest) with feature selection. The models are built using 11,585 features. AUC scores of the two models using the validation and test datasets

## DISCUSSION

Human transcriptomics, epigenomics, proteomics, metabolomics, and microbiome play an important role in health, and there is a strong indication that omics can be used as predictors of diseases. Arneth et. al. [12] conducted a meta-analysis on the metabolomics of Type I and Type II Diabetes mellitus, reporting several significant metabolites. Pinna et. al. [11] reported 16 operational taxonomic units (OTUs) enriched in almost 500 subjects with prediabetes. Huth et. al. [13] examined protein markers associated with T2D and prediabetes. Juvinao-Quintero et. al. [14] identified 77 differentially methylated regions associated with T2D in a meta-analysis. Overmyer et. al.'s [15] multi-omics study investigated the oral microbiome and metabolomics in (n = 97) subjects with prediabetes and found various associations. However, analyzing these omics causes challenges due to their high-dimensional profiles with the help of feature selection, like the multi-dimensional datasets can be easily compressed into low-dimensional features. In our study, when the model was generated with selected features (21 features), the model performance was improved compared to the without feature selection. The ANN model could classify the samples as IR or IS with 21 features, but no single feature could do so. The ANN model was compared with the Random Forest model, both showing similar metric and performance results (AUC), with the Random Forest exhibiting slightly better performance, showcasing its robustness as a method. On the other hand, the Sequential Feature Selector function coupled with forward selection feature selection in ANN model enabled us to focus on specific key bio-markers which was the main focus of the study. Of the 21 features, 9 of them (SCF, LPA, GMCSF, IL7, CR, APOE, MONOAB, TGL, and IGHM) reported in previous studies to be direct and inverse relationship with insulin resistance and 7 of them (HDL, MCV, EOTAXIN, LEPTIN, MCP1, FASL1 and *genus_Coprococcus)* have a positive correlation between prediabetes and diabetes groups. With this study, we proposed 21 features to become distinguishing bio-markers

for prediabetes. Zhao et. al. [25] detected that prediabetes patients had reduced secretion of methyl uric acid and methylxanthine, which are xenobiotics in tea and coffee. Zhou et.al. [7] used the subset of this data longitudinal to analyse the dynamics of microbiomes in prediabetes with more straightforward methods like logistic regression without selecting the significant features. Notably, using the data cross-sectional helped us increase the sample size, and feature selection enabled us to focus on substantial bio-markers. We identified three bio-marker genes, including *SERPINF1, SLC2A2,* and *CHL1*. These three genes linked to diabetes have been studied in a T2D study [26,27]. Results suggested that *SLC2A2* mutation is an autosomal recessive cause of neonatal diabetes mellitus [26]. *SERPINF1* is related to obesity and changes leptin levels in populations at risk of T2D [26]. *CHL1* encodes a protein, and its expression has indicated a decrease in T2D [27]. We can conclude that this study is the first to establish a separation between IR and IS and these five biomarkers: three RNA transcripts (SERPINF1, SLC2A2, and CHL1), and two metabolites (methyl uric acid and methylxanthine).

Our study has some limitations. One limitation of machine learning algorithms is their overfitting problem. To overcome this problem, we used cross-validation for ANN model with the Random Forest model, and feature selection is coupled with ANN for the multi-site variables. Another limitation is the statistical power. In a systems biology study, it is essential to have a sufficient number of samples to get enough power. Although the sample size for multi-omics profiling has increased over the past ten years, the number of samples can still be lower when selecting a stringent significance level required to correct for multiple testing. To detect more bio-markers, the sample size needs to be increased. Another limitation is the multi-dimensional in-person data. The studies should generate system biology data for individuals on multiple biological platforms across different technologies and tissues. An additional limitation of this study is that, while the model was validated using test and validation datasets derived from the original data, further validation on an independent dataset is necessary to fully assess its generalizability and robustness. Overall, the insulin-resistant and insulin-sensitive subjects differed, and multi-omics elements enabled us to explore the early signs of disease development individually. Future studies will help to develop additional information on how the multi-omics elements affect disease development.

## CONCLUSION

Multi-omics analyses of IR and IS cross-sectional profiling demonstrated insight into disease aetiology. We found 21 features characterising IR from IS using the artificial neural network method with a high AUC measure. Future work is required to assess the bio-markers we propose in this study and applies to other IR and IS cases. Overall, the frequency of T2D is increasing, and the problems it brings are also growing. With this study, we contributed to the literature about the assessment of IR and IS by measuring the 21 significant features using the ANN model.

### Author contribution

Study conception and design: IY; data collection: IY; analysis and interpretation of results: IY; draft manuscript preparation: IY. The author reviewed the results and approved the final version of the manuscript.

### Ethical approval

The study was carried out with published data. The data is open access and freely available on iPOP Project Data Portal (http://hmp2-data.stanford.edu/). No ethical approval was needed.

### Funding

The author declare that the study received no funding.

### Conflict of interest

The author declare that there is no conflict of interest.

## ～ଔଔ REFERENCES ଔଔ～

[1] Çetintepe SP YA, Kılıçarslan A. An Overview of Diabetes Mellitus and Work Life. Acta Medica. 2016;47(2):54-60.

[2] Integrative HMPRNC. The Integrative Human Microbiome Project. Nature. 2019;569(7758):641-8.

[3] Sardaraz M, Tahir M, Ikram AA. Advances in high throughput DNA sequence data compression. J Bioinform Comput Biol. 2016;14(3):1630002.

[4] Shin SY, Fauman EB, Petersen AK, Krumsiek J, Santos R, Huang J, et al. An atlas of genetic influences on human blood metabolites. Nat Genet. 2014;46(6):543-50.

[5] Lightbody G, Haberland V, Browne F, Taggart L, Zheng H, Parkes E, et al. Review of applications of high-throughput sequencing in personalized medicine: barriers and facilitators of future progress in research and clinical application. Brief Bioinform. 2019;20(5):1795-811.

[6] Vujkovic M, Keaton JM, Lynch JA, Miller DR, Zhou J, Tcheandjieu C, et al. Discovery of 318 new risk loci for type 2 diabetes and related vascular outcomes among 1.4 million participants in a multi-ancestry meta-analysis. Nat Genet. 2020;52(7):680-91.

[7] Zhou W, Sailani MR, Contrepois K, Zhou Y, Ahadi S, Leopold SR, et al. Longitudinal multi-omics of host-microbe dynamics in prediabetes. Nature. 2019;569(7758):663-71.

[8] Lloyd-Price J, Mahurkar A, Rahnavard G, Crabtree J, Orvis J, Hall AB, et al. Erratum: Strains, functions and dynamics in the expanded Human Microbiome Project. Nature. 2017;551(7679):256.

[9] Beaumont M, Goodrich JK, Jackson MA, Yet I, Davenport ER, Vieira-Silva S, et al. Heritable components of the human fecal microbiome are associated with visceral fat. Genome Biol. 2016;17(1):189.

[10] Gilbert JA, Quinn RA, Debelius J, Xu ZZ, Morton J, Garg N, et al. Microbiome-wide association studies link dynamic microbial consortia to disease. Nature. 2016;535(7610):94-103.

[11] Pinna NK, Anjana RM, Saxena S, Dutta A, Gnanaprakash V, Rameshkumar G, et al. Trans-ethnic gut microbial signatures of prediabetic subjects from India and Denmark. Genome Med. 2021;13(1):36.

[12] Arneth B, Arneth R, Shams M. Metabolomics of Type 1 and Type 2 Diabetes. Int J Mol Sci. 2019;20(10).

[13] Huth C, von Toerne C, Schederecker F, de Las Heras Gala T, Herder C, Kronenberg F, et al. Protein markers and risk of type 2 diabetes and prediabetes: a targeted proteomics approach in the KORA F4/FF4 study. Eur J Epidemiol. 2019;34(4):409-22.

[14] Juvinao-Quintero DL, Marioni RE, Ochoa-Rosales C, Russ TC, Deary IJ, van Meurs JBJ, et al. DNA methylation of blood cells is associated with prevalent type 2 diabetes in a meta-analysis of four European cohorts. Clin Epigenetics. 2021;13(1):40.

[15] Overmyer KA, Rhoads TW, Merrill AE, Ye Z, Westphall MS, Acharya A, et al. Proteomics, Lipidomics, Metabolomics, and 16S DNA Sequencing of Dental Plaque From Patients With Diabetes and Periodontal Disease. Mol Cell Proteomics. 2021;20:100126.

[16] Jihad M, Yet I. Multiomics Integration at Single-Cell Resolution Using Bayesian Networks: A Case Study in Hepatocellular Carcinoma. OMICS. 2023;27(1):24-33.

[17] Kang M, Ko E, Mersha TB. A roadmap for multi-omics data integration using deep learning. Brief Bioinform. 2022;23(1).

[18] Albaradei S, Thafar M, Alsaedi A, Van Neste C, Gojobori T, Essack M, et al. Machine learning and deep learning methods that use omics data for metastasis prediction. Comput Struct Biotec. 2021;19:5008-18.

[19] Tran KA, Kondrashova O, Bradley A, Williams ED, Pearson JV, Waddell N. Deep learning in cancer diagnosis, prognosis and treatment selection. Genome Med. 2021;13(1):152.

[20] Joshi A, Rienks M, Theofilatos K, Mayr M. Systems biology in cardiovascular disease: a multiomics approach. Nat Rev Cardiol. 2021;18(5):313-30.

[21] Snyder M. iPOP and its role in participatory medicine. Genome Med. 2014;6(1):6.

[22] Pedregosa F, Varoquaux G, Gramfort A, Michel V, Thirion B, Grisel O, et al. Scikit-learn: Machine Learning in Python. J Mach Learn Res. 2011;12:2825-30.

[23] Wickham H. ggplot2: Elegant Graphics for Data Analysis. Springer-Verlag New York2016.

[24] Sarica A, Cerasa A, Quattrone A. Random Forest Algorithm for the Classification of Neuroimaging Data in Alzheimer's Disease: A Systematic Review. Front Aging Neurosci. 2017;9:329.

[25] Zhao X, Fritsche J, Wang J, Chen J, Rittig K, Schmitt-Kopplin P, et al. Metabonomic fingerprints of fasting plasma and spot urine reveal human pre-diabetic metabolic traits. Metabolomics. 2010;6(3):362-74.

[26] Huang Y, Cai L, Liu X, Wu Y, Xiang Q, Yu R. Exploring biomarkers and transcriptional factors in type 2 diabetes by comprehensive bioinformatics analysis on RNA-Seq and scRNA-Seq data. Ann Transl Med. 2022;10(18):1017.

[27] Taneera J, Lang S, Sharma A, Fadista J, Zhou Y, Ahlqvist E, et al. A systems genetics approach identifies genes and pathways for type 2 diabetes in human islets. Cell Metab. 2012;16(1):122-34.

acta medica

# Flaps of the abdominal wall

Alaz Çırak[1]
ORCID: 0000-0002-8025-6844

Gökhan Sert[1]
ORCID: 0000-0002-8005-5049

Galip Gencay Üstün[1]
ORCID: 0000-0002-3538-1152

Hakan Uzun[1]
ORCID: 0000-0002-7584-3833

◦◦◦◦ A B S T R A C T ◦◦◦◦

Objective: The deep inferior epigastric artery perforator (DIEP) and transverse-vertical rectus abdominis myocutaneous (TRAM, VRAM) flaps are derived from the anterior abdominal wall and can be free or pedicled. This study aimed to analyze the differences in postoperative complication rates among various types of abdominal flaps and to assess the impact of chemotherapy (CT) and radiotherapy (RT) on surgical outcomes.

Materials and Methods: A retrospective study was conducted, analyzing abdominal flap operations performed between 2016 and 2023. Data on demographics, defect location, mesh use, and postoperative chemo-radiotherapy were collected. Quantitative variables were evaluated as means, minimum-maximum values, and categorical variables were assessed as percentages.

Results: A total of 37 patients underwent 38 operations. Of these, nine patients had pedicled TRAM flaps, 16 had free-TRAM flaps, 6 had free DIEP flaps, and 6 had VRAM flaps. The defect locations were predominantly for breast reconstruction (81.08%), followed by head and neck (8.1%), extremity (8.1%), and thoracic wall (2.7%). The overall donor site complication rate was 5.4%, and the flap site complication rate was 13.51%. The lowest donor site complications were observed in the free-TRAM and VRAM groups (0%), while the highest were in the DIEP group (16.66%). The lowest flap site complication rate was 0% in the free-TRAM group, and the highest was 33.33% in the VRAM group. Donor site complication rates were similar between the mesh-used (5.88%) and non-mesh-used (5%) groups. All donor site complications occurred in patients who received postoperative CT and RT.

Conclusion: Abdominal flaps were primarily utilized for breast reconstruction. The free-TRAM group exhibited the lowest donor and flap site complication rates, while the DIEP group had the highest donor site complication rates. Mesh use did not affect donor site complication rates. Postoperative administration of CT and RT was associated with increased donor site complications.

Keywords: Abdominal Wall, Free Tissue Flaps, Microsurgery, Musculocutaneous Flap, Pedicled Flap, Perforator Flap.

[1] Department of Plastic Reconstructive and Aesthetic Surgery, Faculty of Medicine, Hacettepe University, Ankara, Türkiye

Corresponding Author: Alaz Çırak
E-mail: cirakalaz@gmail.com

## INTRODUCTION

The abdominal wall has been used as a flap donor site to reconstruct various defects. Flaps harvested from the abdominal wall have been used mainly in autologous breast reconstruction; nevertheless, the abdominal wall can be used in many oncologic, traumatic, or various settings such as head and neck [1,2], upper [3] and lower [4] extremity, gynecological [5,6] and penoscrotal reconstruction [7]. The rectus abdominis myocutaneous (RAM) flap was first defined by Mathes and Bostwick in 1977 [8, 9]. Later, in 1979, Robbins described the pedicled vertically oriented RAM (VRAM) flap for breast reconstruction [10]. Holmström, in 1979, described essentially the transversely oriented RAM (TRAM) flap [11]. Later, in 1982, Hartrampf described a pedicled TRAM flap [12]. In order to decrease donor site morbidity and to reduce the muscle bulk, the deep inferior epigastric artery perforator (DIEP) flap was described in 1989 by Koshima and Soeda for defects in the groin and oral cavity [13] and in 1994 by Allen and Treece for breast reconstruction [14].

Abdominal flaps are versatile and trustworthy but bear certain complication risks. Complications can be observed related to the flap site or donor site. Microvascular complications and other flap site complications are generally related to primary complications, and donor site complications are frequently underreported. Following the removal or damage of the rectus abdominis muscle, its nerves and fascia, or intercostal nerves, the abdominal wall is weakened [15], and abdominal bulges or hernias can occur. Multiple studies have shown that regarding donor site complication rates, the TRAM flap has the highest rates, while the DIEP flap has the lowest rates. However, differences regarding microvascular and flap-related complications among various abdominal flaps remain controversial [15,16].

This study analyzed abdominal flap operations performed in a single clinic. Patient characteristics, defect location, timing of the reconstruction surgery, postoperative treatment, and postoperative complication rates were investigated. We aimed to demonstrate differences between postoperative complication rates of different types of flaps and show the effect of chemotherapy and radiotherapy on surgical outcomes.

## MATERIALS AND METHODS

A retrospective analysis was conducted on abdominal flap procedures performed between 2016 and 2023, totaling 37 operations. Demographic data, comorbidities, defect locations, and donor site closure techniques (including using meshes) were recorded. Additionally, postoperative chemotherapy and radiotherapy records were analyzed for patients with primary malignant diseases.

### Exclusion criteria

Immediate breast reconstruction cases were excluded from the analysis. Flaps from the anterior abdominal wall other than TRAM, DIEP, and VRAM, such as free superficial circumflex iliac artery perforator (SCIP) flaps or pedicled SCIP flaps, were also excluded. Flaps from the lateral or posterolateral abdominal wall were similarly excluded.

### Statistical analysis

Following data collection, variables were entered into the Statistical Package for Social Sciences for Windows SPSS 23.0 (IBM Corporation, Armonk, New York, United States). Pearson's chi-square test and Fisher's exact test were employed to evaluate categorical data (presence of complications). Quantitative variables were expressed as means, with minimum and maximum values noted. Categorical variables were presented as percentages. Analysis was conducted at a 95% confidence level, with p-values $< 0.05$ deemed statistically significant.

## RESULTS

Between 2016 and 2023, 37 patients underwent surgery involving 38 flaps. Among them, 30 patients underwent breast reconstruction, while three patients each underwent head & neck and extremity reconstruction, and one patient underwent chest wall reconstruction. The flaps comprised 6 DIEP, 25 TRAM, and 6 VRAM flaps. The mean age of the 37 patients was 46.1 years, ranging from 20 to 63. The average hospitalization duration was 12 days, ranging from 5 to 90 days. Out of 37 operations, two donor site-related complications (5.4%) and five flap-related complications (13.51%)

were observed. Of the patients, 24 (64.86%) received adjuvant postoperative radiotherapy (RT), and 30 (81.08%) received postoperative chemotherapy (CT). Information regarding mesh use during donor site closure revealed that polypropylene mesh was used in 17 operations (45.94%) while not in the remaining 20 operations (54.05%). Patient data is summarized in Table 1.

Nine of the 25 TRAM flaps were pedicled, and 16 were free flaps. All pedicled TRAM flaps were supercharged with an additional vein anastomosis (superficial inferior epigastric vein to cephalic vein). Among pedicled TRAM patients, one was bilateral, while others were unilateral. The average age at surgery was 44.5 years, and the average hospitalization duration was 8.8 days. Mesh was used during donor site closure in 5 patients (55.55%) and not in 4 patients (44.44%). Complications in pedicled TRAM flaps included donor site dehiscence (11.11%), microvascular complications necessitating revision surgery (11.11%), and flap site dehiscence treated with a pedicled latissimus dorsi myocutaneous flap (11.11%). Among patients in the pedicled TRAM group, 77.77% received adjuvant postoperative RT, and 88.88% received adjuvant postoperative CT.

Fifteen free TRAM flap surgeries were performed for breast reconstruction, and one was performed for upper extremity reconstruction due to a traumatic arm defect. The average patient was 44.7 years, and the mean hospitalization duration was 9.12 days. Mesh was used during closure of the donor site in 8 patients (50%) and not in the other eight patients (50%). No postoperative complications were observed. Among patients who underwent free TRAM flap surgery, 10 (62.5%) received postoperative adjuvant RT, and 13 (81.25%) received adjuvant CT.

All six free DIEP flaps performed were for breast reconstruction. The average patient was 50.1 years, and the mean hospitalization duration was eight days. Mesh was not used during the donor site closure for any DIEP flap patients. Complications included early postoperative microvascular complications necessitating venous re-anastomosis (16.66%) and late-term donor site complications, such as umbilical hernia (16.66%). Three patients

(50%) received RT postoperatively, and five (83.3%) received CT.

All VRAM flaps were performed for non-breast reconstruction purposes, with 3 for head and neck, 2 for extremity, and 1 for anterior thoracic wall reconstruction. The mean patient age during surgery was 48.1 years, and the mean hospitalization duration was 28.5 days. Mesh was used during closure of the donor site in 4 patients (66.66%) and not in 2 patients (33.33%). Flap site complications were observed in 2 patients (33.33%). One patient developed scalp dehiscence following reconstruction with a free VRAM flap, treated with a scalp rotation flap. Another patient experienced postoperative venous thrombosis and microcirculatory failure, leading to flap loss despite revision attempts. Four patients (66.66%) received postoperative chemo-radiotherapy.

Complication rates among different flap types revealed that free TRAM flaps had the lowest complication rates (0%), with all other types sharing a similar rate of no complications (66.66%). Details of flap types and complication rates are provided in Table 2.

The correlation between complication rates and mesh use during donor site closure and the administration of postoperative adjuvant RT and CT treatments was analyzed. Details regarding mesh use and complication rates are provided in Table 3. Donor site complication rates were similar regarding mesh use during closure, at 5.88% among patients with mesh used during closure and 5% among those without.

Flap site complication rates were 8.33% among patients who received RT and 23.07% among those who did not. The correlation between complication rates and postoperative RT administration is detailed in Table 4.

The effect of CT on complication rates was investigated. Donor site complication rates were 6.66% among patients who received CT and 0% among those who did not. Flap site complication rates were 10% among patients who received CT and 28.57% among those who did not. The correlation between complication rates and postoperative CT administration is outlined in Table 5.

**Table 1.** Flap types and patient characteristics

| | Patient Number | Age | Flap Site | Laterality | Postoperative Hospital Admission Length (days) | Mesh Use | Postoperative Complications | Adjuvant RT | Adjuvant CT |
|---|---|---|---|---|---|---|---|---|---|
| Pedicled TRAM (n=9) | 1 | 48 | Breast | Unilateral | 9 | None | None | Received | Received |
| | 2 | 45 | Breast | Unilateral | 6 | Used | None | None | Received |
| | 3 | 46 | Breast | Bilateral | 12 | Used | Dehiscence at the donor site | Received | Received |
| | 4 | 56 | Breast | Unilateral | 11 | Used | Dehiscence at flap site, reconstructed with pedicled latissimus dorsi flap | Received | Received |
| | 5 | 40 | Breast | Unilateral | 7 | None | None | None | Received |
| | 6 | 38 | Breast | Unilateral | 7 | None | None | Received | Received |
| | 7 | 45 | Breast | Unilateral | 11 | Used | Thrombosis at vein anastomosis | Received | Received |
| | 8 | 30 | Breast | Unilateral | 7 | None | None | Received | Received |
| | 9 | 53 | Breast | Unilateral | 10 | Used | None | Received | None |
| Free TRAM (n=16) | 10 | 43 | Breast | Unilateral | 7 | Used | None | Received | Received |
| | 11 | 55 | Breast | Unilateral | 7 | None | None | None | None |
| | 12 | 32 | Breast | Unilateral | 8 | None | None | Received | Received |
| | 13 | 49 | Breast | Unilateral | 8 | Used | None | None | Received |
| | 14 | 43 | Breast | Unilateral | 7 | Used | None | Received | Received |
| | 15 | 52 | Breast | Unilateral | 9 | None | None | None | None |
| | 16 | 45 | Breast | Unilateral | 9 | Used | None | Received | Received |
| | 17 | 46 | Breast | Unilateral | 11 | None | None | Received | Received |
| | 18 | 37 | Breast | Unilateral | 9 | None | None | Received | Received |
| | 19 | 39 | Arm | Unilateral | 26 | None | None | None | None |
| | 20 | 43 | Breast | Unilateral | 9 | Used | None | Received | Received |
| | 21 | 45 | Breast | Unilateral | 9 | Used | None | None | Received |
| | 22 | 42 | Breast | Unilateral | 8 | None | None | None | Received |
| | 23 | 60 | Breast | Unilateral | 6 | Used | None | Received | Received |
| | 24 | 35 | Breast | Unilateral | 5 | Used | None | Received | Received |
| | 25 | 50 | Breast | Unilateral | 8 | None | None | Received | Received |
| VRAM (n=6) | 26 | 40 | Scalp | Unilateral | 12 | Used | Dehiscence at flap site, reconstructed with Scalp flap | None | None |
| | 27 | 63 | Thigh | Unilateral | 17 | Used | None | Received | Received |
| | 28 | 56 | Leg | Unilateral | 24 | Used | Flap loss due to thrombosis | None | None |
| | 29 | 63 | Face | Unilateral | 16 | None | None | Received | Received |
| | 30 | 20 | Skull base | Unilateral | 90 | None | None | Received | Received |
| | 31 | 47 | Chest Wall | Unilateral | 12 | Used | None | Received | Received |
| Free DIEP (n=6) | 32 | 55 | Breast | Unilateral | 6 | None | None | None | None |
| | 33 | 48 | Breast | Unilateral | 13 | None | Umbilical hernia | Received | Received |
| | 34 | 47 | Breast | Unilateral | 6 | None | None | Received | Received |
| | 35 | 51 | Breast | Unilateral | 10 | None | The postoperative venous appearance of a flap, venous thrombosis, treated vein re-anastomosis | None | Received |
| | 36 | 46 | Breast | Unilateral | 6 | None | None | Received | Received |
| | 37 | 54 | Breast | Unilateral | 9 | None | None | None | Received |

**Table 2.** Flap types and complication rates

| | | Complication | | | Total |
| --- | --- | --- | --- | --- | --- |
| | | Donor site | Flap Site | None | |
| Flap Type | Pedicled TRAM (%) | 1 (11,11%) | 2 (22,22%) | 6 (66,66%) | 9 (100,00%) |
| | Free TRAM (%) | 0 (0,00%) | 0 (0,00%) | 16 (100,00%) | 16 (100,00%) |
| | DIEP (%) | 1 (16,66%) | 1 (16,66%) | 4 (66,66%) | 6 (100,00%) |
| | VRAM (%) | 0 (0,00%) | 2 (33,33%) | 4 (66,66%) | 6 (100,00%) |
| Total (%) | | 2 (5,40%) | 5 (13,51%) | 30 (81,08%) | 37 (100,00%) |

**Table 3.** Mesh use and complication rates

| | | Complication | | | Total |
| --- | --- | --- | --- | --- | --- |
| | | Donor Site | Flap Site | None | |
| Mesh | Used (%) | 1 (5,88%) | 4 (23,52%) | 12 (70,58%) | 17 (100%) |
| | Not Used (%) | 1 (5,00%) | 1 (5,00%) | 18 (90,00%) | 20 (100%) |
| Total (%) | | 2 (5,40%) | 5 (13,51%) | 30 (81,08%) | 37 (100%) |

**Table 4.** Adjuvant RT administration and complication rates

| | | Complication | | | Total |
| --- | --- | --- | --- | --- | --- |
| | | Donor Site | Flap Site | None | |
| Adjuvant RT | Used (%) | 2 (8,33%) | 2 (8,33%) | 20 (83,33%) | 24 (100%) |
| | Not Used (%) | 0 (0,00%) | 3 (23,07%) | 10 (76,92%) | 13 (100%) |
| Total (%) | | 2 (5,40%) | 5 (13,51%) | 30 (81,08%) | 37 (100%) |

**Table 5.** Adjuvant CT administration and complication rates

| | | Complication | | | Total |
| --- | --- | --- | --- | --- | --- |
| | | Donor Site | Flap Site | None | |
| Adjuvant CT | Used (%) | 2 (6,66%) | 3 (10,00%) | 25 (83,33%) | 30 (100%) |
| | Not Used (%) | 0 (0,00%) | 2 (28,57%) | 5 (71,42%) | 7 (100%) |
| Total (%) | | 2 (5,40%) | 5 (13,51%) | 30 (81,08%) | 37 (100%) |

## DISCUSSION

Abdominal flaps represent a cornerstone in autologous breast reconstruction [17,18], recognized for their superior outcomes in terms of patient satisfaction [19]. In our series, the majority of cases involved breast reconstruction (81.08%). Nearly all non-breast reconstruction procedures (83.33%) comprised VRAM flaps, historically serving as primary agents for perineal and thigh reconstruction [4,20]. VRAM cases in our investigation reveal applications in head and neck reconstruction and the reconstruction of extremities and the chest wall.

Our study's overall incidence of complications stands at 5.40% for donor site complications and 13.51% for flap site complications. Remarkably, 81.08% of patients remained complication-free. Donor site complications primarily manifested as early local wound dehiscence and late-term bulges or hernias. Among these, pedicled TRAM flaps exhibited a donor site complication rate of 11.11%, while the highest incidence, 16.66%, was observed in DIEP flaps. Notably, free-TRAM and VRAM groups displayed no instances of bulges or hernias. Literature suggests that muscle-sparing techniques, such as DIEP or muscle-sparing-TRAM flaps, yield fewer donor site complications due to preserving abdominal wall integrity [21, 22]. However, our findings indicate the lowest donor site complication rates within the free-TRAM and VRAM groups. Nonetheless, bilateral TRAM flap operations, as previously reported, correlated with increased donor site complications [23].

The flap site complication rate of 13.51% aligns with prior investigations [23,24]. Specifically, VRAM flaps exhibited a 33.33% complication rate, followed by p-TRAM (22.22%), DIEP (16.66%),

and free-TRAM (0%) groups. Notably, free TRAM flaps demonstrated the lowest incidence of flap site complications, consistent with earlier studies [25,26]. Past research highlights DIEP flaps' susceptibility to fat necrosis, opposing free-TRAM flaps' resilience [27]. TRAM flaps have historically demonstrated lower flap site complication rates than DIEP flaps [24,28]. Conversely, pedicled flaps appear as the least prone to complications among autologous breast reconstruction options [29,30].

The use of mesh correlates with reduced donor site complications, such as bulging or herniation [31-34]. While prior studies emphasize mesh effectiveness, they suggest that fascial grafts are not essential for safety [35]. Nevertheless, some studies report comparable postoperative bulging or herniation rates between mesh-utilized and non-utilized groups [23]. In our investigation, donor site complication rates were similar between the two groups, at 5.88% in the mesh-utilized and 5% in the non-utilized cohorts.

Breast cancer treatment, apart from surgery, includes chemotherapy (CT) and radiotherapy (RT) based on disease characteristics [36]. CT has been associated with wound dehiscence [37], while post-mastectomy microvascular breast reconstruction under CT regimens is linked to increased complications, particularly fat necrosis [38]. Postoperative RT has also been associated with adverse surgical outcomes [39]. The optimal timing of CT or RT with surgery remains abstract about complication rates [40]. In our series, 64.86% of patients received adjuvant postoperative RT, and 81.08% received postoperative CT. Increased complication rates were expected due to the high CT and RT administration rates. Indeed, our analysis revealed that all patients (n=2) who experienced donor site complications were administered both CT and RT postoperatively, confirming prior evidence linking CT and RT with postoperative complications.

Conversely, our investigation examined the correlation between RT and flap site complications, revealing a complication rate of 8.33% in the RT group versus 23.97% in the RT non-administered group. Similarly, analysis of CT's correlation with complications demonstrated 10% and 28.57% flap site complication rates for the CT-administered and

non-administered groups, respectively. However, statistical significance was not established across all cross-tables due to insufficient patient counts.

This study is not without limitations. A retrospective study design limits the depth of analysis, while the small patient cohort limits statistical significance. Future prospective studies with larger patient cohorts are necessary to clarify differences in complication rates among various abdominal flap techniques.

## CONCLUSION

Our findings reveal a donor site complication rate of 5.4% and a flap site complication rate of 13.51% across all operations. Free-TRAM and VRAM groups exhibited the lowest donor site complication rates (0%), while the highest rate was observed in the DIEP group (16.66%). The lowest flap site complication rate was observed in the free-TRAM group (0%), contrasting with the highest rate in the VRAM group (33.33%). Mesh utilization did not significantly impact donor site complication rates. Adjuvant postoperative CT and RT administration correlated with increased donor site complications, with all complications observed in patients receiving combined CT and RT.

### Author contribution

Study conception and design: GS, GU, HU; data collection: AC, GS, and GU; analysis and interpretation of results: AC, GS, GU, HU; draft manuscript preparation: AC, GS and GU. All authors reviewed the results and approved the final version of the manuscript.

### Ethical approval

The study was approved by the institutional review board (Protocol no. 2023/05-04).

### Conflict of interest

The authors declare that there is no conflict of interest.

~ɝɞ᷇ REFERENCES ᷇ɝɞ~

[1] Mayo-Yáñez M, Rodríguez-Pérez E, Chiesa-Estomba CM, et al. Deep inferior epigastric artery perforator free flap in head and neck reconstruction: A systematic review. J Plast Reconstr Aesthet Surg. 2021;74:718-29.

[2] Guinier C, de Clermont-Tonnerre E, Tay JQ, et al. The deep inferior epigastric artery perforator flap: a narrative review on its various uses in non-breast reconstruction. Ann Transl Med. 2023;11:130.

[3] Al-Qattan MM, Alammar AK, Alfaqeeh FA, et al. Pedicled abdominal flaps for hand reconstruction in adults: physiotherapy of the attached hand. Plast Reconstr Surg Glob Open. 2021;9:e3474..

[4] Banuelos J, Kreutz-Rodrigues L, Mills AM, et al. Vertical rectus abdominis myocutaneous flap to reconstruct thigh and groin defects: A retrospective cohort and systematic review. J Plast Reconstr Aesthet Surg. 2022;75:1893-1901.

[5] Caretto AA, Servillo M, Tagliaferri L, et al. Secondary post-oncologic vulvar reconstruction - a simplified algorithm. Front Oncol. 2023;13:1195580.

[6] Qiu SS, Jurado M, Hontanilla B. Comparison of TRAM versus DIEP flap in total vaginal reconstruction after pelvic exenteration. Plast Reconstr Surg. 2013;132:1020e-1027e.

[7] Boczar D, Huayllani MT, Saleem HY, et al. Surgical techniques of phalloplasty in transgender patients: A systematic review. Ann Transl Med. 2021;9:607.

[8] Mathes SJ, Bostwick J 3rd. A rectus abdominis myocutaneous flap to reconstruct abdominal wall defects. Br J Plast Surg. 1977;30:282-3.

[9] McMenamin DM, Clements D, Edwards TJ, et al. Rectus abdominis myocutaneous flaps for perineal reconstruction: modifications to the technique based on a large single-centre experience. Ann R Coll Surg Engl. 2011;93:375-81.

[10] Robbins TH. Rectus abdominis myocutaneous flap for breast reconstruction. Aust N Z J Surg. 1979;49:527-30.

[11] Holmström H. The free abdominoplasty flap and its use in breast reconstruction. An experimental study and clinical case report. Scand J Plast Reconstr Surg. 1979;13:423-7.

[12] Hartrampf CR, Scheflan M, Black PW. Breast reconstruction with a transverse abdominal island flap. Plast Reconstr Surg. 1982;69:216-25.

[13] Koshima I, Soeda S. Inferior epigastric artery skin flaps without rectus abdominis muscle. Br J Plast Surg. 1989;42:645-8.

[14] Allen RJ, Treece P. Deep inferior epigastric perforator flap for breast reconstruction. Ann Plast Surg. 1994;32:32-8.

[15] Macadam SA, Zhong T, Weichman K, et al. Quality of life and patient-reported outcomes in breast cancer survivors: A multicenter comparison of four abdominally based autologous reconstruction methods. Plast Reconstr Surg. 2016;137:758-71.

[16] Blondeel PN, Arnstein M, Verstraete K, et al. Venous congestion and blood flow in free transverse rectus abdominis myocutaneous and deep inferior epigastric perforator flaps. Plast Reconstr Surg. 2000;106:1295-9.

[17] Song Y, Zeng J, Tian X, et al. A review of different breast reconstruction methods. Am J Transl Res. 2023;15:3846-55.

[18] Borrero M, Hilaire HS, Allen R. Modern approaches to abdominal-based breast reconstruction. Clin Plast Surg. 2023;50:267-79.

[19] Stefura T, Rusinek J, Wątor J, et al. Implant vs. autologous tissue-based breast reconstruction: A systematic review and meta-analysis of the studies comparing surgical approaches in 55,455 patients. J Plast Reconstr Aesthet Surg. 2023;77:346-58.

[20] Radwan RW, Tang AM, Harries RL, et al. Vertical rectus abdominis flap (VRAM) for perineal reconstruction following pelvic surgery: A systematic review. J Plast Reconstr Aesthet Surg. 2021;74:523-9.

[21] Espinosa-de-Los-Monteros A, Frias-Frias R, Alvarez-Tostado-Rivera A, et al. Postoperative abdominal bulge and hernia rates in patients undergoing abdominally based autologous breast reconstruction: Systematic review and meta-analysis. Ann Plast Surg. 2021;86:476-84.

[22] Chang EI, Chang EI, Soto-Miranda MA, et al. Comprehensive analysis of donor-site morbidity in abdominally based free flap breast reconstruction. Plast Reconstr Surg. 2013;132:1383-91.

[23] Edalatpour A, Attaluri P, Shaffrey EC, et al. The nuances of abdominal free flap harvest: Technical and patient factors affecting abdominal donor site morbidity in autologous breast reconstruction. J Plast Reconstr Aesthet Surg. 2023;81:105-18.

[24] Sailon AM, Schachar JS, Levine JP. Free transverse rectus abdominis myocutaneous and deep inferior epigastric perforator flaps for breast reconstruction: A systematic review of flap complication rates and donor-site morbidity. Ann Plast Surg. 2009;62:560-3.

[25] Mortada H, AlNojaidi TF, AlRabah R, et al. Morbidity of the donor site and complication rates of breast reconstruction with autologous abdominal flaps: Systematic review and meta-analysis. Breast J. 2022;2022:7857158.

[26] Jeong W, Lee S, Kim J. Meta-analysis of flap perfusion and donor site complications for breast reconstruction using pedicled versus free TRAM and DIEP flaps. Breast. 2018;38:45-51.

[27] Khansa I, Momoh AO, Patel PP, et al. Fat necrosis in autologous abdomen-based breast reconstruction: A systematic review. Plast Reconstr Surg. 2013;131:443-52.

[28] Chun YS, Sinha I, Turko A, et al. Comparison of morbidity, functional outcome, and satisfaction following bilateral TRAM versus bilateral DIEP flap breast reconstruction. Plast Reconstr Surg. 2010;126:1133-41.

[29] Gart MS, Smetona JT, Hanwright PJ, et al. Autologous options for postmastectomy breast reconstruction: A comparison of outcomes based on the American College of Surgeons National Surgical Quality Improvement Program. J Am Coll Surg. 2013;216:229-38.

[30] Friedrich M, Krämer S, Friedrich D, et al. Difficulties of breast reconstruction - Problems that no one likes to face. Anticancer Res. 2021;41:5365-75.

[31] Leon DS, Nazerali R, Lee GK. Using mesh to reinforce the abdominal wall in abdominal free flaps for breast reconstruction: Is there a benefit? What are the risks? Ann Plast Surg. 2018;80:295-8.

[32] Wan DC, Tseng CY, Anderson-Dam J, et al. Inclusion of mesh in donor-site repair of free TRAM and muscle-sparing free TRAM flaps yields rates of abdominal complications comparable to those of DIEP flap reconstruction. Plast Reconstr Surg. 2010;126:367-74.

[33] Chatterjee A, Ramkumar DB, Dawli TB, et al. The use of mesh versus primary fascial closure of the abdominal donor site when using a transverse rectus abdominis myocutaneous flap for breast reconstruction: A cost-utility analysis. Plast Reconstr Surg. 2015;135:682-9.

[34] Kraft CT, Molina BJ, Skoracki RJ. Polypropylene mesh complications in the sublay position after abdominally based breast reconstruction. Plast Surg (Oakv). 2021;29:16-20.

[35] Kim SA, Kim D, Oh DY, et al. Analysis of 461 consecutive patients' donor site morbidity following abdominal tissue-based breast reconstruction without fascia reinforcement graft. Biomed Res Int. 2022;2022:7221203.

[36] Kerr AJ, Dodwell D, McGale P, et al. Adjuvant and neoadjuvant breast cancer treatments: A systematic review of their effects on mortality. Cancer Treat Rev. 2022;105:102375.

[37] Seth I, Bulloch G, Jennings M, et al. The effect of chemotherapy on the complication rates of breast reconstruction: A systematic review and meta-analysis. J Plast Reconstr Aesthet Surg. 2023;82:186-97.

[38] Olawoyin OM, Mehta S, Chouairi F, et al. Comparison of autologous breast reconstruction complications by type of neoadjuvant chemotherapy regimen. Plast Reconstr Surg. 2021;148:1186-96.

[39] El-Sabawi B, Sosin M, Carey JN, et al. Breast reconstruction and adjuvant therapy: A systematic review of surgical outcomes. J Surg Oncol. 2015;112:458-64.

[40] Saldanha IJ, Cao W, Broyles JM, et al. Breast reconstruction after mastectomy: A systematic review and meta-analysis. Rockville (MD): Agency for Healthcare Research and Quality (US); 2021.

acta medica

# Melatonin can mitigate H$_2$O$_2$-induced atrophy and promote muscle fiber hypertrophy in morphological level in mouse myoblast cell line[*]

Nazli Karimi Ahmadi[1]
ORCID: 0000-0002-3534-6621

Yasemin Kartal[1,2]
ORCID: 0000-0003-0112-2969

Murat Timur Budak[1]
ORCID: 0000-0002-5059-9651

[1] Department of Physiology, Faculty of Medicine, Hacettepe University, Ankara, Türkiye

[2] Department of Physiology, Faculty of Medicine, Kırklareli University, Kırklareli, Türkiye

*Our study was partially presented at the Turkish Society of Physiological Sciences 45th National Physiology Congress, held from 31 October to 3 November 2019 in Kuşadası-Aydın, titled 'Investigation of the Effect of Melatonin Administration on Calpain-1 Expression and Atrophic Morphology in a Mouse Myoblast Cell Line Exposed to Hydrogen Peroxide.

*Published as an abstract: 'Investigation of the Effect of Melatonin Administration on Calpain-1 Expression and Atrophic Morphology in a Mouse Myoblast Cell Line Exposed to Hydrogen Peroxide,' by Nazli Karimi, Yasemin Kartal, and Murat Timur Budak. Acta Physiologica, 2019 (Abstract) | WOSUID: WOS:000532415800059.

Corresponding Author: Nazli Karimi Ahmadi
E-mail: nkarimi@hacettepe.edu.tr

∽◌◠◠ A B S T R A C T ◠◠◌∽

Objective: It is known that oxidative stress is the main factor in the formation of disuse muscle atrophy which is the most common type of muscle atrophy. The utilization of antioxidants as supplements, particularly the category known as mitochondrial targeting antioxidants (MTA), such as melatonin, have demonstrated significant potential as an advanced therapeutic approach. In this study, we aimed to investigate the effect of melatonin application on the cellular morphology of the C2C12 cell line.

Materials and Methods: In our experiment, we induced oxidative stress using hydrogen peroxide (H$_2$O$_2$) to create a model of skeletal muscle atrophy. We established four distinct groups of C2C12 cells, all exposed to the same conditions. These groups included Control (C), Melatonin (M), H$_2$O$_2$ (H), and Melatonin + H$_2$O$_2$ (MH). The aim was to examine morphological features, specifically myotube diameters, to assess atrophy.

Results: The analysis revealed significant differences in diameters among the groups (p < 0.05). The melatonin treatment group not only showed a mitigation of diameter change due to atrophy but also exhibited a significant increase in diameter.

Conclusion: The results suggest that H$_2$O$_2$ induces muscle atrophy, and melatonin plays a dual role in maintaining muscle health, protecting against atrophy and promoting hypertrophy, particularly at the morphological level. However, additional research is needed to figure out the details of underlying mechanisms.

Keywords: Melatonin, mitochondria targeted antioxidants, morphological level, H2O2-Induced muscle Atrophy.

## INTRODUCTION

Muscle mass accounts for approximately 40-50% of the total body weight in healthy adult humans and plays a crucial role in regulating metabolism in mammals. Skeletal muscle exhibits a highly organized structure that facilitates motion and generates mechanical tension (1). Muscle atrophy, defined as the involuntary loss of 5-10% of muscle mass, involves a reduction in organelles, proteins, and cytoplasm within muscle cells. Consequently, fiber diameter, strength production, and resistance to fatigue are all reduced. This type of atrophy can occur in various pathological conditions such as denervation, AIDS, cancer, and also during the aging process (2). Moreover, the decline in muscle mass can compromise the efficacy of diverse treatments. Consequently, it is essential to conduct molecular studies focused on preventing and managing muscle atrophy or alleviating its effects (3). Additionally, muscle disuse without underlying diseases can also lead to skeletal muscle atrophy (4). The excessive breakdown of proteins in skeletal muscles, coupled with the subsequent decrease in muscle mass, results in increased morbidity and mortality due to both functional losses and impaired energy metabolism (2). Skeletal muscles not only contribute to physical performance but also play a vital role in maintaining overall health across the lifespan. They are actively involved in various metabolic pathways that impact overall well-being. For instance, skeletal muscles are crucial for insulin-dependent glucose uptake, making them essential for maintaining glucose homeostasis (5). Moreover, these muscles play a significant role in metabolic functions such as fatty acid metabolism and glycogen synthesis. Consequently, metabolic disorders affecting skeletal muscles can contribute to insulin resistance, metabolic syndrome, and obesity (6). The structure and functional characteristics of skeletal muscles adapt to meet the body's demands. Changes in metabolic requirements, such as exercise or inactivity, can initiate alterations in muscle mass. Due to the limited capacity for muscle cell proliferation, the regulation of muscle size relies on maintaining a delicate balance between protein synthesis and protein breakdown. Intense mechanical load or stimulation by anabolic hormones shifts this balance towards protein synthesis, resulting in hypertrophy characterized by an increase in fiber diameter. In contrast, under catabolic conditions where protein breakdown surpasses protein synthesis, it results in muscle weakness and atrophy (3). Increased production of reactive oxygen species (ROS) resulting from oxidative stress has been identified as a significant factor in the development of various diseases (7). The association between ROS and disuse-related atrophy was first identified in 1991. Subsequent studies over the past two decades have consistently confirmed this link (8, 9). In skeletal muscle, oxidative stress serves as a well-established mechanism that triggers atrophy, involving multiple conditions and proteolytic processes (10,11). Research suggests that increased production of ROS and impaired redox signaling in skeletal muscle fibers activate major proteolytic systems, initiating wasting (12). Elevated ROS production is primarily observed in the mitochondria of underused muscles (13). Disuse muscle atrophy induces substantial changes in the morphology, function, and content of mitochondria through the activation of catabolic pathways, directly affecting ROS production (3). In order to preserve mitochondrial morphology and function, a variety of antioxidant agents specifically targeting mitochondria have been synthesized (14) and extensively examined for their efficacy in this regard (15). However, none of these approaches have proven unsatisfactory results mainly due to the limited permeability of the mitochondrial membrane requiring substances to be transported through transmembrane carrier systems. Successful synthetic agents targeting mitochondria, like coenzyme Q10 (MitoQ) and mitochondria-targeted vitamin E (MitoE), overcome these membrane barriers by attaching a lipophilic cation, allowing for significant accumulation within mitochondria (16). Certain substances present in our body possess a unique structure that allows them to accumulate within the mitochondria and act as mitochondria-targeted antioxidants (MTAs). Melatonin is one of the most significant examples, which was isolated and identified by Lerner in 1958(17). According to the findings, melatonin has a stronger protective effect compared to MitoQ and MitoE. Additionally, there is evidence that melatonin is present in high levels inside mitochondria and is even produced by mitochondria themselves (14).

Melatonin's mitochondrial protective effects involve several mechanisms: It acts as a potent radical

scavenger, increases the expression of antioxidant genes, such as superoxide dismutase and glutathione peroxidase.It affects the mitochondrial permeability transition pores (MPTP), preventing the formation of active caspase-3 and apoptosis. and enhances the activity and gene expression of uncoupling proteins (UCPs) leading to reduced ROS production (18). Studies indicate melatonin enhances antioxidant capacity and upregulates antioxidant gene expression in myoblast cells (19).

Experimental models utilizing $H_2O_2$ have been extensively used in both in vitro and in vivo studies to explore disuse atrophy (20-22). $H_2O_2$ -induced oxidative stress upregulates atrogenes, encoding muscle proteases, while concurrently inhibiting protein synthesis at transcription and translation stages. This dual effect reduces the production of new proteins in muscle cells, impairing muscle growth and maintenance. Oxidative stress increases the susceptibility of oxidized proteins to proteolysis, as structural alterations make them more prone to proteolysis, exacerbating muscle atrophy (23). $H_2O_2$ is used to study disuse atrophy models in the C2C12 cell line, derived from myoblasts in the thigh muscles of C3H mice (24). C2C12 cells easily multiply in high-serum conditions. Yet, when they reach over 80% confluence and come into contact, they undergo differentiation during the shift to low-serum media. and have the capacity to form contractile myotubes and characteristic muscle proteins (25). Due to their pure cell line nature, rapid differentiation ability, and the ability to form contractile muscle fibers, make them a preferred choice for in vitro models of muscle diseases.

In this study, we investigated the effectiveness of melatonin in addressing oxidative stress and its impact on muscle atrophy. Specifically, we aimed to examine how melatonin administration influences the morphological changes of the C2C12 cell line exposed to $H_2O_2$.

## MATERIAL AND METHODS

### Cultured myogenic cell line

The C2C12 mouse myoblast cell line from the American Type Culture Collection (ATCC) was cultured in Dulbecco's Modified Eagle's Medium (DMEM) with 20% Fetal Bovine Serum (FBS), 2% L-Glutamine, and 1% streptomycin+penicillin

during proliferation at 37°C with 5% CO2 (26). Upon reaching 80% density, cells were transitioned to differentiation medium (DMEM, 2% heat-inactivated horse serum, 1% streptomycin+penicillin, and 1% L-Glutamine) and allowed to differentiate for 7 days growth and myotube formation were observed using a light microscope (27).

### Determination of half-maximal inhibitory concentration (IC50) for melatonin and $H_2O_2$

For cytotoxicity assessment and dosage optimization of $H_2O_2$ and melatonin treatments on the C2C12 cell line, we utilized the Vybrant MTT Cell Proliferation Assay Kit (28). $H_2O_2$ was administered at varying concentrations (0.025 mM, 0.05 mM, 0.1 mM, and 0.2 mM) and durations (4, 24, 48, and 72 hours). Melatonin treatments included different concentrations (0.001 mM, 0.05 mM, 0.1 mM, 0.5 mM) for a 24-hour duration (29). Upon determining IC50 values and confirming compatibility with literature, the study progressed with the identified optimal concentrations.

### Experimental protocol

After necessary optimizations and determining optimal concentrations, the procedure was implemented with the identified concentrations. The study groups were as follows: control (C) group, melatonin (M) group, $H_2O_2$, (H) group, melatonin and $H_2O_2$ (MH) group. Melatonin and $H_2O_2$ treatments, consistent with MTT assay results and literature, were applied during differentiation. On the 4th day of differentiation, melatonin (0.1 mM, 24 hours) was administered to the M and MH groups. On the 5th day, $H_2O_2$ (0.05 mM, 24 hours) was applied to the H and MH groups.

### Myotube diameter measurement

Myotube thickness was measured using the method described by Van der Meijden et al. (30). Measurements were taken on the 7th day of differentiation using an inverted microscope (Nikon, ECLIPSE TS100). We captured images using a Toupcam Digital Camera (TOUPTEK PHOTONICS, P/N: TP105100A) and used the ToupView 3.7 software program (Toup Tek-Toup View, Version: x64, 3.7.4460). Evaluations of myotube diameters were performed using the ImageJ (NIH) program. In the ImageJ program, the scale length was defined as 200 μm, and measurements were calculated based on this scale. The length of each myotube

segment was considered 100% and divided into 10 equal parts. These parts, representing the cross-sectional (length) equivalent and cross-sectional angles (using the image frame as a reference), were created using the program.

After all calculations were made, the average length of the cross-sections was taken, and the overall average was considered the group average. Figure 1 explains how the Image J program was used to measure the diameter of myotubes.

## Statistical analysis

Statistical analysis employed GraphPad Prism 6 (GraphPad Software, La Jolla, California, USA, www.graphpad.com). Descriptive statistics, mean ± SD deviation was utilized. Group comparisons utilized ANOVA, and Pearson correlation analysis was conducted. A significance level of $p \leq 0.05$ indicated statistical significance.

## RESULTS

### MTT method results

The melatonin concentrations used in the MTT method and the corresponding cell viability percentages are provided in Table 1.

Based on MTT assay results, it was demonstrated that C2C12 cells exposed to 0.1 mM melatonin for 24 hours maintained 95.72% viability which was suitable for our experimental protocol.
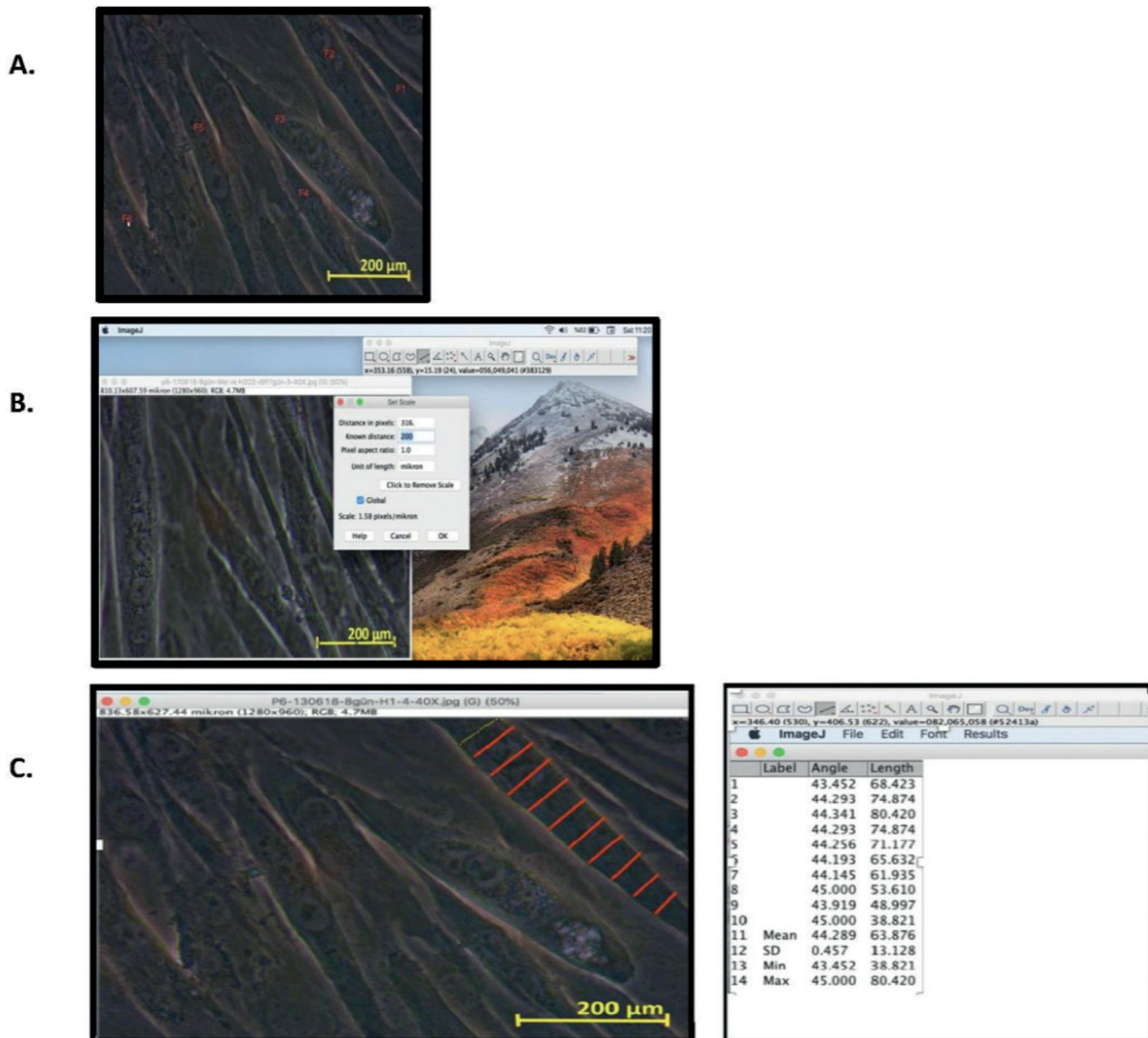


**Figure 1.** At 7th day of differentiation, myotube segments with clearly defined boundaries were selected and numbered in each microscope field 40X magnification **(A)**. 200µm scale bar displayed in the ImageJ program **(B).**Measurements displayed on the ImageJ program screen **(C)**.

**Table 1.** The melatonin concentrations and cell viability percentages at 24h

| Melatonin (mM) | 10 | 5 | 1 | 0.1 | 0.01 |
|---|---|---|---|---|---|
| Viability * % | 15.58 | 50.54 | 100 | 95.72 | 97.74 |

* viability rates were calculated as a percentage relative to the control.

**Table 2.** The $H_2O_2$ concentrations and cell viability percentages at 24h

| $H_2O_2$ (mM) | 1 | 0.5 | 0.1 | 0.05 | 0.001 |
|---|---|---|---|---|---|
| Viability * % | 12.80 | 74.12 | 94.21 | 93.36 | 98.78 |

* viability rates were calculated as a percentage relative to the control.

The concentrations of $H_2O_2$ used in the MTT method and the resulting cell viability percentages are indicated in Table 2.

Based on MTT assay results, the cells exposed to 0.05 mM $H_2O_2$ for 24 hours showed 93.36% viability, which was deemed an appropriate dose.

## Comparing C2C12 cell morphology at different growth and differentiation stages in

### Experimental groups

All cell culture imaging was conducted using a Nikon inverted objective microscope under normal light conditions and processed with the Toupview software. Representative examples of the typical proliferation and differentiation patterns of the C2C12 cells used are shown in Figure 2.

Most cells were observed to differentiate into myotubes as expected. The morphology of C2C12 cells in groups (C), (M), (H) and (MH) on the 7th day of differentiation are shown at 10x and 40x magnifications in Figures 3, 4, 5, and 6, respectively.

The measurements taken from 9 different regions of each group in the Image J program, were transferred to Microsoft Excel. The average and standard deviation of the cross-sectional (length) equivalent and angular measurements for each myotube were calculated.

**Table 3.** Mean myotube diameter and standard deviation (± SD) by experimental group

| Group | Mean ± SD | p-values |
|---|---|---|
| C | 78.12 ± 7.61 | C-H: 0.0262, C-M: 0.0338 |
| H | 60.83 ± 6.89 | H-C: 0.0262, H-M: <0.0001, H-MH: 0.0005 |
| M | 94.78 ± 17.68 | M-C: 0.0338, M-H: <0.0001 |
| MH | 86.69 ± 13.60 | MH-H: 0.0005 |

C: Control; H: H2O2; M: Melatonin; MH: Melatonin +H2O2.

## Comparison of morphological measurement values among experimental groups

At the 7th day of cell differentiation in the experimental groups, the average myotube diameter measurements are illustrated in Figure 7.

The experimental group mean myotube diameter values, along with their respective standard deviations (SD), are detailed in Table 3. These values reveal the differences in mean myotube diameters across the experimental groups (p ≤ 0,000013).

The table displays the mean myotube diameters (± SD) for four experimental groups: C, M, H, and MH. These measurements were obtained through statistical analysis using One-way ANOVA and post-hoc Tukey's HSD test to assess differences between the groups. The p-values indicate the statistical significance of the inter-group differences in mean myotube diameters (p<0.05).
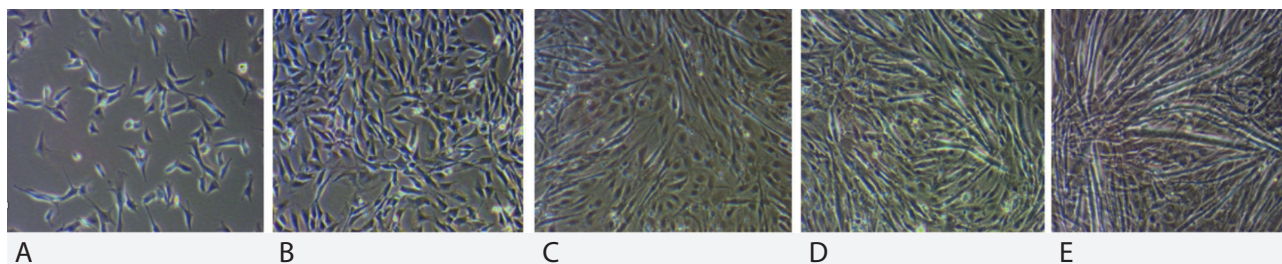


**Figure 2.** Proliferation of C2C12 Cells and Initiation of Their Differentiation Process. 30% density of cells **(A)**, 80% density of cells **(B)**, first day of differentiation **(C)**, second day of differentiation **(D)**, third day of differentiation **(E)**.
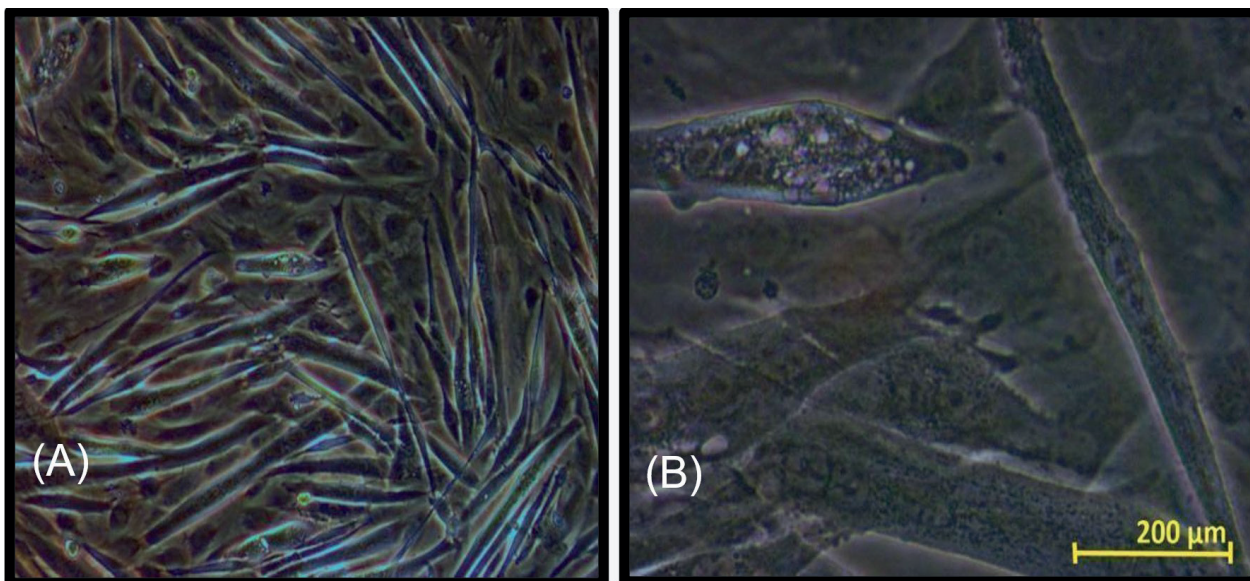
**Figure 3.** Group C at 10x magnification **(A)**, Group C is displayed at 40x magnification with a 200 μm scale bar **(B)**.
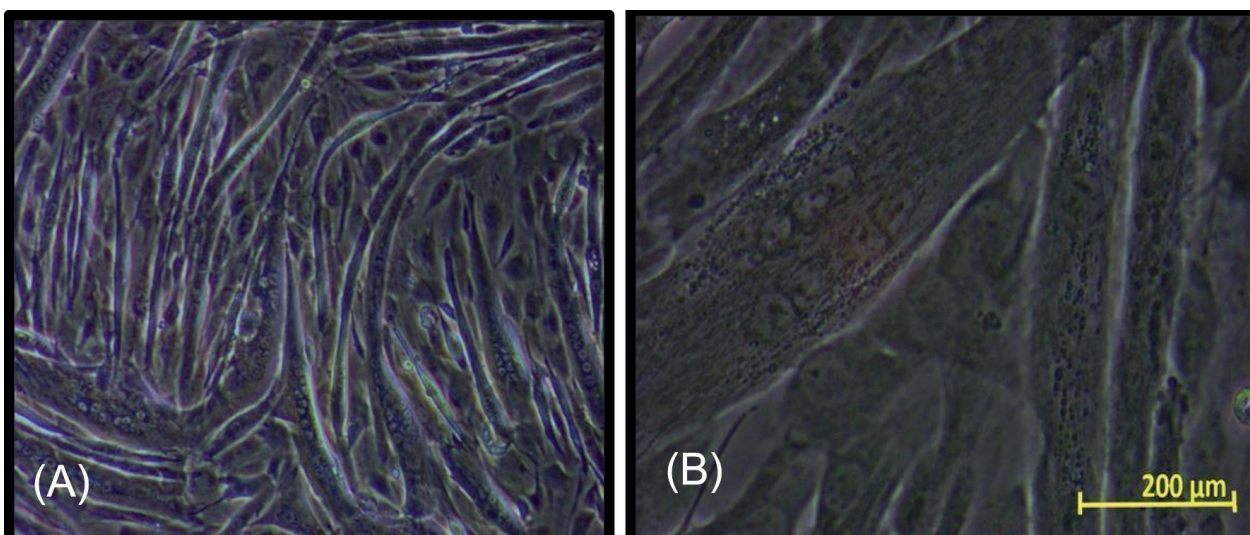


**Figure 4.** Group M at 10x magnification **(A)**, Group M is displayed at 40x magnification with a 200 μm scale bar **(B)**.
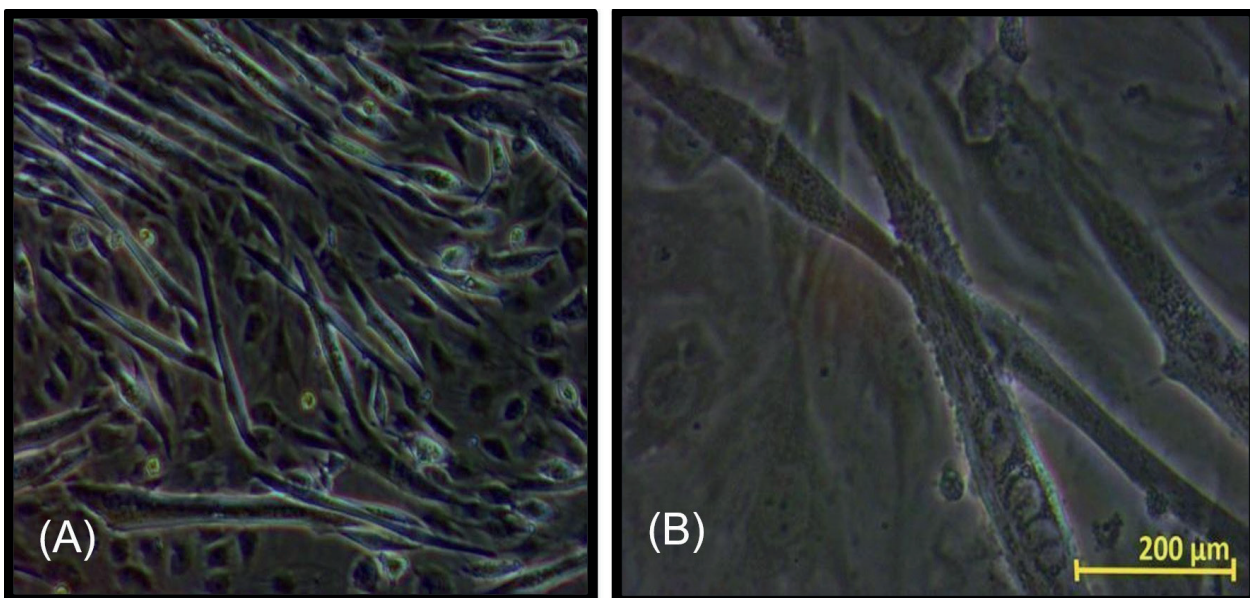


**Figure 5.** Group H at 10x magnification **(A)**, Group H is displayed at 40x magnification with a 200 μm scale bar **(B)**.

**Figure 6.** Group MH at 10x magnification **(A)**, Group MH at 40x magnification with a 200 µm scale bar **(B)**.
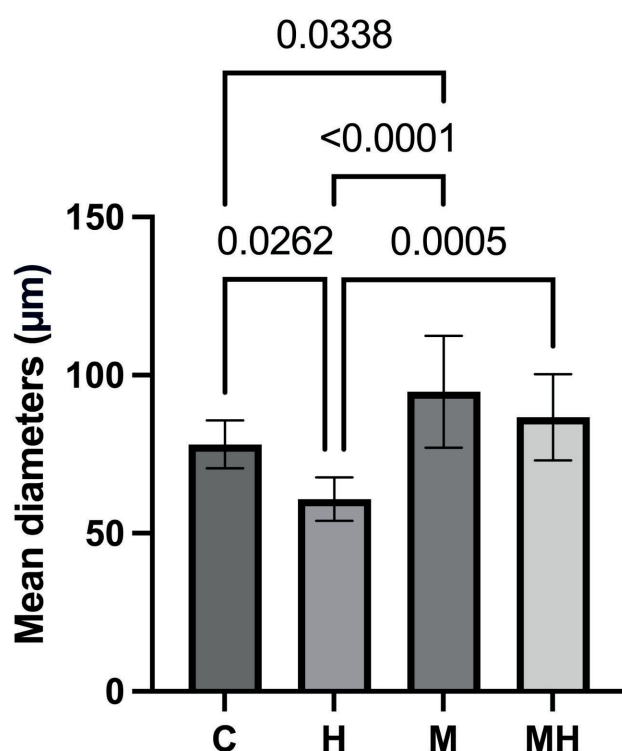


**Figure 7.** The average myotube diameters at the 7th day of differentiation for the experimental groups with standard deviation bars and p values

Statistical analysis revealed significant differences in the mean myotube diameters between the groups. Group H exhibited a 23% reduction in myotube diameter compared to group C ($p = 0.0262$). Group H had significantly smaller myotube diameters compared to all other groups. Specifically, group H showed significantly smaller diameters than group M ($p < 0.000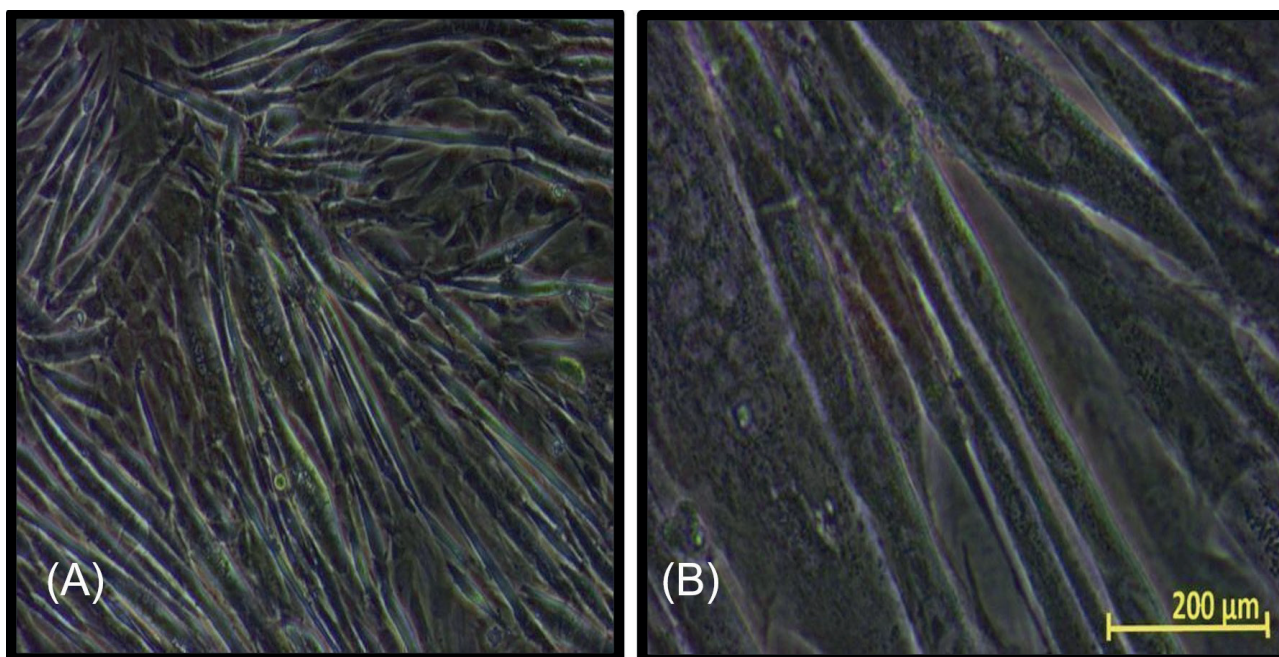1$) and group MH ($p = 0.0005$). Conversely, group M had significantly larger diameters compared to group C ($p = 0.0338$). However, no significant difference in myotube diameters was observed between group M and group MH.

## DISCUSSION

Our study reveals that H2O2 causes muscle atrophy in C2C12 cell line, and melatonin effectively prevents this atrophy. This aligns with the potential therapeutic benefits of melatonin in mitigating oxidative stress-related conditions (31, 32). The ability of melatonin to counteract the harmful effects of H2O2 on muscle cells suggests its potential as a protective agent against disuse-related muscle atrophy. The cells included in our study, having the same passage number, underwent uniform conditions throughout their growth and differentiation phases. Therefore, it can be stated that the observed differences between the groups are attributed to the experimental protocol. In our study, we used 0.05 mM $H_2O_2$ for 24 hours based on MTT assay results and a prior study (27). This led to a 23% reduction in myotube diameter in our atrophy model compared to the control —a recognized indicator of atrophy in the literature (33). We applied 0.1 mM melatonin for 24 hours, consistent with recommended literature dosage and our MTT results (29). Despite previous

evidence of melatonin's antioxidant and anti-apoptotic effects in the C2C12 cell line (29, 34) and its positive impact on muscle wasting, the morphological analysis of muscle atrophy remains unexplored in in vitro research. The 2023 study conducted by Ming Su et al. provides evidence that melatonin enhances muscle regeneration in the stages during the process of skeletal muscle differentiation (35). In our study, we demonstrated the impact of melatonin on muscle atrophy in the C2C12 cell model at the morphological level. Within the group MH, the morphological measurements showed an obvious reversal of muscle atrophy when compared to the group H.This outcome is consistent with previous studies investigating the effects of melatonin on muscle atrophy (31,32,36). Moreover, the group M exhibited a statistically significant increase in fiber diameter compared to the group C. This finding, for the first time implies that melatonin not only prevents atrophy but also induces hypertrophy in C2C12 cell line, which is consistent with a vary recent in vivo study indicating that melatonin has the potential to stimulate skeletal muscle growth and induce muscle fiber hypertrophy primarily through the upregulation of genes associated with skeletal muscle hypertrophy (37). These data allude to a dual role for melatonin in maintaining muscle health, encompassing protection against atrophy and promotion of hypertrophy. Furthermore, a study demonstrated that assessing biochemical markers of atrophy, such as creatine kinase and lactate dehydrogenase, in conjunction with atrogenes, can provide more detailed insights into atrophy (38). Examining these markers alongside atrogene expression is a suitable approach for a more comprehensive evaluation of atrophy. Moreover, to enhance our comprehension of melatonin's role in preventing atrophy and promoting hypertrophy, particularly beyond atrogenic pathways, it is crucial to assess the expression of genes associated with skeletal muscle hypertrophy.

In summary, our study shows that $H_2O_2$ induces muscle atrophy in C2C12 cells, but melatonin not only prevents this atrophy morphologically but also promotes hypertrophy. This underscores melatonin's potential as a versatile therapeutic agent in muscle health and disease prevention.

## Author contribution

Study conception and design: NKA, YK, MTB; data collection: NKA, YK, MTB; analysis and interpretation of results: NKA, YK, MTB; draft manuscript preparation: NKA. All authors reviewed the results and approved the final version of the manuscript.

## Ethical approval

The study was approved by the Hacettepe University Animal Experiments Ethics Committee (Approval No. 52338575-98 on 22 August 2017), confirming that the study on the commercially available C2C12 mouse myoblast cell line, obtained from American Tissue Cell Culture, does not require ethics committee approval.

## Funding

## Conflict of interest

The authors declare that there is no conflict of interest.

~ REFERENCES ~

[1] Sandri M. Autophagy in skeletal muscle. FEBS letters. 2010;584(7):1411-6.

[2] Bonaldo P, Sandri M. Cellular and molecular mechanisms of muscle atrophy. Disease models & mechanisms. 2013;6(1):25-39.

[3] Romanello V, Sandri M. Mitochondrial quality control and muscle mass maintenance. Frontiers in physiology. 2016;6:422.

[4] Sieck GC, Mantilla CB. Effect of mechanical ventilation on the diaphragm. New England Journal of Medicine. 2008;358(13):1392-3.

[5] Otto H. Type 2 diabetes in the middle aged. Strict goals from the very beginning! MMW Fortschritte der Medizin. 2003;145(21):30-2.

[6] Stump CS, Henriksen EJ, Wei Y, Sowers JR. The metabolic syndrome: role of skeletal muscle metabolism. Annals of medicine. 2006;38(6):389-402.

[7] Powers SK, Smuder AJ, Criswell DS. Mechanistic links between oxidative stress and disuse muscle atrophy. Antioxidants & redox signaling. 2011;15(9):2519-28.

[8] Kondo H, Miura M, Itokawa Y. Oxidative stress in skeletal muscle atrophied by immobilization. Acta Physiol Scand. 1991;142(4):527-8.

[9] Powers SK. Can antioxidants protect against disuse muscle atrophy? Sports Med. 2014;44 Suppl 2(Suppl 2):S155-65.

[10] Powers SK, Morton AB, Ahn B, Smuder AJ. Redox control of skeletal muscle atrophy. Free Radical Biology and Medicine. 2016;98:208-17.

[11] Ábrigo J, Elorza AA, Riedel CA, Vilos C, Simon F, Cabrera D, et al. Role of oxidative stress as key regulator of muscle wasting during cachexia. Oxidative medicine and cellular longevity. 2018;2018.

[12] Powers SK, Ozdemir M, Hyatt H. Redox control of proteolysis during inactivity-induced skeletal muscle atrophy. Antioxidants & Redox Signaling. 2020;33(8):559-69.

[13] Talbert EE, Smuder AJ, Min K, Kwon OS, Szeto HH, Powers SK. Immobilization-induced activation of key proteolytic systems in skeletal muscles is prevented by a mitochondria-targeted antioxidant. Journal of applied physiology. 2013;115(4):529-38.

[14] Tan D-X, Manchester LC, Qin L, Reiter RJ. Melatonin: a mitochondrial targeting molecule involving mitochondrial protection and dynamics. International journal of molecular sciences. 2016;17(12):2124.

[15] Oyewole AO, Birch-Machin MA. Mitochondria-targeted antioxidants. Faseb j. 2015;29(12):4766-71.

[16] Kelso GF, Porteous CM, Coulter CV, Hughes G, Porteous WK, Ledgerwood EC, et al. Selective targeting of a redox-active ubiquinone to mitochondria within cells: antioxidant and antiapoptotic properties. J Biol Chem. 2001;276(7):4588-96.

[17] Lerner AB, Case JD, Takahashi Y, Lee TH, Mori W. Isolation of melatonin, the pineal gland factor that lightens melanocyteS1. Journal of the american chemical society. 1958;80(10):2587-.

[18] Kato H, Tanaka G, Masuda S, Ogasawara J, Sakurai T, Kizaki T, et al. Melatonin promotes adipogenesis and mitochondrial biogenesis in 3T3-L1 preadipocytes. Journal of pineal research. 2015;59(2):267-75.

[19] Maarman GJ, Andrew BM, Blackhurst DM, Ojuka EO. Melatonin protects against uric acid-induced mitochondrial dysfunction, oxidative stress, and triglyceride accumulation in C2C12 myotubes. Journal of Applied Physiology. 2017;122(4):1003-10.

[20] Li Y-P, Chen Y, Li AS, Reid MB. Hydrogen peroxide stimulates ubiquitin-conjugating activity and expression of genes for specific E2 and E3 proteins in skeletal muscle myotubes. American Journal of Physiology-Cell Physiology. 2003;285(4):C806-C12.

[21] Prochniewicz E, Lowe DA, Spakowicz DJ, Higgins L, O'Conor K, Thompson LV, et al. Functional, structural, and chemical changes in myosin associated with hydrogen peroxide treatment of skeletal muscle fibers. American Journal of Physiology-Cell Physiology. 2008;294(2):C613-C26.

[22] Higaki Y, Mikami T, Fujii N, Hirshman MF, Koyama K, Seino T, et al. Oxidative stress stimulates skeletal muscle glucose uptake through a phosphatidylinositol 3-kinase-dependent pathway. Am J Physiol Endocrinol Metab. 2008;294(5):E889-97.

[23] Powers SK, Hudson MB, Nelson WB, Talbert EE, Min K, Szeto HH, et al. Mitochondrial-targeted antioxidants protect against mechanical ventilation-induced diaphragm weakness. Critical care medicine. 2011;39(7):1749.

[24] Yaffe D, Saxel O. Serial passaging and differentiation of myogenic cells isolated from dystrophic mouse muscle. Nature. 1977;270(5639):725-7.

[25] Alwan R, Bruel A-L, Da Silva A, Blanquet V, Bouhouche K. An siRNA-based screen in C2C12 myoblasts identifies novel genes involved in myogenic differentiation. Experimental cell research. 2017;359(1):145-53.

[26] Balci-Hayta B, Erdem-Özdamar S, Dinçer P. Overexpression of amyloid beta precursor protein enhances expression and secretion of ST6Gal1 in C2C12 myogenic cell line. Cell biology international. 2011;35(1):9-13.

[27] McClung JM, Judge A, Talbert EE, Powers SK. Calpain-1 is required for hydrogen peroxide-induced myotube atrophy. American Journal of Physiology-Cell Physiology. 2009;296(2):C363-C71.

[28] Choy CK, Cho P, Boost MV. Cytotoxicity and effects on metabolism of contact lens care solutions on human corneal epithelium cells. Clin Exp Optom. 2012;95(2):198-206.

[29] Salucci S, Baldassarri V, Canonico B, Burattini S, Battistelli M, Guescini M, et al. Melatonin behavior in restoring chemical damaged C2C12 myoblasts. Microscopy research and technique. 2016;79(6):532-40.

[30] Van der Meijden K, Bravenboer N, Dirks N, Heijboer A, Den Heijer M, De Wit G, et al. Effects of 1, 25 (OH) 2D3 and 25 (OH) D3 on C2C12 myoblast proliferation, differentiation, and myotube hypertrophy. Journal of Cellular Physiology. 2016;231(11):2517-28.

[31] Park JH, Chung EJ, Kwon HJ, Im SS, Lim JG, Song DK. Protective effect of melatonin on TNF-α-induced muscle atrophy in L 6 myotubes. Journal of pineal research. 2013;54(4):417-25.

[32] Abd Allah ES, Mahmoud AM. Melatonin attenuates chronic immobilization stress-induced muscle atrophy in rats: Influence on lactate-to-pyruvate ratios and Na+/K+ ATPase activity. Pathophysiology. 2018;25(4):353-7.

[33] Menconi M, Gonnella P, Petkova V, Lecker S, Hasselgren PO. Dexamethasone and corticosterone induce similar, but not identical, muscle wasting responses in cultured L6 and C2C12 myotubes. Journal of cellular biochemistry. 2008;105(2):353-64.

[34] Kim CH, Kim KH, Yoo YM. Melatonin protects against apoptotic and autophagic cell death in C2C12 murine myoblast cells. Journal of pineal research. 2011;50(3):241-9.

[35] Su CM, Tsai CH, Chen HT, Wu YS, Chang JW, Yang SF, et al. Melatonin improves muscle injury and differentiation by increasing Pax7 expression. Int J Biol Sci. 2023;19(4):1049-62.

[36] Sayed RKA, Fernández-Ortiz M, Diaz-Casado ME, Rusanova I, Rahim I, Escames G, et al. The Protective Effect of Melatonin Against Age-Associated, Sarcopenia-Dependent Tubular Aggregate Formation, Lactate Depletion, and Mitochondrial Changes. J Gerontol A Biol Sci Med Sci. 2018;73(10):1330-8.

[37] Chen W, Tu Y, Cai P, Wang L, Zhou Y, Liu S, et al. Melatonin supplementation promotes muscle fiber hypertrophy and regulates lipid metabolism of skeletal muscle in weaned piglets. J Anim Sci. 2023;101.

[38] Kaur N, Gupta P, Saini V, Sherawat S, Gupta S, Dua A, et al. Cinnamaldehyde regulates H2O 2-induced skeletal muscle atrophy by ameliorating the proteolytic and antioxidant defense systems. Journal of cellular physiology. 2019;234(5):6194-208.

acta medica

# Malignant pleural effusions: Are we better than the past?

Oğuz Karcıoğlu[1]
ORCID: 0000-0002-6071-0851

Fatih Tekin[2]
ORCID: 0000-0001-6688-1427

Ebru Öztürk[3]
ORCID: 0000-0001-9206-6856

Sevgen Önder[4]
ORCID: 0000-0002-5523-0669

Ziya Toros Selçuk[1]
ORCID: 0000-0003-4220-8128

[1] Department of Chest Diseases, School of Medicine, Hacettepe University, Ankara, Türkiye

[2] Department of Chest Diseases, Van Education and Research Hospital, University of Health Sciences, Van, Türkiye

[3] Division of Biostatistics, School of Medicine, Hacettepe University, Ankara, Türkiye

[4] Department of Pathology, School of Medicine, Hacettepe University, Ankara, Türkiye

*This study was presented at 23rd Annual Congress of Turkish Thoracic Society

Corresponding Author: Oğuz Karcıoğlu
E-mail: oguzkarcioglu@gmail.com

꧁ A B S T R A C T ꧂

Objective: Malignant pleural effusion (MPE) is indicative of advanced-stage disease and a poor prognosis in almost all cancer types. Lung and breast cancers are the predominant malignancies causing MPE, collectively representing over 60% of the total. In recent years, cancer has become a type of chronic disease, with advancements in diagnostic tools and treatment strategies. Our objective was to assess the evolution of primary diagnoses, survival rates, and associated variables among individuals with MPE in recent years.

Materials and Methods: A retrospective search was conducted on the demographics, comorbidities, primary cancer sites, diagnostic interventions, and laboratory results of patients diagnosed with MPE between January 1, 2005, and July 30, 2018.

Results: Of the 663 patients who have MPE, the female/male ratio was 373/290. The mean age was 59.2 ± 14.0 at the time of diagnosis. The most common cancers were lung cancer (30.9%), breast cancer (23.3%), and gastrointestinal system cancers (16.62%). It was observed that the rate of MPE due to lung cancer increased gradually over the years. Initially, breast cancer constituted the most prevalent diagnosis in 28.2% of cases, whereas lung cancer rose to the top as the most prevalent in the second and third five-year periods (28.9% and 37.4%, respectively). Overall, the median survival time was 2.07 months. Kaplan-Meier analysis also revealed that survival times did not change significantly over fourteen years.

Conclusion: Advances in diagnostic methods and treatment modalities have altered the most common primary cancer causing MPE in recent years but have not contributed to survival time.

Keywords: pleurisy, effusion, diagnosis, lung, malignancy.

## INTRODUCTION

Malignant pleural effusion (MPE), refers to malignant involvement of the pleural space, is the second most common cause of exudative pleural effusion, following parapneumonic effusions [1]. It affects approximately 15% of all cancer patients during the course of those diseases [2]. MPE indicates advanced disease and reduced survival in almost all cancer types. Although it may vary depending on the type of primary cancer, the median life expectancy ranges from 1 to 12 months [2-4]. The most common cancers causing MPE are lung and breast cancers, which together account for more than 60% of all cases [5].

Advances in diagnostic tools and treatment modalities have transformed cancer into a chronic disease. The average survival of patients, even in the metastatic stage, significantly improved [6]. Five-year survival of metastatic breast cancer increased from 10% to 27% during the last 40 years [7]. Similarly, the median overall survival of metastatic colorectal cancer doubled in the previous two decades [8,9]. Moderate progress was also present

in lung cancer, and 5-year survival rates approached 20% [6,10].

The management of pleural effusion aims not only to provide definitive treatment but also to control symptoms and allow time for the treatment of the underlying disease [11]. Options include serial thoracentesis, chest tube or indwelling pleural catheter placement, pleurodesis, and pleurectomy [2]. Despite improvements in the management of MPE as well as treatment options for primary cancers, MPE is still associated with a reduced lifetime expectancy, regardless of the primary site. We aimed to evaluate the changes in primary diagnoses, survival rates, and related factors in patients with MPE from 2005 to 2018 in our institution.

## MATERIALS AND METHODS

### Study design

We retrospectively reviewed MPEs between 01.01.2005 and 30.07.2018. We obtained the pathological reports from the database of the pathology department. MPE was defined as the detection of tumor cells in the cytopathological examination of pleural fluid or pleural biopsy material. We obtained the demographic data, comorbidities, primary cancer sites, diagnostic interventions, and laboratory results at the time of diagnosis from the database of our hospital. Survival status, and date of death data were double checked from the database of the hospital and the Death Notification System (DNS) of the Turkish Ministry of Health.

### Statistical analysis

We present the descriptive statistics for continuous variables as mean ± standard deviation, or median, minimum-maximum values based on the normality assumption of distributions. In order to specify

significant variables for survival time, we split the data into five-year periods. For survival analysis, we considered five-year periods as strata, and then we applied univariate stratified Cox regression to determine the candidate variables for multiple stratified Cox regression models. The variables with a p-value<0.25 in univariate models are taken as candidate variables for the multiple Cox regression model. We also present the survival probabilities for 1-year, 2-years, 3-years, and 4-years, median survival times, and survival curves based on the final Cox regression model. The survival analysis part was conducted using R (R Core Team, 2021) [12], "survival" [13], "ggplot2" [14], and "survminer" [15] packages. The other analysis was using IBM SPSS Statistics for Windows, Version 23.0 (IBM Corp., 2015). The results are condisered statistically significant if the p value is< 0.05.

### Ethical approval

Researchers assure that the study fully complies with the Declaration of Helsinki. The clinical research ethics committee of Hacettepe University Faculty of Medicine approved the study protocol (GO 18/883, 25.09.2018).

## RESULTS

Of the 663 patients with MPE, 56% were female, and the female/ male ratio was 1.29 (373 and 290, respectively). The mean age was 59.2±14.0 years at the time of diagnosis. Among those 277 patients whose smoking status information can be accessed, 164 had a smoking history, and 113 were non-smokers. At the time of analysis 21, (4.3%) patients were alive, and 462 (95.7%) were dead. Since the Ministry of Health started using a properly organized DNS in 2013, we could not achieve reliable survival data of 180 patients from previous years. The demographic data of the study population is shown in Table 1.

**Table 1.** Demographics

| Characteristics | 2005-2009 (N= 281) | 2010-2014 (N= 207) | 2015-2018 (N= 175) | Total  (N= 663) |
|---|---|---|---|---|
| Mean Age (years±SD) | 57.3 (14.2) | 59.8 (14.0) | 61.5 (13.4) | 59.2 (14.0) |
| Gender (Female) N, (%) | 175 (62.3) | 105 (37.7) | 93 (53.1) | 373 (56.3) |
| Smoking N, (%) (N= 277) | 53 (59.6) | 64 (66.6) | 47 (51.1) | 164 (59.2) |
| Mortality N, (%) (N= 483) | 124 (94.7) | 177 (97.8) | 161 (94.2) | 462 (95.7) |
| Lung cancer (%) | 78 (27.8) | 62 (30.0) | 65 (37.1) | 205 (30.9) |

The most common diagnoses were lung cancer (30.9%), followed by breast cancer (23.2%) and gastrointestinal system (GIS) cancers (16.6%) overall (Table 2). Breast cancer was the most prevalent diagnosis in the first 5-year period (28.2%), while lung cancer became the most common diagnosis in the second and third 5-year periods (28.9% and 37.4%, respectively) (Figure 1). Evaluation of factors associated with death showed that elder age (HR: 1.010) and low serum protein levels (HR: 1.496) were associated with shorter survival. GIS and hematologic cancers reduce the time to death 1.441 and 1,157 times compared to lung cancers, respectively (Table 3).

Examination of mortality data over 5-year periods showed that there was no significant difference in survival. Although the rate of 1-year survivors is higher in Groups 2 and 3 than in Group 1, death rates have converged over the years. The median survival was 2.07 months overall. Kaplan-Meier analysis also revealed that there was no significant change in survival times during five-year periods over 14 years (Table 4, Figure 2).

## DISCUSSION

Current study confirmed that lung cancer is the most common tumor causing MPE. The fraction of lung cancer among cancers causing MPE has increased over the years, and that of breast cancer has decreased. Elder age and low serum protein levels were associated with shortened survival. While GIS and hematologic cancers with MPE were more risky for reduced survival compared to lung cancer, the lifespan was longer in breast cancers. Despite the minor increase in 1-year survival time, which did not reach statistical significance, survival time did not change during the 14 years.

In the late 1990s, Sahn et al. reported that lung cancer (36%), breast cancer (25%), and lymphoma (10%) were the most common cancer types associated with MPE [16]. In a large-scale research conducted almost 20 years later, the most common causes of MPE were determined to be lung (37%), breast (16%), hematological (10%), and unknown origin (10%) [17]. These results indicate that breast cancer is the second-leading cause of MPE, although its impact is decreasing, whereas lung cancer preserves its leading role. The results of our

**Table 2.** Distribution of primary tumors

| Lung 205 (30.9%) | Breast 154 (23.2%) | Non-lung 458 (69.1%) | | | |
|---|---|---|---|---|---|
| | | GIS 110 (16.6%) | Gynecology-Urinary 69 (10.4%) | Hematology 43 (6.5%) | Others 82 (12.4%) |
| Adenocarcinoma 148 (22.3%) | 154 (23.2%) | Gastric 59 (8.9%) | Ovary 47 (7.1%) | Lymphoma 32 (4.8%) | Mesothelioma 31 (4.7%) |
| NSCLC 29 (%4.4) | | Pancreas 24 (3.6%) | RCC 7 (1.1%) | MM 6 (0.9%) | CUP 29 (4.4%) |
| SCLC 22 (3.5%) | | Colorectal 19 (2.9%) | Endometrium 5 (0.8%) | ALL 2 (0.3%) | Sarcoma 9 (1.2%) |
| Squamous cell carcinoma 6 (0.9%) | | Cholangiocarcinoma 4 (0.6%) | Bladder 4 (0.6%) | CLL 2 (0.3%) | Malignant melanoma 4 (0.6%) |
| | | Esophagus 2 (0.3%) | Prostate 3 (0.5%) | AML 1 (0.2%) | Thyroid 3 (0.5%) |
| | | Small intestine 1 (0.2%) | Tuba uterina 1 (0.2%) | | Yolk sac 2 (0.3%) |
| | | Gall bladder 1 (0.2%) | Cervics 1 (0.2%) | | Cutenous SCC 1 (0.2%) |
| | | | | | Parotis 1 (0.2%) |
| | | | | | Thymus 1 (0.2%) |
| | | | | | PNET 1 (0.2%) |
| | | | | | Cystadenocarcinoma 1 (0.2%) |

GIS: Gastrointestinal system, NSCLC: Non-squamous cell lung cancer, SCLC: Small cell lung cancer, MM: Multiple myeloma, ALL: Acute lymphocytic leukemia, CLL: Chronic Lymphocytic leukemia, AML: Acute myeloid leukemia, RCC: Renal cell carcinoma, CUP: Cancer of unknown primary site, SCC: Squamous cell carcinoma, PNE: Primitive neuroectodermal tumor

**Table 3.** Factors related with reduced survival

| | Univariate Cox Regression | Multiple Cox Regression** | HR (95% CI) | p-value |
|---|---|---|---|---|
| | HR (95% CI) | p-value | | |
| Age of diagnosis | 1.005 (0.998-1.012) | 0.148 | 1.010 (1.002-1.017) | 0.014 |
| Gender (M/F) | 1.448 (1.203-1.742) | <0.001 | - | - |
| Smoking | 1.199 (0.914-1.573) | 0.191 | - | - |
| Lactate dehydrogenase | 1.000 (1.000-1.000) | 0.363 | - | - |
| Pleural glucose | 1.000 (0.999-1.000) | 0.26 | - | - |
| Pleural protein | 1.000 (0.996-1.004) | 0.992 | - | - |
| Serum protein | 0.707 (0.641-0.779) | <0.001 | 0.669 (0.627-0.779) | <0.001 |
| Organ systems | | | | |
| Gastrointestinal system | 1.705 (1.300-2.235) | <0.001 | 1.441 (1.079-1.926) | 0.013 |
| Hematologic malignancy | 1.413 (0.952-2.096) | 0.086 | 1.157 (0.752-1.780) | 0.507 |
| Breast cancer | 0.649 (0.503-0.837) | 0.001 | 0.619 (0.471-0.814) | 0.001 |
| Gynecologic-Urologic malignancy | 0.939 (0.677-1.301) | 0.704 | 0.709 (0.493-1.019) | 0.063 |
| Others | 0.936 (0.680-1.288) | 0.683 | 0.949 (0.679-1.325) | 0.758 |

**In the final model, the year period is considered as strata. Therefore, the stratified Cox regression results were given.

**Table 4.** Survival rates up to 5 year-periods

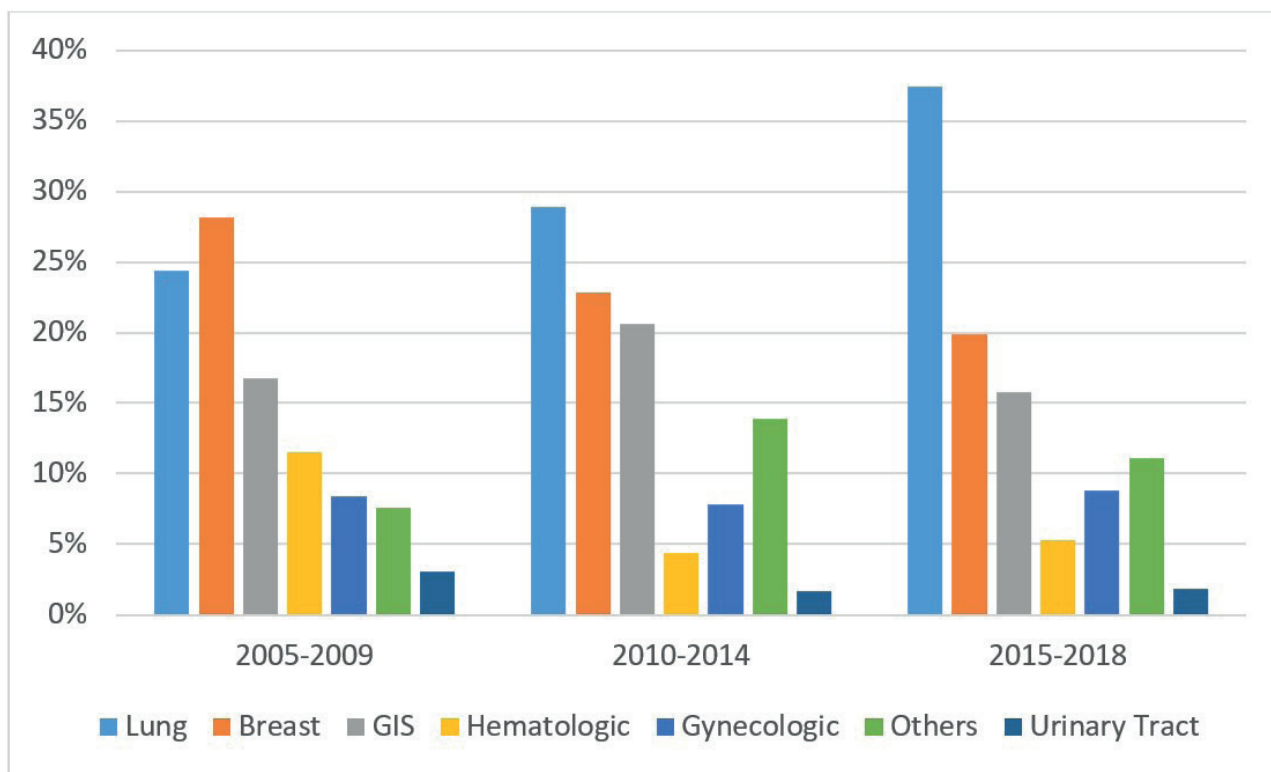| Survival | 2005-2009 (Group 1) | 2010-2014 (Group 2) | 2015-2018 (Group 3) | OVERALL |
|---|---|---|---|---|
| 1-year (%) | 16.47 | 25.51 | 22.81 | 21.89 |
| 2-year (%) | 9.01 | 13.88 | 10.03 | 11.02 |
| 3-year (%) | 6.49 | 6.40 | 7.12 | 6.69 |
| 4-year (%) | 3.69 | 2.92 | 4.92 | 3.79 |
| Median (months) | 1.57 | 1.87 | 2.30 | 2.07 |



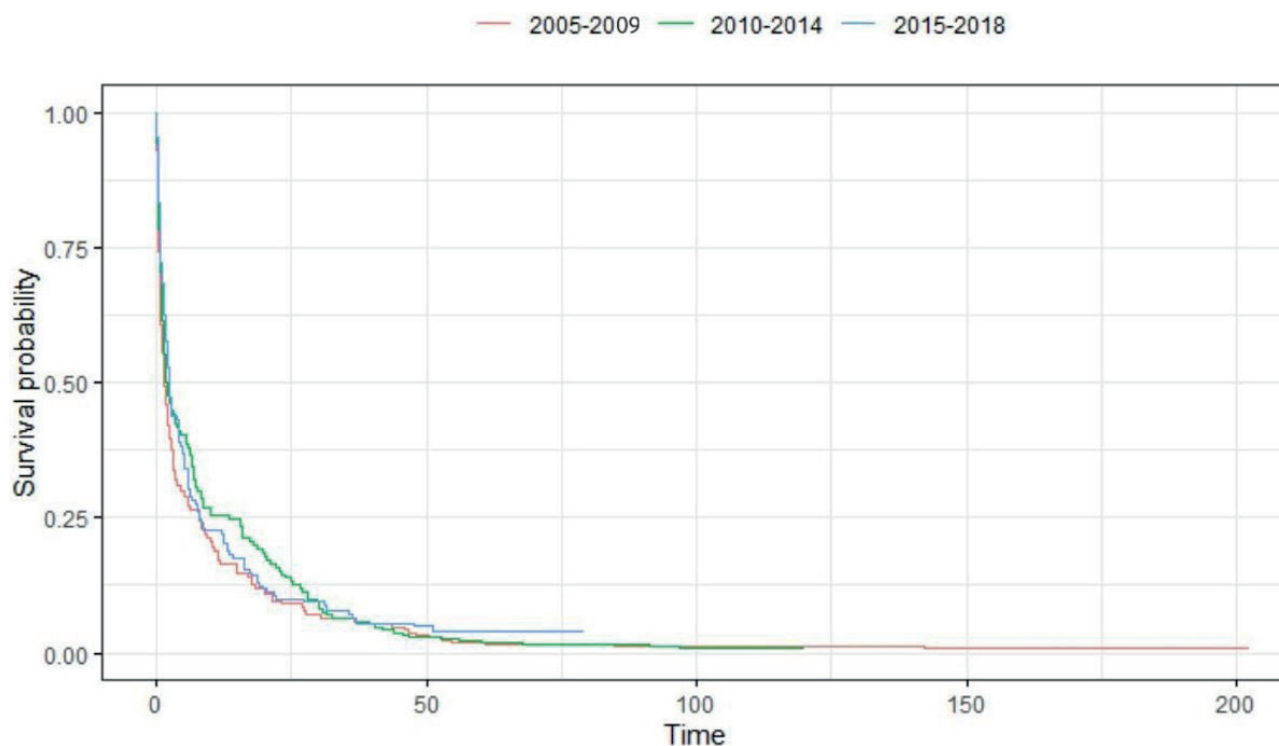**Figure 1.** Diagnoses by five-year periods

**Figure 2.** Kaplan-Meier analysis of survival by five-year periods

study appear to be in accordance with previous research, with the exception that gastrointestinal malignancies rank third. Analyses of 5-year intervals revealed a rise in the incidence of lung cancer, a decrease in breast cancer, and no change in the other malignancies. This finding may be related to the established breast cancer screening program. Indeed, Bleyer et al. have shown that screening with mammography contributes to early detection and has reduced the diagnosis of advanced breast cancer over the past three decades [18].

Extensive research has been conducted on the factors associated with the prognosis of MPE. First, the primary tumor site constitutes an independent risk factor for survival. While chemotherapy-sensitive malignancies, including breast cancer, and hematologic malignancies have a more favorable prognosis, solid tumors like lung, GIS, urologic cancers, and sarcomas are associated with a shorter life time [19-21]. In our study, GIS cancers with MPE were associated with a lower survival rate than lung cancer with MPE. Contrary to the literature, hematological malignancies with MPE were also associated with a slightly shorter survival compared to lung cancers with MPE. This may be due to the different grades of diseases included in our study and previous studies.

Other predictors of mortality were sought in the clinical state and laboratory results of individuals. Performance, age, and blood and pleural fluid test results have all been associated with mortality [2,19,20,22]. Being elder and having low serum protein levels were found to be associated with decreased life expectancy in our study. These parameters may be associated with the performance status of the patient rather than the tumor's behavior. In fact, the scores generated to predict survival in MPE utilize not only the laboratory values induced by the tumor but also the patient's performance [19]. Although LENT [19] and PROMISE [23] scores have been reported to be useful in predicting survival, doubt exists due to their limited clinical use and lack of validation in different studies. Due to the reciprocal impact of laboratory data and characteristics such as general health, comorbidities, and nutritional status on each other, it appears difficult to determine which is the main cause and to develop a simple survival prediction model.

In their 1966 article, Ariel et al. stated that while the average life expectancy for colon cancer and MPEs of unknown primary is 3 to 4 months, patients with breast, ovarian cancers and lymphoma have an improved prognosis [24]. Similarly, in the 1970s, the average MPE survival rate was about 16 months

for breast and mesothelioma malignancies and 6 months for lung and other solid cancers [25,26]. Despite the fact that new treatment methods for many cancers have resulted in longer survival in recent years, it is difficult to state that significant progress has been made in the treatment of MPE. Although it varies depending on the primary tumor site, with the best prognosis for ovarian tumors and the worst prognosis for the lungs, the average survival time remains between 3 and 12 months [2,27]. We also found no change in the mean lifespan after diagnosis across the 14-year research period. When prognostic factors are also considered, it becomes apparent that the development of MPE is an indicator of the progression of cancer from a local to a systemic disease, regardless of the primary site, and that it impairs the overall health status.

Our study's strengths include a significant number of patients over an extended period of time. In addition, describing the primary tumor's site in great detail and analyzing the change in mortality over time adds value to this study. Important limitations include the retrospective design, the inability to access the data of some patients due to deficiencies in the death notification system, and the absence of performance score and symptom data.

MPE remains associated with a poor prognosis despite advances in diagnostic procedures and treatment modalities. Indicators of a poor prognosis in MPE are closely associated with the primary tumor, clinical features, and laboratory findings. Unfortunately, the intended increase in MPE's average survival has not been realized. Hopefully, further research and progress in the management of MPE will contribute to better survival in the future.

## Author contribution

Study conception and design: OK, and ZTS; data collection: OK, and FT; analysis and interpretation of results: OK, SÖ, and EÖ; draft manuscript preparation: OK, SÖ, FT and ZTS. All authors reviewed the results and approved the final version of the manuscript.

## Ethical approval

The study was approved by the Clinical Research Ethics Committee of Hacettepe University (GO 18/883, 25.09.2018).

## Funding

The authors declare that the study received no funding.

## Conflict of interest

The authors declare that there is no conflict of interest.

~⁓◌◍ REFERENCES ◌◍⁓~

[1] Feller-Kopman DJ, Reddy CB, DeCamp MM, et al. Management of malignant pleural effusions. An official ATS/STS/STR clinical practice guideline. American journal of respiratory and critical care medicine 2018;198(7):839-849.

[2] Bibby AC, Dorn P, Psallidas I, et al. ERS/EACTS statement on the management of malignant pleural effusions. European journal of cardio-thoracic surgery 2019;55(1):116-132.

[3] DeBiasi E, Puchalski J. Pleural effusions as markers of mortality and disease severity: a state-of-the-art review. Current Opinion in Pulmonary Medicine 2016;22(4):386-391.

[4] Özyurtkan MO, Balcı AE, Çakmak M. Predictors of mortality within three months in the patients with malignant pleural effusion. European Journal of Internal Medicine 2010;21(1):30-34.

[5] Penz E, Watt KN, Hergott CA, et al. Management of malignant pleural effusion: challenges and solutions. Cancer management and research 2017;9:229.

[6] National Cancer Institute: Surveillance, Epidemiology, and End Results Database. Cancer stat facts: lung and bronchus cancer. https://seer.cancer.gov/statfacts/ Accessed January 17, 2022.

[7] Sundquist M, Brudin L, Tejler G. Improved survival in metastatic breast cancer 1985–2016. The Breast 2017;31:46-50.

[8] Karimi S, Biemans HJ, Naderi Mahdei K, et al. Testing the relationship between personality characteristics, contextual factors and entrepreneurial intentions in a developing country. International Journal of Psychology 2017;52(3):227-240.

[9] Fenocchio E, Colombi F, Calella MG, et al. Improvement of metastatic colorectal cancer patient survival: single institution experience. Cancers 2019;11(3):369.

[10] Heuvers ME, Hegmans JP, Stricker BH, et al. Improving lung cancer survival; time to move on. BMC pulmonary medicine 2012;12(1):1-4.

[11] Kulandaisamy PC, Kulandaisamy S, Kramer D, et al. Malignant Pleural Effusions—A Review of Current Guidelines and Practices. Journal of Clinical Medicine 2021;10(23):5535.

[12] R Core Team A, Team RC. R: A language and environment for statistical computing. R Foundation for Statistical Computing, Vienna, Austria. 2012

[13] Terry M Therneau TL, Atkinson Elizabeth, Crowson Cynthia. A Package for Survival Analysis in R_. R package version 3.2-10. 2021.

[14] Wickham H, Chang W, Wickham MH. Package 'ggplot2'. Create elegant data visualisations using the grammar of graphics Version 2016;2(1):1-189.

[15] •Alboukadel Kassambara MK, Przemyslaw Biecek. Drawing Survival Curves using 'ggplot2'. R package version 0.4.9. 2021.

[16] Sahn S. Pleural diseases related to metastatic malignancies. European Respiratory Journal 1997;10(8):1907-1913.

[17] Porcel JM, Esquerda A, Vives M, et al. Etiology of pleural effusions: analysis of more than 3,000 consecutive thoracenteses. Archivos de Bronconeumología (English Edition) 2014;50(5):161-165.

[18] Bleyer A, Welch HG. Effect of three decades of screening mammography on breast-cancer incidence. New England Journal of Medicine 2012;367(21):1998-2005.

[19] Clive AO, Kahan BC, Hooper CE, et al. Predicting survival in malignant pleural effusion: development and validation of the LENT prognostic score. Thorax 2014;69(12):1098-1104.

[20] Popowicz N, Cheah HM, Gregory C, et al. Neutrophil-to-lymphocyte ratio in malignant pleural fluid: Prognostic significance. Plos one 2021;16(4):e0250628.

[21] Qiao X, Zhang Z-R, Shi X-Y, et al. Total Protein–Chloride Ratio in Pleural Fluid Independently Predicts Overall Survival in Malignant Pleural Effusion at the First Diagnosis. Frontiers in Oncology 2022;11:777930.

[22] Bielsa S, Salud A, Martínez M, et al. Prognostic significance of pleural fluid data in patients with malignant effusion. European journal of internal medicine 2008;19(5):334-339.

[23] Psallidas I, Kanellakis NI, Gerry S, et al. Development and validation of response markers to predict survival and pleurodesis success in patients with malignant pleural effusion (PROMISE): a multicohort analysis. The Lancet Oncology 2018;19(7):930-939.

[24] Ariel IM, Oropeza R, Pack GT. Intracavitary administration of radioactive isotopes in the control of effusions due to cancer: results in 267 patients. Cancer 1966;19(8):1096-1102.

[25] Martini N, Bains MS, Beattie Jr EJ. Indications for pleurectomy in malignant effusion. Cancer 1975;35(3):734-738.

[26] Friedman MA, Slater E. Malignant pleural effusions. Cancer treatment reviews 1978;5(2):49-66.

[27] Roberts ME, Neville E, Berrisford RG, et al. Management of a malignant pleural effusion: British Thoracic Society pleural disease guideline 2010. Thorax 2010;65(Suppl 2):ii32-ii40.

h acta medica

# Comparison of the safety profile of tofacitinib and etanercept in rheumatoid arthritis patients aged 60 years and over: The real-life data from the HUR-BIO registry

Emine Sarıyıldız[1]
ORCID: 0000-0003-0257-1061

Erdinç Ünaldı[1]
ORCID: 0009-0005-4381-202X

Levent Kılıç[1]
ORCID: 0000-0003-1064-9690

Ömer Karadağ[1]
ORCID: 0000-0002-3443-3117

Umut Kalyoncu[1]
ORCID: 0000-0001-7129-2109

Ali İhsan Ertenli[1]
ORCID: 0000-0002-3904-0769

Sedat Kiraz[1]
ORCID: 0000-0003-2802-6061

[1] Department of Internal Medicine, Division of Rheumatology, Faculty of Medicine, Hacettepe University, Ankara, Türkiye

Corresponding Author: Emine Sarıyıldız
E-mail: docemineduran@gmail.com

~⟲⟳ A B S T R A C T ⟲⟳~

Objective: To investigate the safety profile of tofacitinib in rheumatoid arthritis (RA) patients aged 60 and over and to compare these findings with etanercept.

Materials and methods: HUR-BIO (Hacettepe University Rheumatology Biologic Registry) is a single-center registry for biological and targeted synthetic DMARDs since 2005. We included RA patients aged ≥ 60 years who were prescribed tofacitinib or etanercept as their first bDMARD or tsDMARD and had at least one control visit. MACE (major adverse cardiovascular event), VTE (venous thromboembolism), malignancy, herpes zoster, and infections requiring hospitalization were recorded for the safety profile. Incidence rate (IR) and incidence rate ratios (IRR) per 1000 patient years were calculated for all safety data.

Results: This study consisted of 123 RA patients (tofacitinib n=70, etanercept n=53). In the overall population, the mean age was 67.9 ± 6.2 years and the median follow-up period was 2.1 years. Among the traditional cardiovascular risk factors, smoking history and hyperlipidemia were more common in the tofacitinib group. The IRR per 1000 patients years for MACE, herpes zoster, and infections requiring hospitalization was similar between the groups. All three patients who diagnosed with DVT or PE were in the tofacitinib group, and the significance level of the increase in IR was close to the statistical threshold (p=0.057). There was only one patient who developed non-melanoma skin cancer, and that patient was in the tofacitinib group.

Conclusion: The incidence of MACE, herpes zoster, and infections requiring hospitalization was comparable between tofacitinib and etanercept. However, the occurrence of VTE exclusively in the tofacitinib group suggests that this issue needs careful evaluation for these patients.

Keywords: tofacitinib, rheumatoid arthritis, safety profile.

## INTRODUCTION

Rheumatoid arthritis (RA) is a chronic, systemic autoimmune disease that predominantly affects peripheral joints by targeting synovial tissues [1]. Modern treatment guides recommend adding biological disease-modifying antirheumatic drugs (bDMARDs) or targeted synthetic (ts) DMARDs in patients whose treatment goal is not accomplished with conventional synthetic DMARDs (csDMARDs) [2, 3]. However, the findings of the ORAL Surveillance research have caused some concerns about the safety profile of tofacitinib, one of the tsDMARDs [4].

Tofacitinib is known a pan-JAK inhibitor that inhibits the JAK family, which plays a pivotal role in inflammation by participating intracellular signal transduction. JAK inhibitors suppress inflammatory mediators by inhibiting the autophosphorylation and activation of JAK [5]. The United States Food and Drug Administration (FDA) approved tofacitinib for the treatment of moderate-to-severe RA patients in 2012, and the European Medicines Agency (EMA) authorized it in 2017 [6]. In Turkey, it was approved by the Ministry of Health in 2015 and subsequently implemented.

Although there are no discuss about the effectiveness of tofacitinib, concerns about safety have increased significantly. The FDA's post-marketing safety study in 2019 stated that the incidence of pulmonary embolism and all-cause death in the tofacitinib 10 mg group was higher than in the TNF inhibitor (TNFi) group [7]. Then, the ORAL Surveillance trial displayed that the risk of malignancy and major adverse cardiovascular events (MACE) was increased in the tofacitinib group among RA patients aged 50 and over who had at least one cardiovascular risk factor. Moreover, the incidences of opportunistic infections and all herpes zoster infections were higher in this group [4]. Therefore, the European Alliance of Associations for Rheumatology (EULAR 2022) update prioritized the use of bDMARDs in patients who have failed csDMARDs. It was stated that relevant risk factors should be taken notice when prescribing JAK inhibitors [8].

Following the ORAL Surveillance trial, many researches containing safety data of tofacitinib were published [9-14]. Assumed the augmented risk of adverse events (AEs) in elderly patients, our

study aimed to examine safety profile in RA patients aged 60 and over who were using tofacitinib, and to compare with those in patients who were using etanercept as their first bDMARD.

## MATERIALS AND METHODS

This study was a observational cohort study of prospectively registered RA patients from the Hacettepe University Rheumatology (HUR-BIO) database, conducted at a primary referral center in central Türkiye. In the HUR-BIO database, established in 2005, patient data are recorded distinctly for each patient and there are no repeat patient records [15]. RA was diagnosed regarding to the doctor desicion and/or 2010 EULAR/ACR criteria [16]. We screened RA patients who received tofacitinib or etanercept as first b/tsDMARDs and had at least one visit from the date it became available in Türkiye until January 2022. The exclusion criteria for the study were being under 60 years of age, having used another bDMARD or tsDMARD before the use of tofacitinib/etanercept, not attending any visits after the prescription of tofacitinib/etanercept, and being unable to reach patients who did not attend their routine follow-ups by phone. Our study was performed according to the Helsinki Declaration and approved by the Ethical Committee (Number: GO 21/1251).

All data were performed from the HUR-BIO database. Patients with at least one visit who did not attend their follow-up visits were contacted by the physician via phone to inquire about their continuation of the medication and any AEs. With the patients' consent, information obtained from the Turkish Ministry of Health National Electronic Database, E-pulse was utilized to check for the presence of metabolic comorbidities and AEs. The demographic data and disease features included gender, age, body mass index (BMI), smoking status, disease duration, follow-up time, seropositivity status, accompanying DMARD usage (methotrexate or leflunomide), current prednisolone dose, disease activity score (DAS)-28, and health assessment questionnaire-disability index (HAQ-DI).

Safety outcomes contained MACE, malignancies (excluding non-melanoma skin cancer [NMSC]),

NMSC, venous thromboembolism (VTE), herpes zoster, and all infections requiring hospitalization. Adjudicated MACE was described as myocardial infarction (MI), stroke, and/or cardiovascular death after 60 days of drug exposure and within 28 days after drug discontinuation. Cardiovascular risk factors (diabetes mellitus, hypertension, hyperlipidemia, low HDL level) and coronary artery disease at an early age in first-degree relatives were also recorded. All safety profile data were investigated during the period of drug exposure.

## Statistical analysis

Statistical analyses were performed using SPSS software (version 25.0; IBM Corporation, Armonk, NY, USA). Both visual methods (histogram, probability plots) and analytical techniques (Kolmogorov-Smirnov, skewness, and kurtosis) were employed to assess the normality of variable distributions. For continuous data, either the median (interquartile range, IQR) or the mean (standard deviation, SD) was reported, while categorical data were presented as percentages. Categorical variables were examined using the Chi-square or Fisher's exact test, and continuous variables were evaluated using the Mann-Whitney U test or Student's T test. Incidence rates (IR) and incidence rate ratios (IRR) per 1000 patient-years were calculated for all safety data. Drug retention rates were analyzed with the log-rank test, and Kaplan-Meier survival estimates were generated. A p value of less than 0.05 was deemed statistically significant.

## RESULTS

A total of 123 patients were included in this study. In the overall population, the mean age was 67.9 ± 6.2 years and 96 (78.0%) patients were female. The median (IQR) disease duration was 13 (12) years and the median (IQR) follow-up duration under tofacitinib or etanercept was 27 (45) months. The treatment of 72 (58.5%) patients receiving tofacitinib or etanercept was discontinued for various causes. The most frequent causes for discontination the drug were: secondary failure (n=25), primary failure (n=14), patient's preference (n=9) and allergic reaction/rash (n=6). The mean baseline DAS-28 (ESR) score of patients was 4.8 ± 1.2 and the rate of concomitant methotrexate (MTX) or leflunomide (LEF) usage was 57.7%. There

was no distinction between the groups in terms of age, gender, and BMI. Ever smoking condition was more common in the tofacitinib group (47.1% vs 24.5%, p=0.010). While the median disease duration was longer in the etanercept group (18 years vs 10.5 years, p<0.001), the median duration under tofacitib or etanercept use was similar. In the tofacitinib group, 55.7% of patients continued treatment; this rate was significantly higher than the etanercept group (55.7% vs 22.6%, p<0.001). Additionally, both the mean baseline DAS-28 (ESR) score (4.6 vs 5, p=0.021) and the rate of concomitant MTX or LEF use (48.6% vs 84.1%, p<0.001) were lower in this group (Table 1).

Comorbidities and safety outcomes of the groups were displayed in table 2. Hyperlipidemia (58.6% vs 25%, p<0.001) was significantly higher in the tofacitinib group, whereas the distribution of metabolic comorbidities such as hypertension, diabetes mellitus, and obesity was similar for both groups. The results for safety data were as follows: coronary heart disease (CHD) (n=7), cerebrovascular disease (CVD) (n=2), NMSC (n=1), VTE (n=3), herpes zoster (n=8), and infection requiring hospitalization (n=9). One patient who developed NMSC was in the tofacitinib group and her diagnosis was squamous cell carcinoma (SCC) of the skin. The time from tofacitinib initiation to SCC development was 18 months. In the tofacitinib group, one patient was diagnosed with DVT and 2 patients were diagnosed with PE. Tofacitinib exposure durations were 63 months, 15 months, and 4 months, respectively. Reasons for hospitalization were pneumonia (n=3), COVID-19 disease (n=3), gastrointestinal infection (n=2) and soft tissue infection (n=1). Six patients deceased under the medication. The reason of death of the patient in the etanercept group was CVD, the cause of death of one of the 5 patients in the tofacitinib group was pneumonia, and the others was unknown.

For drug retention, survival rates of the tofacitinib and etanercept was similar in our study population (log rank, p=0.194) (Figure 1). The IRR per 1000 patients years for MACE was not different between the groups [IRR:0.8 (0.07–7.01), p=0.837]. One of the 2 patients in the tofacitinib group had MI (smoking and hyperlipidemia history) and the other had CVD (smoking and hypertansion history). One of the 3 patients in the etanercept group died due to CVD. Two others had experienced MI; one had

**Table 1.** Comparison of the demographic and disease characteristics of tofacitinib and etanercept groups

| Variables* | Tofacitinib (n=70) | Etanercept (n=53) | p |
|---|---|---|---|
| Age (mean, SD) | 67.5 (6.3) | 68.5 (6) | 0.387 |
| Gender (female) | 59 (84.3) | 37 (69.8) | 0.055 |
| BMI (kg/m$^2$) | 28.9 (8) | 30.1 (8.1) | 0.446 |
| Smoking status | | | |
| - Ever smoker | 33 (47.1) | 13 (24.5) | **0.010** |
| - Never smoker | 37 (52.9) | 40 (75.5) | |
| Disease duration, years | 10.5 (11) | 18 (13) | **<0.001** |
| Duration under tofacitinib or etanercept, months | 25 (30.5) | 26.5 (57.2) | 0.341 |
| Total follow-up time, months | 37.5 (30.2) | 105 (68.5) | **<0.001** |
| Current tofacitinib or etanercept status | | | |
| - Ongoing | 39 (55.7) | 12 (22.6) | **<0.001** |
| - Discontinued | 31 (44.3) | 41 (77.4) | |
| RF and/or anti-CCP positivity | 58 (82.9) | 38 (73.1) | 0.192 |
| Glucocorticoids use at last visit | 49 (74.2) | 26 (59.1) | 0.095 |
| Glucocorticoids dose at last visit | 5 (5) | 2.5 (5) | 0.110 |
| Concomitant MTX or LEF use | 34 (48.6) | 37 (84.1) | **<0.001** |
| Baseline DAS-28 (ESR) (mean, SD) | 4.6 (1.3) | 5 (1.1) | **0.021** |
| Baseline HAQ-DI (mean, SD) | 1 (0.7) | 1.1 (0.7) | 0.440 |

*n (%) for categorical values and median (IQR) for numeric values, if not otherwise specified

BMI: Body mass index, CCP: cyclic-citrulinated peptide, DAS28: disease activity score 28, ESR: erythrocyte sedimentation rate, HAQ: health assessment questionnaire, IQR: interquartile range, MTX: Methotrexate, LEF: Leflunomide, RF: rheumatoid factor, SD: Standart derivation.

**Table 2.** Comorbidities and safety outcomes of tofacitinib and etanercept groups

| Variables* | Tofacitinib (n=70) | Etanercept (n=53) | p |
|---|---|---|---|
| Hypertension | 40 (57.1) | 26 (51) | 0.501 |
| Diabetes mellitus | 15 (21.4) | 10 (21.7) | 0.968 |
| BMI ≥30 kg/m$^2$ | 29 (42) | 27 (50.9) | 0.327 |
| Hyperlipidemia | 41 (58.6) | 11 (25) | <0.001 |
| HDL level (<40 mg/dl) | 2/62 (3.2) | 1/16 (6.2) | 0.617 |
| Family history of early CHD | 8 (11.9) | 4 (8.5) | 0.557 |
| CHD | 3 (4.4) | 4 (7.5) | 0.464 |
| Myocardial infarction | 1 (1.5) | 2 (3.8) | 0.581 |
| Cerebrovascular disease | 1 (1.9) | 1 (1.5) | 0.999 |
| NMSC | 1 (1.4) | 0 | NA |
| Family history for cancer | 11 (16.2) | 12 (27.9) | 0.137 |
| DVT or PE | 3 (4.5) | 0 | NA |
| Herpes zoster | 4 (5.9) | 4 (9.1) | 0.521 |
| Infection requiring hospitalization | 6 (8.8) | 3 (6.7) | 0.678 |
| Exitus | 5 (7.1) | 1 (1.9) | 0.327 |

*n (%) for categorical values

BMI: Body mass index, CHD: Coronary heart disease, DVT: Deep vein thrombosis, HDL: High density lipoprotein, NMSC: Non-melonom skin cancer, PE: Pulmonary embolism

only hypertension as a risk factor, while the other had risk factors including smoking, hypertension, diabetes mellitus, and hyperlipidemia. Similar to MACE, the IRR for herpes zoster and infection displayed no significant difference between the groups [herpes zoster IRR:1.2 (0.22–6.46), p=0.798; infections IRR:2.4 (0.51-14.89), p=0.223]. All three patients who developed DVT or PE were in the tofacitinib group, and the significance level of the increase in IRR was close to the statistical threshold (p=0.057) (Table 3).

**Table 3.** Incidence rate and incidence rate ratios for safety outcomes of tofacitinib and etanercept groups

|  | Tofacitinib (n=70) | | Etanercept (n=53) | | | |
|---|---|---|---|---|---|---|
|  | n | IR (95% CI) | n | IR (95% CI) | IRR (95% CI) | P value for IRR |
| MACE | 2 | 12 (1.46-43.55) | 3 | 15 (3.09-43.528) | 0.8 (0.07-7.01) | 0.837 |
| NMSC | 1 | 6 (0.15-33.56) | 0 | 0 | NA | 0.272 |
| DVT or PE | 3 | 18.1 (3.73-52.81) | 0 | 0 | NA | 0.057 |
| Herpes zoster | 4 | 24.1 (6.57-61.7) | 4 | 20 (5.45-51.21) | 1.2 (0.22-6.46) | 0.798 |
| Infection requiring hospitalization | 6 | 36.1 (13.26-78.67) | 3 | 15 (3.09-43.84) | 0.51-14.89 | 0.223 |

IR: Incidence rate and IRR: Incidence rate ratios were calculated per 1000 patient years. DVT: Deep vein thrombosis, MACE: major adverse cardiovascular event; NA: not applicable, NMSC: Non-melonom skin cancer, PE: Pulmonary embolism
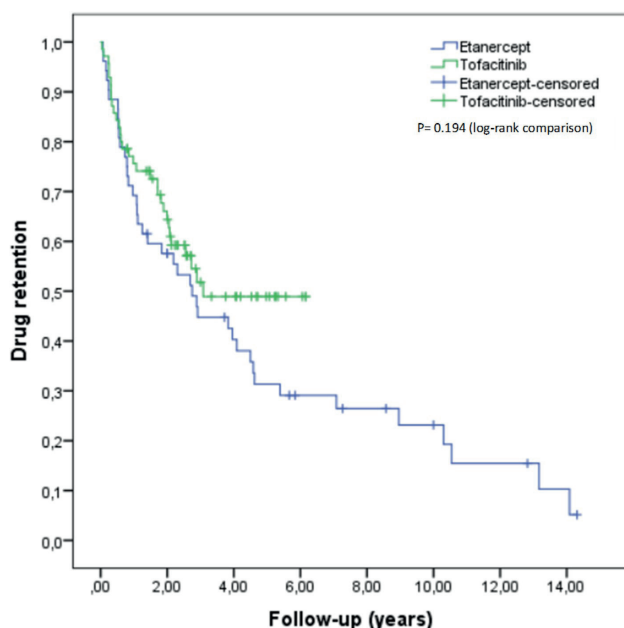


**Figure 1.** Kaplan–Meier analysis of tofacitinib and etanercept for drug retention

## DISCUSSION

In this study, we compared the real-world safety data of tofacitinib and etanercept as the first bDMARD/tsDMARD used in RA patients aged 60 and over. Although the presence of smoking history and hyperlipidemia was more common in the tofacitinib group, we found the risk of MACE to be similar in both groups through a median follow-up time of 25 months. Additionally, the risk of herpes zoster and infections requiring hospitalization were not distinct between the groups. One patient who developed non-melanom skin cancer and three patients who diagnosed VTE were in the tofacitinib group.

Patients with RA have an elevated risk of cardiovascular disease compared to the general population. This increased risk is attributed not only to traditional risk factors but also to endothelial dysfunction related to the inflammation and

the medications used in treatment, particularly glucocorticoids [17, 18]. A study conducted on RA patients who experienced MI demonstrated that cardiovascular risk increased in association with both the current and the cumulative glucocorticoid dose [19]. Therefore, current guidelines for RA treatment advise administering the minimal effective dose of glucocorticoids for the shortest feasible duration [3, 8]. Similar apprehension for cardiovascular disease risk was enhanced for tofacitinib in the ORAL Surveillance (A3921133) study [4]. This research focused on patients aged 50 and above with at least one cardiovascular risk factor, and the safety profile comparison between tofacitinib and TNFi (adalimumab or etanercept) did not show non-inferiority for MACE. The post-hoc analysis of the ORAL Surveillance study revealed that MACE risk was higher in the tofacitinib (2x5 mg) group compared to the TNFi group among patients with a history of atherosclerotic cardiovascular disease (ASCVD). In contrast, the risk of MACE was similar for patients without a history of ASCVD but with common cardiovascular risk factors [20]. The STAR-RA study outcomes in the United States did not provide any evidence of an elevated risk of cardiovascular outcomes for tofacitinib compared to TNFi. However, RA patients with cardiovascular risk factors or a history of cardiovascular disease showed an observed, yet not statistically significant, elevated risk of cardiovascular events. Additionally, the subgroup analysis of patients over 65 years of age with cardiovascular risk factors showed that the tofacitinib group had a higher cardiovascular risk, although this tendency did not attain statistical importance [21]. Similarly, the German observational RABBIT registry, which included 8000 RA patients, stated that the incidence of MACE did not increase in RA patients when comparing JAKi therapy with TNFi therapy [22]. Results from the French national health system comparing JAK inhibitors and adalimumab revealed reassuring

outcomes for MACE and these results were also valid for patients ≥ 65 years with at least one cardiovascular disease risk [23]. Consistent with previously published studies, we also indicated that MACE risk was not raised in the tofacitinib group compared to the etanercept group. Since data from large cohorts also include patients without cardiovascular disease risk, the necessity for careful monitoring of cardiovascular events in older patients and those with cardiovascular disease risk is evident.

Another safety issue that emerged from the ORAL Surveillance study was the increased frequency of cancer and the most frequent cancer was lung cancer in the tofacitinib group [4]. A meta-analysis examining the association between the JAKi class and malignancy found that JAK inhibitors were linked to a higher incidence of malignancy compared to TNFi. However, this result was mainly owing to the ORAL Surveillance study. When the ORAL Surveillance study was excluded from the analysis, the incidence of malignancy with JAK inhibitors remained higher compared to TNFi, but the statistical significance of this difference disappeared [24]. Likewise, the STAR-RA study found no evidence of a high risk of malignancy between tofacitinib and TNFi [25]. In the long-term safety results of tofacitinib, extending up to 9.5 years, the IRs for both NMSC and malignancies (excluding NMSC) were found to be similar to those informed in RA populations receiving bDMARD [9]. The fact that only one patient had squamous cell carcinoma in our study and no other malignancy (excluding NMSC) was detected makes it difficult to comment on this issue. However, the increased malignancy findings from the ORAL Surveillance study cannot be ignored and they remain up to date [26].

The other safety concern regarding tofacitinib is venous thromboembolism. VTE risk in RA patients is approximately twice as high compared to healthy controls and is closely related to disease activity [27]. In the ORAL Surveillance study, the most significant rise in VTE risk was in the tofacitinib 10 mg twice daily group. Although the signal for VTE was higher in the tofacitinib 5 mg twice daily group compared to TNFi, the difference did not reach statistical significance. Additionally, obesity, history

of VTE in the past, advanced age, and chronic lung disease were risk factors for VTE [28]. Data from the French national health system also indicated that the risk of VTE was not elevated in the JAKi group compared to the TNFi group [23]. We identified three patients who experienced VTE, and all of them were in the tofacitinib group. This increase in the VTE signal in the tofacitinib group indicates that caution should be exercised in RA patients over 60 years of age.

Like most bDMARDs, the most prevalent adverse events for tofacitinib are infections. In the ORAL Surveillance study, opportunistic infections, particularly herpes zoster, were more frequent with all doses of tofacitinib compared to TNFi [4]. The long-term safety data of tofacitinib highlighted a high risk of serious infections, opportunistic infections, and herpes zoster [9]. Findings of the US Corrona RA registry indicated that the percentage of serious infections was similar for tofacitinib compared to adalimumab [29]. In a study that included all patients using tofacitinib from the HUR-BIO database, herpes zoster was shown to be more common in the tofacitinib group [13]. In our study, the incidence of both herpes zoster and infections requiring hospitalization was found to be similar in both groups. Clinicians need to be particularly vigilant regarding infections in all elderly RA patients receiving immunosuppressive therapy.

**Study Limitations**

Although all patients who discontinued follow-up were called and questioned by phone, disease activation data at the time when MACE and VTE developed were unknown. The study group included data from a single center, and the sample size was small. Particularly in the etanercept group, lipid levels were assessed in a small number of patients and we did not have any data on how blood sugar and blood pressure regulation was progressing in patients diagnosed with DM and/or HT. Finally, since patients who did not continue their follow-up and could not be reached by phone were excluded from the study, data on the drug safety profile could not be obtained in these patients. Despite all these limitations, the results we have presented in elderly RA patients provide to the understanding of the safety profile of tofacitinib.

## CONCLUSION

Tofacitinib and etanercept had similar incidence for MACE, herpes zoster, and infections requiring hospitalization. The fact that all patients who developed VTE were in the tofacitinib group indicates that this situation warrants careful review. It is difficult to make a conclusive statement regarding cancer risk in this study. Large, observational, population-based controlled studies are needed to specifically investigate the safety profile of tofacitinib in RA patients and to evaluate factors that may be associated with adverse effects.

## Author contribution

Study conception and design: UK, AIE, and SK; data collection: ES and EÜ; analysis and interpretation of results: ES, LK, ÖK; draft manuscript preparation: ES, LK, UK, and SK. All authors reviewed the results and approved the final version of the manuscript.

## Ethical approval

## Funding

## Conflict of interest

The authors declare that there is no conflict of interest.

~∞∞ REFERENCES ∞∞~

[1] Smolen JS, Aletaha D, McInnes IB. Rheumatoid arthritis. Lancet 2016;388(10055):2023-38. https://doi.org/10.1016/S0140-6736(16)30173-8

[2] Smolen JS, Landewé RBM, Bijlsma JWJ, et al. EULAR recommendations for the management of rheumatoid arthritis with synthetic and biological disease-modifying antirheumatic drugs: 2019 update. Annals of the rheumatic diseases 2020;79(6):685-99. https://doi.org/10.1136/annrheumdis-2019-216655

[3] Fraenkel L, Bathon JM, England BR, et al. 2021 American College of Rheumatology Guideline for the Treatment of Rheumatoid Arthritis. Arthritis care & research 2021;73(7):924-39. https://doi.org/10.1002/acr.24596

[4] Ytterberg SR, Bhatt DL, Mikuls TR, et al. Cardiovascular and Cancer Risk with Tofacitinib in Rheumatoid Arthritis. The New England journal of medicine 2022;386(4):316-26. https://doi.org/10.1056/NEJMoa2109927

[5] McLornan DP, Pope JE, Gotlib J, Harrison CN. Current and future status of JAK inhibitors. Lancet (London, England) 2021;398(10302):803-16. https://doi.org/10.1016/S0140-6736(21)00438-4

[6] Kawalec P, Śladowska K, Malinowska-Lipień I, et al. European perspective on the management of rheumatoid arthritis: clinical utility of tofacitinib. Therapeutics and clinical risk management 2018;14:15-29. https://doi.org/10.2147/TCRM.S138677

[7] US Food and Drug Administration. Safety trial finds risk of blood clots in the lungs and death with higher dose of tofacitinib (Xeljanz, Xeljanz XR) in rheumatoid arthritis patients; FDA to investigate. 2019. Available https://www.fda.gov/media/120485/download (accessed 11 Mar 2020).

[8] Smolen JS, Landewé RBM, Bergstra SA, et al. EULAR recommendations for the management of rheumatoid arthritis with synthetic and biological disease-modifying antirheumatic drugs: 2022 update. Annals of the rheumatic diseases 2023;82(1):3-18. https://doi.org/10.1136/ard-2022-223356

[9] Cohen SB, Tanaka Y, Mariette X, et al. Long-term safety of tofacitinib up to 9.5 years: a comprehensive integrated analysis of the rheumatoid arthritis clinical development programme. RMD open 2020;6(3):e001395. https://doi.org/10.1136/rmdopen-2020-001395

[10] González Mazarío R, Fragío Gil JJ, Ivorra Cortés J, et al. Real-world Effectiveness and Safety of JAK Inhibitors in Rheumatoid Arthritis: A Single-centre Study. Reumatologia clinica 2022;18(9):523-30. https://doi.org/10.1016/j.reumae.2021.08.004

[11] Iwamoto N, Sato S, Kurushima S, et al. Real-world comparative effectiveness and safety of tofacitinib and baricitinib in patients with rheumatoid arthritis. Arthritis research & therapy 2021;23(1):197. https://doi.org/10.1186/s13075-021-02582-z

[12] Lanzillotta M, Boffini N, Barone E, et al. Safety of Janus Kinase Inhibitors: A Real-World Multicenter Retrospective Cohort Study. The Journal of rheumatology 2023. https://doi.org/10.3899/jrheum.2023-0145

[13] Bilgin E, Ceylan F, Duran E, et al: Efficacy, retention, and safety of tofacitinib in real-life: Hur-bio monocentric experience. Turkish journal of medical sciences 2021;51(1):297-308. https://doi.org/10.3906/sag-2007-123

[14] Bilgin E, Duran E, Ünaldı E, et al. Comparison of cardiovascular, cancer and herpes zoster risk of tofacitinib versus etanercept: single-centre observational study. Rheumatology (Oxford, England) 2022;61(9):e267-e269. https://doi.org/10.1093/rheumatology/keac226

[15] Nikiphorou E, Buch MH, Hyrich KL. Biologics registers in RA: methodological aspects, current role and future applications. Nature reviews Rheumatology 2017;13(8):503-10. https://doi.org/10.1038/nrrheum.2017.81

[16] Aletaha D, Neogi T, Silman AJ, et al. 2010 Rheumatoid arthritis classification criteria: an American College of Rheumatology/European League Against Rheumatism collaborative initiative. Arthritis Rheum. 2010;62(9):2569-81. https://doi.org/10.1002/art.27584

[17] England BR, Thiele GM, Anderson DR, Mikuls TR. Increased cardiovascular risk in rheumatoid arthritis: mechanisms and implications. BMJ. 2018;361:k1036. https://doi.org/10.1136/bmj.k1036

[18] Soubrier M, Barber Chamoux N, Tatar Z, et al. Cardiovascular risk in rheumatoid arthritis. Joint Bone Spine. 2014;81(4):298-302. https://doi.org/doi:10.1016/j.jbspin.2014.01.009

[19] Aviña-Zubieta JA, Abrahamowicz M, De Vera MA, et al. Immediate and past cumulative effects of oral glucocorticoids on the risk of acute myocardial infarction in rheumatoid arthritis: a population-based study. Rheumatology (Oxford). 2013;52(1):68-75. https://doi.org/10.1093/rheumatology/kes353

[20] Charles-Schoeman C, Buch MH, Dougados M, et al. Risk of major adverse cardiovascular events with tofacitinib versus tumour necrosis factor inhibitors in patients with rheumatoid arthritis with or without a history of atherosclerotic cardiovascular disease: a post hoc analysis from ORAL Surveillance. Ann Rheum Dis. 2023;82(1):119-29. https://doi.org/10.1136/ard-2022-222259

[21] Khosrow-Khavar F, Kim SC, Lee H, et al. Tofacitinib and risk of cardiovascular outcomes: results from the Safety of TofAcitinib in Routine care patients with Rheumatoid Arthritis (STAR-RA) study. Ann Rheum Dis. 2022;81(6):798-804. https://doi.org/10.1136/annrheumdis-2021-221915

[22] Meissner Y, Schäfer M, Albrecht K, et al. Risk of major adverse cardiovascular events in patients with rheumatoid arthritis treated with conventional synthetic, biologic and targeted synthetic disease-modifying antirheumatic drugs: observational data from the German RABBIT register. RMD Open. 2023;9(4):e003489. https://doi.org/10.1136/rmdopen-2023-003489

[23] Hoisnard L, Pina Vegas L, Dray-Spira R, et al. Risk of major adverse cardiovascular and venous thromboembolism events in patients with rheumatoid arthritis exposed to JAK inhibitors versus adalimumab: a nationwide cohort study. Ann Rheum Dis. 2023;82(2):182-8. https://doi.org/10.1136/ard-2022-222824

[24] Russell MD, Stovin C, Alveyn E, et al. JAK inhibitors and the risk of malignancy: a meta-analysis across disease indications. Ann Rheum Dis. 2023;82(8):1059-67. https://doi.org/10.1136/ard-2023-224049

[25] Khosrow-Khavar F, Desai RJ, Lee H, et al. Tofacitinib and Risk of Malignancy: Results From the Safety of Tofacitinib in Routine Care Patients With Rheumatoid Arthritis (STAR-RA) Study. rthritis Rheumatol. 2022;74(10):1648-59. https://doi.org/10.1002/art.42250

[26] Curtis JR, Yamaoka K, Chen YH, et al. Malignancy risk with tofacitinib versus TNF inhibitors in rheumatoid arthritis: results from the open-label, randomised controlled ORAL Surveillance trial. Ann Rheum Dis. 2023;82(3):331-43. https://doi.org/10.1136/ard-2022-222543

[27] Molander V, Bower H, Frisell T, Askling J. Risk of venous thromboembolism in rheumatoid arthritis, and its association with disease activity: a nationwide cohort study from Sweden. Ann Rheum Dis. 2021;80(2):169-75. https://doi.org/10.1136/annrheumdis-2020-218419

[28] Charles-Schoeman C, Fleischmann R, Mysler E, et al. Risk of Venous Thromboembolism With Tofacitinib Versus Tumor Necrosis Factor Inhibitors in Cardiovascular Risk-Enriched Rheumatoid Arthritis Patients. Arthritis Rheumatol. Published online March 13, 2024. https://doi.org/10.1002/art.42846

[29] Winthrop KL, Citera G, Gold D, Henrohn D, et al. Age-based (<65 vs ≥65 years) incidence of infections and serious infections with tofacitinib versus biological DMARDs in rheumatoid arthritis clinical trials and the US Corrona RA registry. Ann Rheum Dis. 2021;80(1):134-6. https://doi.org/10.1136/annrheumdis-2020-218992

acta medica

# Pelger-Huët Anomaly (PHA) Case Report

Hamza Sümter[1]
ORCID: 0000-0002-0224-9438

[1] Uşak Training and Research Hospital, Clinic of Hematology, Uşak, Türkiye

Corresponding Author: Hamza Sümter
E-mail: hamzasumter@gmail.com

~~● A B S T R A C T ●~~

Pelger-Huët anomaly is a rare benign hematological disorder. It was first described in the 1920s. It is inherited in an autosomal dominant manner. Nuclear hypolobulation, which can also be seen in other leukocytes, especially neutrophils, is a characteristic feature. This morphological change does not cause a defect in the immune system. It should be differentiated clinically from pseudo-Pelger-Huët anomaly (PPHA). In this study, Pelger-Huët anomaly is presented which is noticed in the peripheral smear of a 22-year-old female patient who came to the hematology outpatient clinic due to her sibling having Hodgkin's lymphoma. The family members of the case were also evaluated in this respect.

Keywords: Pelger-Huët anomaly, benign, hyposegmentation, lamin B receptor, Pince-Nez.

## INTRODUCTION

Pelger-Huët anomaly (HPA) is known as hypolobulation in leukocytes. A well-prepared peripheral smear and careful evaluation is essential for diagnosis. While the incidence of the mono allelic form of Pelger-Huët anomaly is 1 in 6000, the biallelic form is much more rare [1,2]. Hypolobulation in neutrophil nuclei can be bilobed (2-lobed) as well as non-lobulated (1-lobed). In the two-lobed nuclear structure, the lobes are connected by a thin chromatin. This change in the neutrophil nucleus can also be seen in eosinophils, lymphocytes and monocytes [3]. Neutrophilia is not expected in the blood count. In studies, the immunological functions of PHA cells were found to be normal [3]. Although different prevalence rates were reported due to its asymptomatic nature, the real frequency of this hematological disorder cannot be known [4].

## CASE REPORT

A 22-year-old female patient, who applied for examination due to her sibling's history of Hodgkin lymphoma, was evaluated at the hematology outpatient clinic. The patient's anamnesis showed no medical or herbal drug use. She had no known systemic disease. No lymphadenopathy was detected on physical examination. B symptoms(fever, weight loss, night sweats) were not present. Biochemical tests (transaminases, renal function tests) were within the normal range. Complete blood count: Leukocyte (WBC): 6160/ μL, Neutrophil(ANC): 3640/μL, Hemoglobin(Hgb): 14.2 g/dL, Platelet: 409000/ μL. Peripheral smear examination reported 60% neutrophils, 35% lymphocytes, 5% monocytes. Neutrophil classification was as follows: 80% 2-lobed, 10% 1-lobule (nonlobule), 10% band formation (Figure 1-4). Peripheral blood smear was performed every 2-3 months for approximately 8 months and it was observed that hypolobulation continued at similar rates. In the genetic study conducted for the LBR gene, p.Leu177(c.530T>G) mono allelic was detected. Ten people were contacted as close relatives (mother, father, sibling, 5 aunts, 1 cousin, 1 uncle) and evaluated for Pelger-Huët anomaly. However, their peripheral smears were found normal.
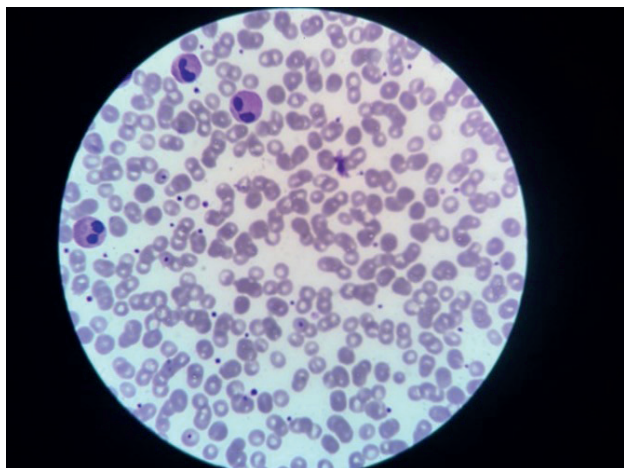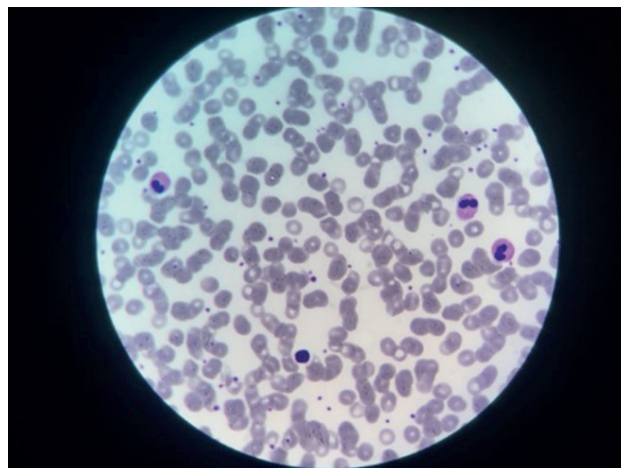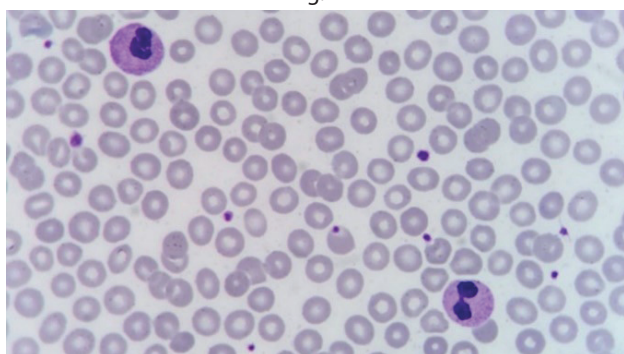
Fig. 1


Fig. 2


Fig. 3


Fig. 4

## DISCUSSION

In a normal peripheral blood smear, the majority of neutrophils (approximately 70-75%) have 3-4 segments, while a small number of cells may have more than 4 or less than 3 segments [1].

Pelger-Huët anomaly (PHA) was first described in 1928 by the Dutch doctor Pelger in a tuberculosis patient. This anomaly was considered to have a poor prognosis since the patient died during clinical follow-up [5,6]. It was also described in 1932 by the Dutch pediatrician Dr. Huët in another tuberculosis patient. However, since the patient recovered during the follow-up, it was concluded that this malformation in the leukocytes did not have a bad prognosis [7].

Autosomal dominant transmission is seen in PHA. The mutation is in the gene encoding the lamin B receptor (LBR) protein. This gene is located on the long arm of chromosome 1 (1q41-43). Deficiency in the amount of lamin B receptor (LBR) protein is associated with neutrophil hyposegmentation[8]. Peripheral smear findings may differ in biallelic and mono allelic interactions. Bilobulation is predominant in neutrophils in the mono allelic form. In the biallelic form, non-lobulated neutrophil morphology is more prominent [3,7]. The nuclear structure in non-lobulated cells may be round, oval or peanut shaped [3,7]. In homozygotes, in addition to hyposegmentation in blood cells, mental retardation, epilepsy, developmental delay, skeletal anomalies, macrocephaly with prominent forehead, ventricular septal defect, and metacarpal shortness may occur[8]. In experimental studies, it was observed that the lifespan and immunological functions of PHA cells were normal [1,2]. Although the studies conducted in animals lead to different results, in humans no mortality risk was detected in Pelger-Huët anomaly [5].

Biallelic PHA, which is much less common compared to the mono allelic form, was first described in rabbits. biallelic rabbits have severe chondrodystrophy, skeletal anomalies, and increased prenatal and postnatal mortality (>80% mortality) [5, 8]. The biallelic form was first described in humans in 1952 in a Dutch girl. Convulsions (familial convulsions), psychomotor and mild physical developmental delay were observed in

this patient. In the peripheral smear of the same patient, it is detected that 94% of the neutrophils were round-shaped, non-lobulated neutrophils [6]. Biallelic PHA is known to be very rare in humans, in fact even in a study conducted in 2021 as to biallelic PHA, it was reported that there were      fewer than 10 known cases [3]. In a few cases identified as biallelic in humans, congenital anomalies were rarely reported [5]. Although the neutrophils in rabbits and humans are structurally similar, it was concluded that the biallelic disorder does not cause death and skeletal disorder in humans [5].

Patient history (medication use, infection status) and the percentage of pelgeroid cells in the peripheral smear are important in distinguishing PHA from pseudo-Pelger-Huët anomaly (PPHA). In PPHA, three-lobed neutrophils predominate, while a small number of pelgeroid cells are present. In HPA, the predominant cells are 2-lobed. Even in biallelic HPA cases, there is a dominance of non-lobulated neutrophils. In addition to hyposegmentation in neutrophils, band form may be seen in a small number of cells. In PPHA There is a secondary cause that may cause hypolobulation in the peripheral smear. Myelodysplastic syndrome, acute myeloid leukemia, myeloproliferative neoplasia, lymphoproliferative disease, some drugs (ibuprofen, tacrolimus, ganciclovir, co-trimaxazole, itraconazole, fludarabine, rituximab, citalopram, lorezepam, valproic acid, colchicine, mycophenolate mofetil), infections (HIV, tuberculosis , mycoplasma, malaria, influenza) can cause PPHA [1,3].

Hyposegmentation in PHA cells must be distinguished from granulocyte precursors (myeloid precursor cells). While the nucleus to cytoplasm ratio is high in granulocyte precursors, this ratio is low in neutrophils with PHA[3]. While normal neutrophil segmentation is absent or minimal in congenital PHA, hypolobulation is found in a small number of cells in MDS or other acquired PPHA conditions [7]. Additionally, in hypolobulation in PPHA, the lobes are non-symmetrical [9]. A distinction should also be made between PHA cells with a single lobe (round - oval nucleus) and myelocytes. Compared to typical myelocytes, the nucleus in a HPA cell is smaller, denser and more compact. The nucleus to cytoplasm ratio is lower than the one for myelocyte [9]. Another nuclear shape, the peanut-shaped Pelger-Huët cell may resemble a metamyelocyte [7].

According to Ham's classification, neutrophils are divided into 3 groups [3]:

Type A: Nucleus more than 2 lobes

Type B: The nucleus is 2-lobed (dumbbell-shaped). Pince-nez cells consist of a symmetrical 2-lobed nucleus.

Type C: Nucleus non lobule. Round or oval shaped. They are known as Stodmeister cells.

In congenital mono allelic HPA, type B (2-lobed) neutrophils are dominant, while type A and type C are found in small numbers.

In congenital biallelic HPA, type C neutrophils are dominant, while type A and type B are present in small numbers.

In PPHA, type A neutrophils are dominant, while type B and type C are found in small numbers [3].

Mutation in the LBR gene has been identified also in Greenberg/HEM dysplasia, which can show hypolobulation like HPA in peripheral blood smear. Greenberg/HEM dysplasia results in in utero exitus. A total of 8 cases were described in the article published in 2015. HPA was also detected in the peripheral blood smear of two patients with this diagnosis [5]. However, no information was available about the peripheral smear of the other cases. For this reason, it was stated that a neutrophil morphology connection cannot be established between Greenberg/HEM dysplasia and PHA [5,7].

## CONCLUSION

Pelger-Huët anomaly (HPA) is a rare hematological disorder and is caused by lobulation deficiency in the leukocyte nucleus. It is noticed by hypolobulation due to a defect in the LBR gene. Although it is stated that it is effective in the diapedesis and chemotaxis of lobulated leukocytes in the nucleus, there is no retardation in immune functions in people with HPA compared to normal people. People with HPA may not even be diagnosed since it is asymptomatic. However, it is important to distinguish it from pseudo Pelger-Huët anomaly (PPHA), which may develop due to secondary causes.

## Author contribution

Study conception and design: HS; data collection: HS; analysis and interpretation of results: HS; draft manuscript preparation: HS. The author reviewed the results and approved the final version of the manuscript.

## Conflict of interest

The authors declare that there is no conflict of interest.

∼⌒ R E F E R E N C E S ⌒∼

[1]  Ayan M S, et al. Case of acquired or pseudo-Pelger-Huët anomaly. Oxf Med Case Reports 2015. 2015(4): 248-50.

[2]  Shah S S, et al. Familial Pelger-Huet Anomaly. Indian J Hematol Blood Transfus 2016. 32(Suppl 1): 347-50.

[3]  Padmapriya B, et al. Pelger-Huet anomaly: A Rare case report. 2020. 9(4): 255-258.

[4]  Konishi T, et al. Familial case of hereditary Pelger-Huët anomaly. Int J Hematol 2019. 110(2): 127-128.

[5]  Oosterwijk J C, et al. Congenital abnormalities reported in Pelger-Huët homozygosity as compared to Greenberg/HEM dysplasia: highly variable expression of allelic phenotypes. J Med Genet 2003. 40(12): 937-41.

[6]  Haverkamp Begemann N and A Van Lookeren Campagne. Homozygous form of Pelger-Huët's nuclear anomaly in man. Acta Haematol 1952. 7(5): 295-303.

[7]  Cunningham J M, et al. Historical perspective and clinical implications of the Pelger-Hüet cell. Am J Hematol 2009. 84(2): 116-9.

[8]  Hoffmann K, et al. Mutations in the gene encoding the lamin B receptor produce an altered nuclear morphology in granulocytes (Pelger-Huët anomaly). Nat Genet 2002. 31(4): 410-4.

[9]  Colella R and S C Hollensead. Understanding and recognizing the Pelger-Huët anomaly. Am J Clin Pathol 2012. 137(3): 358-66.